UNIVERSITAT DE BARCELONA

New Strategies for Black Hole Physics

Raimon Luna

Tesi doctoral

New Strategies for Black Hole Physics

Raimon Luna

Director: Roberto Emparan

UNIVERSITAT DE BARCELONA

New Strategies for Black Hole Physics

Programa de doctorat en Física

Autor: Raimon Luna

Director: Roberto Emparan

Tutor: Joan Soto

Universitat de Barcelona

UNIVERSITAT DE BARCELONA

"Als meus pares, Gonçal i Agnès,
i a la meva germana, Magalí,
sense els quals res d'això
hagués estat possible."

Acknowledgements

I would like to start by thanking my advisor, Roberto Emparan, for all his help, advice and orientation during my PhD and Master studies. Thank you so much, Roberto, for such an amazing time working with you, and for your nearly infinite patience, kindness and support. Your knowledge of gravitation and black holes and your physical intuition are impressive. You have always known the right approach to take in every problem during research, and you seem to already know the answer before any complicated calculations are done. I have enjoyed very much collaborating with you, and I really hope this collaboration continues for many years in the future.

I am very much grateful to Vítor Cardoso, Miguel Zilhão, João L. Costa and José Natário in the group at CENTRA, *Instituto Superior Técnico* in Lisbon (Portugal) for their hospitality and collaboration on Strong Cosmic Censorship. In particular, many thanks to Miguel Zilhão for his lessons on numerical relativity, computation and code development, and for his continuous advice on academic life.

I want to thank Luis Lehner and Laura Bernard for a wonderful time at the Perimeter Institute for Theoretical Physics in Waterloo, Ontario (Canada). Spending six months working in such an amazing research center as PI, in such a welcoming scientific environment, was a highly enriching phase of my PhD. The vast knowledge of numerical relativity of Luis Lehner and the analytic skill of Laura Bernard allowed me to learn a lot during my stay.

Many thanks to my other collaborators during research in my PhD. Marina Martínez introduced me to symbolic calculations and showed me extremely powerful tools such as spectral methods, widely used in all my research. David Licht, with his impressive knowledge of gravity and theoretical physics, has been of great importance in several projects. Ryotaku Suzuki, Kentaro Tanabe and Keisuke Izumi have shown absolutely remarkable analytic computational skills and have made possible the large D research projects. Tomás Andrade has contributed enormously in finding unexpected and very interesting uses of the large D effective equations. Alejandro Fernández-Piqué worked with us in a very instructive project on holography and AdS Love numbers.

I would also like to thank the Theoretical Physics, Gravitation and Cosmology group in Barcelona for their support, especially professors Tomeu Fiol, Jaume Garriga, David Mateos, Enric Verdaguer, Federico Mescia and Jorge Casalderrey; and postdocs Miguel Zilhão, Jorge Rocha, Christiana Pantelidou, Aron Jansen, Jakob Salzer, Yago Bea, Antonia Micol Frassino, Benson Way, Antón Faedo and Ricardo Ferreira. Special thanks to Helvi Witek for her help and her very instructive lectures on the 3+1 decomposition and numerical relativity.

I have enjoyed a good time and interesting physics discussions with the other PhD students in the group, including Marija Tomašević, Mikel Sánchez, Genís Torrents, Javier Gómez Subils, Miquel Triana and David Pravos.

I would like to thank the administrative staff of the *Física Fonamental* and *Física Quàntica i Astrofísica* departments in Barcelona, and Perimeter Institute, for their efforts in solving problems and making our lives much easier. Many thanks to Kayla, Bea, Cristina, Elena, Rosa and Lenka. I would like to thank as well Domènec Espriu and Joan Soto for tutoring this PhD.

I could not continue without thanking all the people who have accompanied me throughout my career in the wonderful world of physics. Starting with my undergraduate studies, I am very grateful to Aitor, Alex, Alvaro, Anna, Carles, Carlota, David, Gemma, Júlia and Raimon for all the good times we have spent together. Also, obviously, everyone I met during my PhD, both at the University of Barcelona and at Perimeter Institute, especially Iván, Ricard, Joan, Xavi, Isa, Elena, Adrià, Jaime, Tony, Frede; and to Bruno, Adrián, Javi, Victor, Nanna, Hugo, Hyun, Pablo, Andrés, Ruoshui and Michael. Thanks to the physics choir in the University of Barcelona (*Cor-Iolis*), the Perimeter Institute Choir, *Cor Jove Cantus Firmus*, and the physics outreach group *Encontres amb el Tercer Cicle*.

None of this would have been possible without the unconditional support from my family, especially my parents and my sister. I want to express my deepest gratitude to all my family, including my grandparents Gonzalo Luna and Caridad Tomás, who will always be remembered.

My collaboration with *Instituto Superior Técnico*, including a stay in Lisbon, has been supported by the GWverse COST Action CA16104, "Black holes, gravitational waves and fundamental physics".

My long visit to Perimeter Institute has been funded by the Visiting Graduate Fellowship program, that covered all my expenses during my 6 months in Canada. This research was supported in part by Perimeter Institute for Theoretical Physics. Research at Perimeter Institute is supported by the Government of Canada through the Department of Innovation, Science, and Economic Development, and by the Province of Ontario through the Ministry of Research and Innovation.

Last but not least, this PhD has been possible thanks to the PhD grant *Formación del Profesorado Universitario* FPU15/01414 from Spanish *Ministerio de Ciencia, Innovación y Unversidades*, to which I am very grateful. This work is also supported by ERC Advanced Grant GravBHs-692951 and MEC grants FPA2013-46570-C2-2-P and FPA2016-76005-C2-2-P.

Contents

Chapter 1

Introduction

General Relativity (GR) has proven to be an extremely successful theory of gravity. This beautiful theory, formulated in a purely geometric language, produces predictions that have been accurately verified in a plethora of historic experiments. More recently, and almost precisely a century after the formulation of the theory, LIGO gave us a confirmation of one of the most spectacular predictions of GR, together with a brand new way of obtaining valuable information from astrophysical events: gravitational waves [1]. From a fundamental point of view, we have reasons to think that GR is incomplete. This means that the theory should cease to be trustworthy at a large enough energy scale (or small enough length scale), with this scale being at most the Planck scale.

Black holes are the most basic objects in GR, and a good knowledge of them seems to be a key to understanding gravity. They are extremely important as astrophysical objects, also from the early Universe (primordial black holes), in Mathematical Relativity, String Theory and Quantum Gravity, and last but not least, in many seemingly non-gravitational systems through applied holographic dualities [2] (AdS/QFT, AdS/QGP, AdS/CMT). Black holes are probably the simplest macroscopic objects in Nature, which are completely described by their mass, spin, and charge. This fact makes them mathematically very appealing and beautiful, allowing us to describe astrophysically sized objects with very simple equations, often even analytically. Although apparently very simple, we have clues, such as black hole thermodynamics or the Information Paradox, which are somehow warning us that there should be a more complex structure underlying the theory of GR. It is our goal, therefore, to try to find the right theory of quantum gravity. For now, the most accepted candidates are encapsulated in what we know as String Theory. This family of theories comes at a cost: we need to formulate them in more than four dimensions, usually 10 or 11, and they almost certainly require supersymmetry.

In this thesis we will be applying novel approaches and developing new techniques to touch on a number of issues that are all related to fundamental aspects of modern gravitational theory and black holes. We will now give a brief preview of the context for these problems, which we will elaborate on in more detail in subsequent separate sections of this introduction.

Having a fundamental dimension larger than four is a problem that can be circumvented by requiring that the extra dimensions are compactified in some

(D-4)-dimensional manifold, so that physics takes place in an effective 4-dimensional spacetime at large enough distances. This fact, however, encourages us to explore the behavior of gravity and black holes in dimensions larger than four. The black hole physics in higher dimensions is immensely richer than in dimension four: many of the uniqueness theorems do not hold anymore, thus allowing for a wide variety of gravitational phenomena. Particularly, you can now have black holes with extended directions (black strings and black branes), that allow for extended gauge charges. Extended black holes also display the so-called Gregory-Laflamme (GL) instability [3,4], which causes black strings and black branes to spontaneously develop non-uniformities that may lead to violations of Weak Cosmic Censorship (WCC), that is to the formation of *naked* singularities. Research has been done on violations of the WCC in the large D approach, *i.e.,* in the limit of a very large number of dimensions as a $1/D$ expansion, both in extended and localized black holes. Recently, [5] found evidence of a possible violation of WCC in colliding black holes by this technique, and there is evidence that this happens in dimensions possibly as low as $D = 6$. Research on this hypothesis is still ongoing. Many extensions of this work are promising, including the endpoint of axisymmetric unstable modes of rotating (Myers-Perry) black holes, addition of charge, or further analysis of the scattering problem in large D. It is important to notice that higher dimensional black holes, when treated in the large D formalism, simplify enormously. Even when numerical solutions are needed, these are dramatically simpler than the ones required for general finite D simulations, and are usually run in a regular laptop in a matter of seconds or minutes.

Moving away from astrophysical scenarios, gravity and black holes can give us valuable information about strongly coupled Quantum Field Theories (QFTs). This is made possible through the AdS/CFT correspondence [2], also known as the holographic principle, in which there is a one-to-one duality between certain types of conformally invariant QFTs and classical gravity theories. Therefore, relatively simple gravitational calculations can be used to obtain qualitative, and sometimes even quantitative information about strongly coupled theories that are extremely difficult to solve otherwise.

On the other hand, quantum effects may lead to to some modified theory of classical gravity at low energies, *i.e.,* some deviation from conventional GR. This ex-

pectation is calling for us to explore which possibilities in the landscape of theories are good candidates for the description of Nature. Although the space of possible theories of modified gravity may seem unaffordably wide at first sight, many constraints exist, both from observation and from the mathematical structure of the theories. Since gravity theories are classically described by nonlinear partial differential equations, one must check whether they satisfy some minimal requirements that would otherwise render the theory highly suspicious. It is generally expected that the equations of motion for a sensible theory should be well posed. Also, a fully nonlinear evolution should not lead to pathologies such as loss of hyperbolicity, formation of shocks, or violations of causality.

Even in conventional GR itself, there exist some issues that need to be understood in order to be ready for gravity modifications. A common issue is the existence of solutions which contain Cauchy Horizons (CH), where physics stops being predictable from asymptotic data, thus violating the Strong Cosmic Censorship (SCC) conjecture. These solutions are typically eternal and stationary, and so the Cauchy Horizons are expected to be dynamically destroyed once dynamical effects are taken into account. However, some configurations have been recently proven to present stable Cauchy Horizons that can be crossed by an observer with finite tidal deformations. These solutions, although astrophysically not very relevant, could give us clues about the extreme behavior of GR.

We now proceed to discuss more specifically the problems and approaches that constitute the bulk of this thesis.

1.1 Large D black branes and black strings

Black $p-$branes are higher-dimensional black holes that extend along p spatial directions. They are known to exist in $D \geq 5$. In the neutral case, they can be easily obtained from the Schwarzschild-Tangherlini solution as

$$ds^2 = -\left(1 - \left(\frac{r_0}{r}\right)^n\right) dt^2 + \frac{dr^2}{1 - \left(\frac{r_0}{r}\right)^n} + dz^i dz_i + d\Omega_{n+1}^2 \tag{1.1}$$

with $i = 1, ..., p$ labeling the spatial directions along the brane. $d\Omega_{n+1}^2$ is a $(n+1)$-dimensional sphere metric, and n is defined as $n = D - p - 3$. Typically, the

brane *worldvolume* spatial directions z^i are compactified in a circle, restricting any dependence along them to be periodic with a given wavenumber $k_i = 2\pi/L_i$. Black branes were shown to be unstable [3, 4]. As a consequence of this instability, the so-called Gregory-Laflamme instability, branes develop non-uniformities along their extended directions z^i. The instability appears at low wavenumbers k, starting from some threshold value k_{GL}, and follows a dispersion relation $\Omega(k)$ that depends only on n.

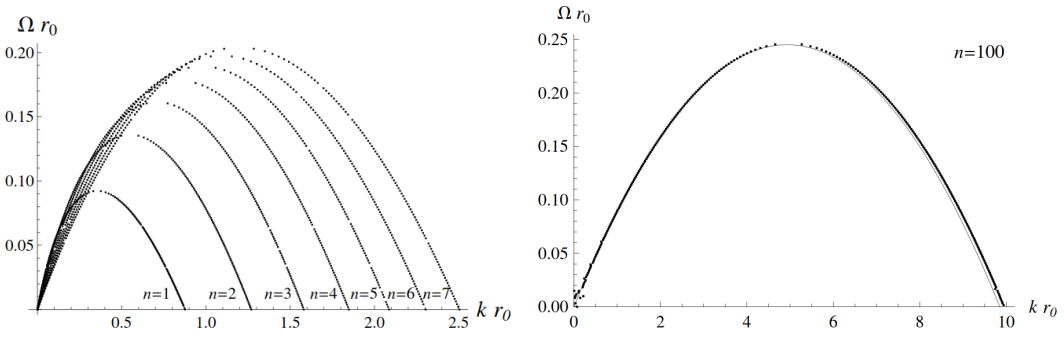

Figure 1.1: Left: Dispersion relation $\Omega(k)$ of the unstable Gregory-Laflamme mode for black branes. Right: Dispersion relation for $n = 100$. (numerical data courtesy of P. Figueras). Plots taken from Ref. [6]

In this thesis we approach the behavior of black branes in the large-D approximation, *i.e.,* considering a very large number of spacetime dimensions, as an asymptotic expansion in $1/D$. This approach, developed in [7–9], allows us to obtain a set of very simple equations that capture many of the physical phenomena in gravity. This technique uses the fact that the gravitational field around a massive object decays as $1/r^n$, and therefore, as one takes the limit $n \to \infty$, it becomes extremely concentrated in a thin region of size $1/D$ around the black hole horizon. In this way, the horizon can be seen as an effective membrane embedded in an essentially flat background geometry (see [10] for details). The region where the black hole lives is in some sense excised from the background spacetime.

Equations for this effective membrane have been derived in recent years in [11–17], in different formulations and in regimes that overlap but do not entirely coincide. In particular, ref. [11] obtained fully covariant equations for static black holes, both

in vacuum ($R_{\mu\nu} = 0$) and in (Anti-)deSitter ($R_{\mu\nu} = \pm\Lambda g_{\mu\nu}$), including leading order (LO) and next-to leading order (NLO) terms in the $1/D$ expansion. To leading order, the effective equations for the dynamics of the black brane can be written as

$$\begin{aligned} \partial_t m - \partial_i \partial^i m &= -\partial_i p^i \,, \\ \partial_t p_i - \partial_j \partial^j p_i &= \epsilon \partial_i m - \partial^j \left(\frac{p_i p_j}{m} \right) \,. \end{aligned} \tag{1.2}$$

with m being the energy density of the fluid, and p_i giving (essentially, see later) the momentum density of the fluid, hence the local velocity of the flow. The parameter ϵ has the value +1 for asymptotically flat (AF) spacetimes, and -1 for asymptotically Anti-de Sitter (AdS) spacetimes. One can also obtain corrections to these equations to higher orders in $1/n$, which are in fact used (up to $1/n^4$) for the case of a black string in Chapter 3.

A basic question is whether the equations of the effective theory can be understood in terms of familiar physics. We can, in fact, write the equations for the dynamical evolution of the black brane in hydrodynamic form, but for stationary configurations they are more naturally viewed as soap-bubble-type equations. These two views (none of which were manifest in [15]) are complementary in that the same variable is interpreted, in one case as the energy density of the fluid, in the other case as the 'height function' measuring the deformation of an elastic membrane.[1] Indeed this reflects a basic feature of black holes: the same variable that gives their mass also sets the horizon size.

In Chapter 3, we use these effective equations to investigate the phases and the stability of black strings at different values of the dimension D and the compactification length L. The case of the black string, *i.e.,* with $p = 1$, has been widely studied. Non-uniform black strings were first numerically constructed in $D = 6$ by [20] and then followed up in [21–26]. The endpoint of the instability depends on the dimension of spacetime, and on the compactification length. Dynamical evolutions in $D = 5$ were performed in [27], signaling a violation of Penrose's Weak Cosmic Censorship [28]. In these simulations, the instability of the string leads to

[1] Despite similarities in wording, this is very different from the blackfold effective fluid on an elastic membrane [18], and also from the usual membrane paradigm [19], which does not possess these elastic aspects.

the formation of very thin necks that pinch-off with diverging curvature, producing an endless cascade of self-similar structures of satellite black holes. In some cases, the instability of uniform black strings (UBS) can lead to stable non-uniform black strings (NUBS). The type of symmetry-breaking transition form UBS to NUBS was shown to change at a critical value of the spacetime dimension $D_* \approx 13.5$ by [29]. Black strings and their stability have been analyzed by using several analytical techniques, such as the so-called blackfold approximation and fluid gravity. We use $1/D$ corrections to estimate the value of Sorkin's critical dimension, which turns out to be remarkably accurate. In fact, our analytical determination of the critical dimensions gives quite possibly the most accurate value so far, surpassing currently existing numerical calculations. We use both perturbative analytical solutions and numerical calculations (using a coefficient fitting spectral algorithm) to obtain thermodynamic data that we compare with finite-D results in the literature. The comparison shows that the large-D technique can give accurate analytical results with excellent level of detail.

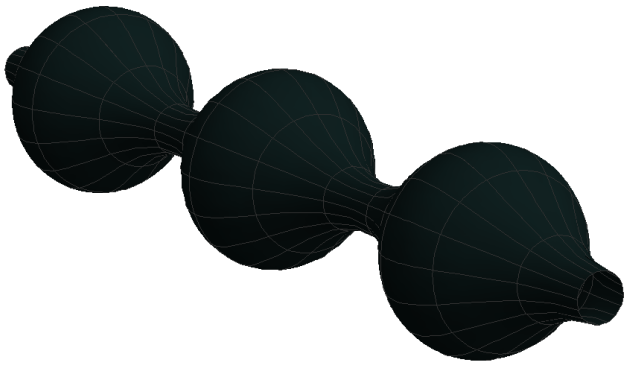

Figure 1.2: Non-uniform black string: endpoint of the Gregory-Laflamme instability on a black string with $z \sim z + \frac{2\pi}{k}$ boundary conditions as $D \to \infty$. In this case, $k = 0.98 k_{GL}$. Profile obtained via the nonlinear fitting of 10 Fourier coefficients.

In general, all these issues about the existence and the local and global stability of solutions depend on the values of the parameters of the system, such as its charges and the number of dimensions. Typically the linear instability is present only within certain parameter ranges, but also the non-linear evolution, and its most probable

endpoint, depend in general on what region of parameter space the initial system lies in. For black strings and black branes these details are not fully understood; the non-linear regime requires the numerical solution of Einstein's equations, both to find highly non-uniform static phases, and to determine their stability and time-evolution (see [30–32] for early reviews and [33] for a very recent one).

Studies so far have mostly focused on the properties of neutral, asymptotically flat black strings in different numbers of dimensions D.[2] The latter is possibly the simplest and most natural parameter that can be varied to explore this problem. Indeed, since a number $D-3$ of the dimensions are fixed in the shape of a S^{D-3}, the equations reduce to a three-dimensional dynamics where D is a parameter that can be varied continuously.

We also perform a study of highly non-uniform black strings in increasing number of dimensions, in order to establish when they can be expected to transition into localized black holes. This study would be extremely cumbersome and time-consuming with conventional numerical techniques, due to the increasing difficulty of these methods as the number of dimensions grows. We do this by a combination of methods—dynamical evolution leading to large non-uniformities until the numerical evolution breaks down, and studies of static solutions that develop identifiable pathologies (specifically, negative tensions) when the non-uniformity grows too large.[3] In dynamical evolutions we aim mostly at qualitative information, for which NLO effects seem enough[4], but in the construction of static solutions we strive for accuracy comparable to previous studies and thus we include up to 4NLO corrections (four terms after the leading order).

Besides UBS and NUBS it is also possible to have black holes localized in the compact circle. Less is known in the literature about these phases, except when they are either very small and far from merging into a NUBS [36,37], or else at relatively low values of D [26, 38, 39]. They are expected to be the dominant phase in the canonical ensemble in the regions below the curves of existence of NUBS. However, there are also regions of the plane where they coexist with NUBS, and in which they may dominate thermodynamically over the latter. In particular, this is expected to

[2] See [34,35] for recent work on non-uniform black membranes.

[3] Ref. [34] made similar studies to NLO.

[4] At times we have gone to NNLO, to confirm our conclusions.

be the case in low dimensions up to values of $\boldsymbol{\beta}$ and $\mathbf{M}$ larger than the threshold for the GL instability. However, the details of what are the dominant phases, either at fixed temperature or at fixed mass, can be fairly complicated and require information about localized black holes that we have not explored. Nevertheless, our study provides the most complete picture so far of the properties of phases of non-uniform black strings in arbitrary dimensions, both below and above the critical dimension.

1.2 Weak Cosmic Censorship violation in higher dimensions

The use of the effective equations 1.2 for the description of black strings already gives useful insight into the violation of Penrose's WCC [28], as initially pointed out by [3, 27]. The WCC conjecture states that no naked singularities can be formed by dynamical evolution of a gravitational system starting from classical initial data. It can also be defined as the impossibility for distant observers to probe Plank scale physics (and hence quantum gravity) if the energy of the initial configuration is low and the system follows the classical gravitational evolution of Einstein's equations.

WCC has been shown to be violated in different scenarios [27, 40, 41], but some aspects of WCC violations are still not completely explored. For instance, it is not clear how generic the initial conditions leading to CC violation can be. Different gravitational setups can require different amounts of fine-tuning in order to lead to the formation of naked singularities in a finite evolution time. The presence of naked singularities is expected to require a theory of quantum gravity to describe further evolution of the system. In other words, the future of the system ceases to be predictable from classical gravity. The importance of this loss of predictability, and the amount of energy transfered to a Plankian density are currently not completely clear.

Chapter 4 explores possible events of WCC violation in $D > 4$ black hole collisions. The technique of large D, through the use of the effective equations (1.2), gives a powerful tool to analyze this type of scenarios that are otherwise very heavy to approach via numerical finite D simulations [41, 42]. It has been recently [43, 44] been shown that localized rotating black holes can actually be described as blobs

on a black brane in the so-called *blob* formalism.

The phenomenon of CC violation can be summarized as follows: When two black holes collide, their event horizons merge and form a single, highly deformed black hole. At a low enough angular momentum, this resulting horizon will relax through a Quasinormal Mode (QNM) ringdown to a rotating Myers-Perry stationary solution. If the angular momentum of the collision lies above a certain threshold, however, the Myers-Perry black hole is affected by an ultraspinning instability that leads to the formation of an elongated bar-like object. These black bars are always a transient phase of the evolution at finite D, due to the emission of gravitational radiation. They can instead last for a long time, even indefinitely, at large D, since gravitational waves are strongly suppressed as D becomes very large [8, 45].

The black bar happens to be affected by an instability, which is analogous to the GL instability [3], that can induce the horizon to form a thin neck in its center. The resulting object, which we call a dumbbell, can pinch off by evaporation once the neck reaches a Plank size, and break into two separate (now stable) black holes that fly apart from each other. The competition between the GL instability growth rate and the depletion of angular momentum due to gravitational wave emission (and thus driving the black hole towards stability) will determine whether WCC is eventually violated.

1.3 Strong Cosmic Censorship in the presence of a cosmological constant

Cauchy horizons appear in many exact solutions to gravitational systems, particularly in the Reissner-Nordström (RN) and Kerr solutions. These horizons are a boundary beyond which GR ceases to be a deterministic theory. Indeed, the future of an observer that enters the region of spacetime beyond the inner horizon of a RN black hole cannot be predicted from the outside initial data. The observer will at this point have a timelike singularity in its null past, and therefore information from this singularity can affect the fate of the black hole interior.

It is generally believed that the appearence of Cauchy horizons is an artifact that arises in exact eternal solutions. By constraining the spacetime to be stationary

we are ruling out the dynamical evolution that would prevent the formation of such horizons. This idea is encapsulated in Penrose's Strong Cosmic Censorship hypothesis. According to this conjecture, external perturbations falling into the black hole would suffer an infinite blueshift when they arrive to the CH, triggering an instability. The resulting unstable horizon would then become singular, creating a terminal boundary of spacetime. This effect was confirmed in asymptotically flat spacetimes by [46], due to the *mass inflation* effect. The Misner-Sharp mass was shown to increase exponentially as one approaches the CH.

The stability of Cauchy horizons depends therefore on the decay of perturbations in the exterior of the black hole. A scalar field ϕ perturbation in AF black holes will decay as a power-law tail given by the well-known Price's law [47]. This behavior is enough to guarantee the appearance of mass inflation and thus the validity of SCC. This scenario, however, changes drastically when a cosmological constant $\Lambda > 0$ is present. In this case, ϕ will instead decay as an exponential law. This fact has recently motivated [48–55] to put into question the SCC conjecture for nearly-extremal RN black holes in asymptotically de Sitter spacetimes (RNdS).

In order to go beyond previous studies, Chapter 5 summarizes the results of fully nonlinear simulations of highly charged RNdS spacetimes. In order to perform such (spherically symmetric) nonlinear integrations, a novel spectral double-null code has been developed. Even though the results presented here are far from conclusive, they do show a dramatic decrease in mass inflation as the charge of the back hole approaches the threshold derived in [51], to the point where mass inflation is not observed through the time domain capability of the code.

1.4 Plasma polarization and Love numbers of AdS black branes

Any continuous system that can be described as a quantum field theory will react to a change in the geometry it lives in. It will do so by changing the distribution of the energy density, pressure and stresses. In other words, the system (which we will call from now on as *plasma*) polarizes, and its stress energy tensor acquires some non-trivial expectation values. This effect is in general quite difficult to compute,

especially if the QFT happens to be strongly coupled. In this case, perturbation theory is not applicable, and only numerical and lattice computations can be performed.

In this context, the gauge-gravity duality, also known as AdS/CFT correspondence, is extremely useful to extract qualitative valuable information from the system [2]. According to this conjecture, strongly-coupled quantum field theories that are conformally invariant, those called conformal field theories (CFT), are dual to classical gravity in Anti-de Sitter space in the limit where the rank of their gauge group is very large ($N \to \infty$). Therefore, there exists a one-to-one correspondence between classical gravity in $(n+1)$-dimensional AdS, and n-dimensional strongly coupled CFTs (in particular $SU(N)$ Super Yang-Mills theories) living in in the boundary of AdS. This fact can be used to extract information of the quantum theory, otherwise extremely difficult to obtain, from calculations in gravity.

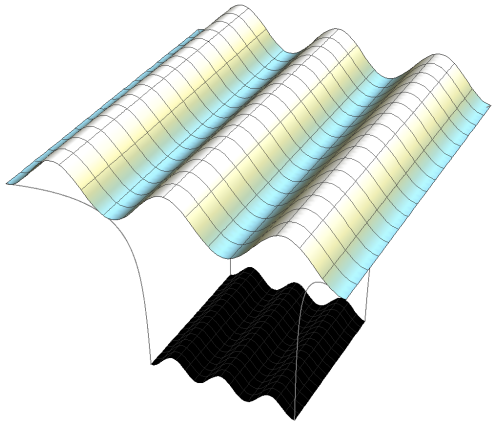

Figure 1.3: Fluctuations of the energy of the plasma are represented by deformations of the bulk geometry.

This technique has been used in the past in both fully-nonlinear numerical calculations and in some particular geometries that allow for analytic results to exist [56–59]. There is also the possibility to consider linear deformations of the geometry where the plasma lives, which can be represented as Fourier modes. Perturbations of the boundary geometry will produce tidal deformations on the underlying geometry in the bulk. In order to compute this deformation, we solve the equations

for a linearized perturbation of the geometry that satisfies an appropriate boundary condition at infinity. Namely, the metric perturbation must not vanish asymptotically, but instead approach the non-zero value that matches the source, *i.e.,* the metric perturbation specified at the boundary. This is exactly the goal of Chapter 6. Having a CFT at finite temperature is equivalent to introducing a black hole in the AdS bulk. In particular, a black brane, whose worldvolume spatial directions will correspond to the spatial directions of the boundary.

If the perturbations are small, the deformations of the brane are well described by linear response coefficients, called the Love numbers. These numbers, firstly introduced to describe deformations on astrophysical objects under external potentials [60, 61], encode the information needed for the characterization of the response of the plasma at a linear level. Furthermore, they are in principle measurable experimentally. In recent times these Love numbers have been a matter of interest in this area, since they may be measured from the gravitational wave signal of inspiralling black holes and neutron stars [62, 63]. One can then use them to test the predictions of General Relativity, and also to extract information about the internal constitution and equation of state of neutron stars. These Love numbers can be classified, depending on the transformation properties of the perturbation under rotations, as tensor, vector and scalar-type. They can be determined from linearized master second order equations first derived in [64], where we use the holographic coordinate $v = 1/r$. From these master equations, the Love numbers can be read in a straightforward manner as coefficients in the near-boundary expansion of the gauge-invariant quantities $Z_i(v)$. The two independent solutions of the master equations are classified as non-normalizable, and normalizable parts. The former can be seen as the external source forcing the system, and the later as the linear response (or vacuum expectation value) of the system to the external forcing. The ratio between the amplitudes of these two solutions, imposed by regularity at the black hole horizon, determines the Love numbers. This can be done both numerically, and analytically as a hydrodynamic expansion (power series in the wavenumber k). A non-linear calculation of the hydrodynamic response of the plasma to an external gravitational force was made in [65, 66], to lowest order for small k.

The quantum expectation value of the CFT stress tensor is obtained from the Love numbers [67] as the renormalized quasilocal stress tensor of the bulk geometry.

Once we know $\langle T_{\alpha\beta}\rangle$ as a function of the metric perturbation $\gamma_{\rho\sigma}$, we can easily obtain the two-point function by functional differentiation

$$\langle T_{\alpha\beta}T_{\rho\sigma}\rangle = -\frac{2}{\sqrt{-\gamma}}\frac{\delta\langle T_{\alpha\beta}\rangle}{\delta\gamma^{\rho\sigma}}. \tag{1.3}$$

This two-point function gives the geometric polarizability of the plasma. We will provide a detailed description of how the polarization coefficients are related to this two-point function and to the Love numbers of the black brane. Finally, as a natural extension of our study, we also compute the linear-response coefficients of the electric polarizability of the plasma.[5]

1.5 Global solutions in Horndeski's theory

When trying to build extensions to General Relativity, it is natural to consider the inclusion of new degrees of freedom to describe the gravitational field. It is, however, desirable for the resulting equations of motion to be at most of second order type, to guarantee the absence of Ostrogradski ghosts [69], which would potentially lead to catastrophic instabilities in the theory. If we only allow a metric tensor in the gravitational part of the Lagrangian, we are left with Lovelock theories. The richness of possible theories increases drastically if one allows gravity to be describes both by a metric $g_{\mu\nu}$ and a scalar field ϕ. Thus, the most general scalar-tensor diffeomorfism-invariant theory that leads to second order equations of motion is known as Horndeski's Theory [69–71]. Special cases of this theory have been used under different names to describe dark energy [72–75] and possible extensions of GR that could hopefully be detected by gravitational wave signals [76–83]. In the former front, particular examples include quintessence [84, 85]; kinetic quintessence or k-essence [86, 87] and chameleon/galileon [88, 89] theories.

In the later case, strong constraints have indeed been introduced on the spectrum of allowed theories from the GW170817 detection [90–92]. These constraints are a result of the comparison of the experimental signals with linearized predictions of

[5]The literature on AdS black branes deformed by boundary electric fields is too large, and more importantly, too differently motivated than ours, to properly refer to all of it here. We shall mention, though, that a linearized perturbation analysis was performed in [68].

Horndeski's theories. It is nevertheless important to keep in mind that the predictions at a linear level do not necessarily agree with the fully nonlinear solution, even if initial conditions are weak. Some phenomena are intrinsically nonlinear, and could in principle challenge the linear predictions in case of a disagreement. In the particular case of Horndeski's theory, the nonlinear behavior has been analyzed in the literature [93–95].

Independently of the experimental constraints, it is generally assumed that a theory that is intended to describe Nature must be *well posed* [96]. Well posed theories are those who have a unique solution which depends continuously on initial and boundary conditions. A theory that is not well posed would arguably fail to give reliable physical predictions.

Chapter 7 studies a subset of Horndeski's theories whose equations of motion are rendered symmetric hyperbolic when a generalized harmonic gauge is used. These theories are then locally well posed. It is however nontrivial to determine whether global solutions exist, and if these solutions are sufficiently well-behaved. It is a useful technique to express the Lagrangian in the so-called Einstein frame, with the Ricci tensor appearing without any multiplicative factor containing the scalar field. In the Einstein frame, much of the physics can be extracted from the behavior of the equation of motion of the scalar field, whose principal part is described in terms of an effective metric $\gamma_{\mu\nu}$.

This effective metric depends both on the fundamental metric $g_{\mu\nu}$ and on the scalar field ϕ, and can show a number of pathological behaviors at a non-linear level. If these phenomena occur outside of horizons, *i.e.,* if they are causally connected to null infinity, they would render the theory suspicious. It is important to consider that characteristics for the effective metric do not generally coincide with the light cones of the fundamental metric, and therefore we can in general find *sound horizons* for the scalar and *light horizons* for the metric. Since $g_{\mu\nu}$ and ϕ are coupled together, only the innermost horizon will be a true boundary for the causal connection with infinity. The speed of propagation of the scalar is in fact not bounded from above, and can even diverge in certain special circumstances.

Another worrisome possibility (which has been confirmed by numerical simulations), is a change of the character of the equation of motion, from hyperbolic to parabolic, and to elliptic afterwards. This happens when an eigenvalue of $\gamma_{\mu\nu}$

switches sign. This produces a change on the causal structure of the geometry.

Chapter 2

Large D effective equations

This chapter introduces the notion of the large D expansion of General Relativity, and in particular the derivation of effective equations for black branes and black strings at leading order in $1/D$. These are derived for both neutral black branes, and $p-$brane charged black branes (corresponding to a $(p+2)$-form gauge field strength).

Further analysis shows that the equations admit both a hydrodynamic and an elastic interpretation, the so-called *hydro-elastic* complementarity. According to this view, the black branes at very high dimensions can be dynamically described as a viscous, compressible fluid. When they settle down, on the other hand, they behave like an elastic membrane, or a soap bubble. This chapter is based on the research published in [97].

2.1 Notation and conventions

Many expressions can be given in unified form by introducing a parameter

$$\epsilon = \begin{cases} +1 & \text{for AF}\,, \\ -1 & \text{for AdS}\,. \end{cases} \tag{2.1}$$

For AF black p-branes we define

$$n = D - p - 3\,, \tag{2.2}$$

and for AdS black branes

$$n = D - 1\,. \tag{2.3}$$

p will be the finite number of spatial dimensions, out of all of its worldvolume directions, along which we will allow the brane to fluctuate. We will often use n as the large parameter instead of D. In order to obtain finite magnitudes in the effective theory we have scaled by appropriate powers of n the physical magnitudes of the theory, beginning with (2.17), which indicates that physical length scales along the brane are $1/\sqrt{n}$ times the corresponding lengths in the effective theory. The physical magnitudes discussed in this chapter, written with a tilde, are related to the effective ones as

$$\tilde{\omega} = \omega\,, \qquad \tilde{k}_i = \sqrt{n}\,k_i\,, \tag{2.4}$$

$$\tilde{\partial}_i = \sqrt{n}\,\partial_i\,, \qquad \tilde{v}^i = \frac{v^i}{\sqrt{n}}\,, \tag{2.5}$$

$$\tilde{m} = nm\,, \qquad \tilde{P} = P\,, \tag{2.6}$$

$$\tilde{T} = nT\,, \qquad \tilde{s} = s\,, \tag{2.7}$$

$$\tilde{q}_p = \sqrt{n}\,q_p\,, \qquad \tilde{\Phi}_p = \frac{\Phi_p}{\sqrt{n}}\,, \tag{2.8}$$

$$\tilde{\eta} = \eta\,, \qquad \tilde{\kappa} = n\kappa\,. \tag{2.9}$$

Our length units are $r_0 = 1$, where r_0 is measured from the trace of the extrinsic curvature K of the solution at $\mathsf{R} \to \infty$ so that

$$K = \frac{n}{r_0} + \mathcal{O}(n^0, \mathsf{R}^{-1})\,. \tag{2.10}$$

We use units where $16\pi G = \Omega_{n+1} =$ area of the unit S^{n+1}.[1]

2.2 The neutral black brane

Let us begin by identifying how to take the large-D limit. This can be inferred from the properties of static, uniform black branes. In Eddington-Finkelstein coordinates, the AF black brane metric is[2]

$$ds^2 = 2dt\,dr - \left(1 - \frac{r_0^n}{r^n}\right) dt^2 + \delta_{ij} d\tilde{\sigma}^i d\tilde{\sigma}^j + r^2 d\Omega_{n+1}\,, \tag{2.11}$$

with spatial indices along the brane

$$i, j = 1, \ldots, D - n - 3 = p\,, \tag{2.12}$$

and in AdS

$$ds^2 = 2dt\,dr + r^2 \left(- \left(1 - \frac{r_0^n}{r^n}\right) dt^2 + \delta_{ij} d\tilde{\sigma}^i d\tilde{\sigma}^j \right)\,, \tag{2.13}$$

[1] The fact that $G \sim \Omega_{n+1} \sim n^{-n/2} \to 0$ at large n can be related to the vanishing of the gravitational field outside the near-horizon region [8, 9].

[2] We denote by t the ingoing null coordinate. When n is large, dependence on t is the same as dependence on the asymptotic time that measures time in the effective theory.

with

$$i, j = 1, \ldots, D-2 = n-1\,. \tag{2.14}$$

In the latter, the cosmological constant is set to $\Lambda = -n(n-1)/2$. As $D \to \infty$ we will keep p finite in AF, while in AdS we will assume that the metric functions depend on only a finite number of coordinates.

The equation of state relating the energy density $\tilde{m} = (n+\epsilon) r_0^n$ and pressure $\tilde{P}$ of the branes is (using (2.1))

$$\tilde{P} = -\epsilon \frac{\tilde{m}}{n+\epsilon}\,, \tag{2.15}$$

so the speed of sound of long-wavelength perturbations is[3]

$$c_s = \sqrt{\frac{\partial \tilde{P}}{\partial \tilde{m}}} = \sqrt{\frac{-\epsilon}{n+\epsilon}}\,. \tag{2.16}$$

Since c_s is small when $n \gg 1$, we expect the large-n dynamics to be non-relativistic. This dictates the scalings with n required to capture this physics: we rescale

$$\tilde{\sigma}^i = \frac{\sigma^i}{\sqrt{n}}\,, \tag{2.17}$$

in order to focus on small, $\mathcal{O}(1/\sqrt{n})$ lengths along the brane, and in addition consider worldvolume velocities $\mathcal{O}(1/\sqrt{n})$. Thus we take the metric along brane directions to be[4]

$$g_{tt} = \mathcal{O}(1)\,, \qquad g_{ij},\, g_{ti} = \mathcal{O}(1/n)\,. \tag{2.18}$$

Ref. [15] sought solutions in Bondi-type gauge for the AF neutral brane

$$ds^2 = -2\left(u_t dt + \frac{u_i}{n} d\sigma^i\right) dr - A dt^2 - \frac{2}{n} C_i d\sigma^i dt + \frac{1}{n} G_{ij} d\sigma^i d\sigma^j + r^2 d\Omega_{n+1}\,, \tag{2.19}$$

and the AdS black brane

$$ds^2 = -2\left(u_t dt + \frac{u_i}{n} d\sigma^i\right) dr + r^2 \left(-A dt^2 - \frac{2}{n} C_i d\sigma^i dt + \frac{1}{n} G_{ij} d\sigma^i d\sigma^j\right)\,. \tag{2.20}$$

A convenient way to proceed is to integrate over the sphere Ω_{n+1} in the AF case, and over the cyclic brane directions in AdS, and obtain theories of gravity in the reduced finite-dimensional spacetimes with a dilaton field for the size of the compactified

[3] Imaginary c_s for AF black branes corresponds to the GL instability [6, 18].

[4] As already mentioned, this scaling is not covered by the analysis of [12, 17].

spaces (see *e.g.,* appendix B of [11]). The reduced AF and AdS theories can be related by analytic continuation in n, so only one of them needs to be explicitly solved [98, 99]. One finds that $1/n$ terms in G_{ij} must be included for consistency of the Einstein equations at this order.

The solution found in [15] has $u_t = -1$, $u_i = 0$ (by gauge choice), and

$$A = 1 - \frac{m(t,\sigma)}{\mathsf{R}}\,, \qquad C_i = \frac{p_i(t,\sigma)}{\mathsf{R}}\,, \qquad G_{ij} = \delta_{ij} + \frac{1}{n}\frac{p_i(t,\sigma)p_j(t,\sigma)}{m(t,\sigma)\mathsf{R}}\,, \tag{2.21}$$

and finite radial coordinate

$$\mathsf{R} = r^n\,. \tag{2.22}$$

In the AdS solution $p_i \neq 0$ only along the finite number of non-cyclic brane directions. Furthermore, the Einstein equations with a radial index imply that the collective fields $m(t,\sigma)$ and $p_i(t,\sigma)$ must satisfy the effective field equations[5]

$$\partial_t m - \partial_i \partial^i m = -\partial_i p^i\,, \tag{2.23}$$

$$\partial_t p_i - \partial_j \partial^j p_i = \epsilon \partial_i m - \partial^j \left(\frac{p_i p_j}{m}\right)\,. \tag{2.24}$$

Spatial brane indices i, j are raised and lowered with the flat metric δ_{ij}.

2.2.1 Isothermal fluid

Eqs. (2.23) and (2.24) have the form of continuity equations for m and p_i, with $\int d^p\sigma\, m$ and $\int d^p\sigma\, p_i$ being conserved in time. This suggests that we change the variable p^i to v^i as

$$p_i = m v_i + \partial_i m\,. \tag{2.25}$$

Then (2.23) becomes the continuity equation for mass,

$$\partial_t m + \partial_i \left(m v^i\right) = 0\,, \tag{2.26}$$

and (2.24) the momentum-stress equation

$$\partial_t (m v^i) + \partial_j \left(m v^i v^j + \tau^{ij}\right) = 0\,, \tag{2.27}$$

[5] We believe these are the conservation equations of the quasilocal stress-energy tensor at $\mathsf{R} \to \infty$ (with appropriate subtraction). However, extracting this stress tensor is subtle [11], so we omit it.

with

$$\tau_{ij} = -\epsilon m\, \delta_{ij} - 2m\partial_{(i}v_{j)} - m\, \partial_j\partial_i \ln m\,. \tag{2.28}$$

These are the equations of a non-relativistic, compressible fluid with mass density m, velocity v^i, and stress tensor τ_{ij}. The first two terms in (2.28) correspond, respectively, to isothermal-gas pressure

$$P = -\epsilon m\,, \tag{2.29}$$

and to shear and bulk viscosities

$$\eta = m\,, \qquad \zeta = \frac{1+\epsilon}{p}\eta \tag{2.30}$$

(recall that $\delta^i{}_i = p$ is finite for the AF black p-brane, but infinite for the AdS brane). Together with the entropy density and temperature,

$$s = 4\pi m\,, \qquad T = \frac{1}{4\pi}\,, \tag{2.31}$$

which satisfy

$$m = Ts\,, \qquad dm = Tds\,, \tag{2.32}$$

these properties reproduce the leading large-n results for AF and AdS black branes in the fluid/gravity correspondences of [6, 66]. That is, if we take the large-n limit of the stress-energy tensor of the latter, including up to viscosity terms, and scale physical quantities as in section 2.1, then we obtain the first two terms in (2.28). Negative P for $\epsilon = +1$ gives rise to the Gregory-Laflamme instability [6, 18].

The constitutive relation (2.28) contains one last term beyond the viscous stress. In fact, since the large-D expansion and the hydrodynamic gradient expansion are different, one might have expected an infinite number of higher-derivative terms in τ_{ij}. Remarkably, the gradient expansion is truncated at a finite order when $D \to \infty$. This implies that an infinite number of higher-order transport coefficients vanish in this limit [6]. In order to match the last term in (2.28) to the hydrodynamic second-order coefficients computed in [66] one must focus on the regime where both expansions agree. Hence we must not only take the large-n limit of [66], but also regard (2.28) as a perturbative gradient expansion, so that the hydrodynamic equations at first-derivative order can be used to rewrite the second-order term, with gradients of m, in terms of velocity gradients.

In the hydrodynamic interpretation, the last term in τ_{ij} is associated to creation or dissipation of density inhomogeneities. But we can also interpret it in other ways. Let us write its divergence as

$$\partial_j \left(m\, \partial^j \partial_i \ln m \right) = m \partial_i \left(\frac{\partial_j \partial^j m}{m} - \frac{\partial_j m \partial^j m}{2m^2} \right) , \tag{2.33}$$

i.e., as a term proportional to the gradient of a potential. In this manner we can view this term as yielding an external gravitational force, proportional to the mass density, acting on the fluid. However, the origin of the gravitational potential from second derivatives of m is obscure. Since this rewriting will not be possible for dynamical charged black branes, we shall not dwell anymore on it.

2.2.2 Hydro-elastic complementarity

The variable m sets the horizon size $\mathsf{R} = \mathsf{R}_h = m$ in the black brane solutions (2.19), (2.20), and as such it also determines the radial position of the effective membrane in the background geometry. Namely, the 'near-zone' solutions (2.19), (2.20) are matched to either the Minkowski background

$$ds^2 = -dt^2 + \frac{1}{n} \delta_{ij} d\sigma^i d\sigma^j + r^2 d\Omega_{n+1} + dr^2 , \tag{2.34}$$

or to the AdS background

$$ds^2 = -r^2 \left(-dt^2 + \frac{1}{n} \delta_{ij} d\sigma^i d\sigma^j \right) + \frac{dr^2}{r^2} \tag{2.35}$$

at a 'membrane surface' $r = r(\sigma)$, of the form

$$r^n = m(\sigma) . \tag{2.36}$$

When n is large, this is

$$r = 1 + \frac{\ln m(\sigma)}{n} , \tag{2.37}$$

which describes small, $1/n$ deformations of a uniform surface at $r = 1$. Let us calculate the area A and volume V of this surface. In order to ease a bit the notation we use the variable

$$\mathcal{P}(\sigma) = \ln \left(m(\sigma) \right) . \tag{2.38}$$

When n is large, in the Minkowski background (2.34) we have

$$A = \frac{\Omega_{n+1}}{n^{p/2}} \int dt\, d^p\sigma \left(1 + \frac{\mathcal{P}(\sigma)}{n}\right)^{n+1} \left(1 + \frac{1}{2n}(\partial\mathcal{P})^2\right) , \tag{2.39}$$

$$V = \frac{\Omega_{n+1}}{n^{p/2}} \int dt\, d^p\sigma \, \frac{1}{n+2} \left(1 + \frac{\mathcal{P}(\sigma)}{n}\right)^{n+2} , \tag{2.40}$$

and in the AdS background (2.35),

$$A = n^{(1-n)/2} \int dt\, d^{n-1}\sigma \left(1 + \frac{\mathcal{P}(\sigma)}{n}\right)^{n} \left(1 + \frac{1}{2n}(\partial\mathcal{P})^2\right) , \tag{2.41}$$

$$V = n^{(1-n)/2} \int dt\, d^{n-1}\sigma \, \frac{1}{n} \left(1 + \frac{\mathcal{P}(\sigma)}{n}\right)^{n} . \tag{2.42}$$

We compute the trace of the extrinsic curvature K by functional differentiation

$$K = \frac{\delta A}{\delta V} = \frac{\delta A}{\delta \mathcal{P}(\sigma)} \Big/ \frac{\delta V}{\delta \mathcal{P}(\sigma)} . \tag{2.43}$$

In Minkowski we find

$$K = n + 1 - \left(\mathcal{P} + \partial^2\mathcal{P} + \frac{1}{2}(\partial\mathcal{P})^2\right) , \tag{2.44}$$

and in AdS

$$K = n - \left(\partial^2\mathcal{P} + \frac{1}{2}(\partial\mathcal{P})^2\right) . \tag{2.45}$$

In AdS there is a non-trivial gravitational redshift on the surface, namely

$$\sqrt{-g_{tt}} = 1 + \frac{\mathcal{P}(\sigma)}{n} . \tag{2.46}$$

With these results we obtain

$$\sqrt{-g_{tt}}\, K = n + \frac{1+\epsilon}{2} - \left(\epsilon \ln m + \frac{\partial_j \partial^j m}{m} - \frac{\partial_j m \partial^j m}{2m^2}\right) + \mathcal{O}(1/n) . \tag{2.47}$$

Let us collect the velocity-independent terms in Eq. (2.27), and use (2.33) and (2.47) to write it as

$$-m\partial_i \left(\sqrt{-g_{tt}}\, K\right) = \partial_t(m v_i) + \partial^j \left(m v_i v_j - 2m\partial_{(i} v_{j)}\right) . \tag{2.48}$$

In addition, if we take the time derivative of (2.47) and use the mass continuity equation (2.26) we obtain

$$m\partial_t\left(\sqrt{-g_{tt}}K\right) = \partial_i\left(\epsilon m v^i + m\partial^i\frac{\partial_j\left(mv^j\right)}{m}\right) . \tag{2.49}$$

These equations encapsulate the notion of *hydro-elastic complementarity* in the neutral black brane effective theory. Instead of the hydrodynamic equations for the mass and momentum densities of a fluid we can write the elasticity equations (2.48) and (2.49) for the time and space derivatives of extrinsic curvature of the membrane, in terms of the radial variable m and a velocity field along the membrane.

The right-hand sides of equations (2.48) and (2.49) still retain a hydrodynamic flavour. This disappears, however, for configurations with $v^i = 0$, which must be static and satisfy the Young-Laplace equation

$$\sqrt{-g_{tt}}\,K = \text{constant}\,. \tag{2.50}$$

Stationary, time-independent configurations, can have $v^i \neq 0$ as long as there is no viscous dissipation, *i.e.,* $\partial_{(a}v_{b)} = 0$, or in other words $\partial_t + v^i\partial_i$ is a Killing vector. In this case, using (2.26) and (2.33), we find that Eq. (2.27) becomes

$$\partial_i\left(\frac{v^2}{2} + \epsilon\ln m + \frac{\partial_j\partial^j m}{m} - \frac{\partial_j m\partial^j m}{2m^2}\right) = 0\,, \tag{2.51}$$

which, to leading non-trivial order at large n, is equivalent to

$$\sqrt{-g_{tt}\left(1-\frac{v^2}{n}\right)}\,K = 2\kappa\,. \tag{2.52}$$

with constant κ. It is straightforward to check that the latter is actually the surface gravity of the horizon in (2.19) and (2.20). In terms of the physical velocity $\tilde{v}$ this equation is

$$\sqrt{-g_{tt}\left(1-\tilde{v}^2\right)}\,K = 2\kappa\,, \tag{2.53}$$

with equality holding at $\mathcal{O}(n)$ and $\mathcal{O}(1)$. Thus we have obtained the soap-bubble (Young-Laplace) equation. It can be viewed as the statement that the surface gravity of the stationary horizon is constant along the brane, even when the horizon itself is not uniform but has locally-varying extrinsic curvature, and when the time coordinate on the brane is locally redshifted by Lorentz-boost and gravitational factors, relative to the canonical time of static observers in the background.

2.2.3 Static string solutions

For completeness and later reference, we review here the analysis in [11] of static solutions of (2.51), with $v = 0$, for which m depends on only one spatial coordinate z. We refer to these as static string configurations.

Define[6]

$$\mathcal{P}(z) = \ln m(z)\,. \tag{2.54}$$

From (2.37) we see that $\mathcal{P}$ measures the $\mathcal{O}(1/n)$ fluctuation of the radius of the membrane. Eq. (2.51) (with $v = 0$) can be integrated twice to obtain

$$\frac{1}{2}\mathcal{P}'^2 + U(\mathcal{P}) = E\,, \tag{2.55}$$

with

$$U(\mathcal{P}) = \epsilon\left(\mathcal{P} + m_0\, e^{-\mathcal{P}}\right)\,. \tag{2.56}$$

Here E and m_0 are integration constants. We can view this as the classical mechanics of a particle (the undamped Toda oscillator), with position $\mathcal{P}$, time z, potential U, and energy E. When $m_0 > 0$ the potential has an extremum at $e^{\mathcal{P}} = m_0$.

Trajectories of the particle with $\mathcal{P}' \neq 0$ correspond to non-uniform string profiles. The potential is dominated by the linear term $\epsilon\mathcal{P}$ for $\mathcal{P} > 0$, and by $\epsilon m_0 e^{-\mathcal{P}}$ for $\mathcal{P} < 0$. Then, when $\epsilon = -1$ there cannot be any non-trivial, bounded trajectories of the particle, and the only solutions correspond to constant $\mathcal{P}$ at a maximum of U where $e^{\mathcal{P}} = m = m_0 > 0$. These are uniform AdS black branes.

When $\epsilon = +1$ and $m_0 > 0$ the potential has a minimum where $U = 1 + \ln m_0$. The solution that stays at the minimum is the uniform AF black string, but now periodic trajectories also exist (for $E > 1 + \ln m_0$), which give non-uniform black string solutions. Although the equation cannot be integrated exactly, it is easy to obtain analytical approximations and numerical solutions [11], which match very well the profiles that result at the end of the time evolution of the dynamical equations (2.23), (2.24) [15].

[6] This $\mathcal{P}$ is twice the one in [11].

2.3 Brane-charged black branes

Now we study p-brane solutions of the action

$$I = \int d^D x \sqrt{-g} \left(R - \frac{1}{2(p+2)!} H^2_{[p+2]} \right) , \tag{2.57}$$

which carry p-brane charge under the $(p+2)$-form field-strength $H_{[p+2]} = dB_{[p+1]}$. We keep p fixed as the dimension $D = n + p + 3$ grows large.

In this case we do not consider AdS branes: since their worldvolume has $p = D-2$ spatial directions, the field-strength $H_{[p+2]}$ would be a top-form, simply amounting to a renormalization of the cosmological constant.[7]

2.3.1 Choice of large-n limit

In order to get oriented about how to take the large-n limit, we study first the static uniform solutions. At any finite n, refs. [100, 101] give their energy density, pressure, p-brane charge, potential, temperature and entropy density, in terms of two parameters r_0 and α ($r_0 \geq 0$, $|\alpha| < \infty$), in the form

$$\tilde{m} = r_0^n \, n \left(1 + N \sinh^2 \alpha + \frac{1}{n} \right) , \tag{2.58}$$

$$\tilde{P} = -r_0^n (1 + nN \sinh^2 \alpha) , \tag{2.59}$$

$$\tilde{q}_p = r_0^n \sqrt{N} n \sinh \alpha \cosh \alpha , \qquad \tilde{\Phi}_p = \sqrt{N} \tanh \alpha , \tag{2.60}$$

$$\tilde{T} = \frac{n}{4\pi r_0} (\cosh \alpha)^{-N} , \qquad \tilde{s} = 4\pi r_0^{n+1} (\cosh \alpha)^N , \tag{2.61}$$

where we have defined

$$N = \frac{2}{p+1} + \frac{2}{n} . \tag{2.62}$$

The speed of sound is [101]

$$c_s^2 = \left(\frac{\partial \tilde{P}}{\partial \tilde{m}} \right)_{\tilde{q}_p} = -\frac{1}{n+1} \frac{1 + (2 - Nn) \sinh^2 \alpha}{1 + \left(2 - \frac{Nn}{n+1}\right) \sinh^2 \alpha} . \tag{2.63}$$

[7] We might consider lower-form fields $H_{[p+2]}$ in AdS, with p finite as $D \to \infty$. In general these introduce anisotropic worldvolume dynamics, which is beyond the scope of this chapter. The dynamics could be truncated to the isotropic sector, but we shall not study this either.

Let us now take the large-n limit with α fixed, so $\tilde{q}_p/\tilde{m}$ and $\tilde{P}/\tilde{m}$ remain $\mathcal{O}(1)$. Then the speed of sound

$$c_s^2 = \frac{N \sinh^2\alpha}{1+(2-N)\sinh^2\alpha} + \mathcal{O}(1/n) \tag{2.64}$$

is always positive, *i.e.,* we never expect a GL instability, even though the p-brane is in general non-extremal. Moreover, we have $c_s = \mathcal{O}(1)$ instead of $\mathcal{O}(1/\sqrt{n})$, so the system is relativistic. While there is nothing wrong with this limit, it is a regime of brane physics different than we are studying in this chapter.

A different large-n limit is obtained for small charge $\tilde{q}_p/\tilde{m} = \mathcal{O}(1/\sqrt{n})$, *i.e.,* set

$$\alpha = \frac{\hat{\alpha}}{\sqrt{n}} \tag{2.65}$$

and keep $\hat{\alpha}$ finite. Then

$$c_s^2 = -\frac{1-N\hat{\alpha}^2}{n} \tag{2.66}$$

is non-relativistic at large n, and can change sign if the charge is large enough. Therefore, scaling the metric as in (2.18) and the gauge potential $B_{[p+1]}$ as

$$B_{t\sigma^1\ldots\sigma^p} = \mathcal{O}\left(n^{-\frac{p+1}{2}}\right) \tag{2.67}$$

we expect to capture the physics of hydrodynamic sound and the appearance/disappearance of the GL instability.

2.3.2 Large D effective theory

Following these arguments, we take the ansatz (2.19) for the metric and

$$B_{t\sigma^1\ldots\sigma^p} = n^{-\frac{p+1}{2}} F(t,\sigma,\mathsf{R})\,. \tag{2.68}$$

We find the solution

$$A = 1 - \frac{m(t,\sigma)}{\mathsf{R}}\,, \qquad C_i = \frac{p_i(t,\sigma)}{\mathsf{R}}\,, \qquad G_{ij} = \delta_{ij} + \frac{1}{n}\frac{p_i(t,\sigma)p_j(t,\sigma) - q_p^2\delta_{ij}}{m(t,\sigma)\mathsf{R}}\,, \tag{2.69}$$

$$F = \frac{q_p}{\mathsf{R}}\,, \tag{2.70}$$

where now q_p is constant and we set $u_t = -1$, $u_i =$ constant. We may also gauge-transform B to make it vanish at the horizon $\mathsf{R} = m$. The effective field equations for m and p^i are

$$\partial_t m - \partial_i \partial^i m = -\partial_i p^i \,, \tag{2.71}$$

$$\begin{aligned} \partial_t p_i - \partial_j \partial^j p_i &= \partial_i m - \partial^j \left(\frac{p_i p_j - q_p^2 \delta_{ij}}{m} \right) \\ &= \left(1 - \frac{q_p^2}{m^2} \right) \partial_i m - \partial^j \left(\frac{p_i p_j}{m} \right) \,. \end{aligned} \tag{2.72}$$

2.3.3 Fluid dynamics

The change (2.25) casts these equations into explicitly hydrodynamic form. Besides the usual mass continuity equation (2.26) from (2.71), Eq. (2.72) gives

$$\partial_t (m v_i) + \partial^j \left(-m \left(1 + \frac{q_p^2}{m^2} \right) \delta_{ij} + m v_i v_j - 2m \partial_{(i} v_{j)} - m \partial_i \partial_j \ln m \right) = 0 \,. \tag{2.73}$$

The only change in the effective fluid relative to the neutral one is in the pressure,

$$P = -m \left(1 + \frac{q_p^2}{m^2} \right) \,. \tag{2.74}$$

This is indeed the large-n limit of the pressure of the black brane discussed above in sec. 2.3.1, with the appropriate translation between physical and effective magnitudes. The charge q_p is a global parameter of the fluid only affecting its pressure, and not a local degree of freedom. Nevertheless, we can associate to it a 'local potential' [101]

$$\Phi_p = n^{\frac{p+1}{2}} \left(B_{t\sigma^1 \ldots \sigma^p}(\mathsf{R} \to \infty) - B_{t\sigma^1 \ldots \sigma^p}(\mathsf{R} \to m) \right) = \frac{q_p}{m} \,. \tag{2.75}$$

Since in the large-n limit as we have taken it, the entropy density and temperature of the effective theory are the same as in the neutral fluid (2.31), q_p and Φ_p do not enter the first and second law of thermodynamics, and the entropy is conserved.

2.3.4 Elastic interpretation

Eq. 2.48 (with $g_{tt} = -1$) applies again to this system and gives $\partial_t K$, while Eq. (2.73) can be written in the hydro-elastic form

$$-m \partial_i \left(\left(1 - \frac{q_p^2}{2nm^2} \right) K \right) = \partial_t (m v_i) + \partial^j \left(m v_i v_j - 2m \partial_{(i} v_{j)} \right) \,, \tag{2.76}$$

with the extrinsic curvature of the brane embedding in Minkowski being (2.44). For stationary branes we can write

$$\left(1-\frac{q_p^2}{2nm^2}-\frac{v^2}{2n}\right)K=2\kappa\,, \tag{2.77}$$

which expresses how the surface gravity κ remains constant over the entire horizon of the non-uniform, locally boosted brane.

2.3.5 Sound mode and GL instability

The shear mode is the same as in the absence of charge. Sound modes have frequency

$$\omega_\pm=\pm ik\sqrt{1-\frac{q_p^2}{m^2}}-ik^2\,. \tag{2.78}$$

When $q_p<m$ the frequency ω_+ presents a GL instability for wavenumber k smaller than

$$k_{GL}=\sqrt{1-\frac{q_p^2}{m^2}}\,, \tag{2.79}$$

that is, if *e.g.,* a string has length $L<2\pi/k_{GL}$, in units where the horizon radius is $r_0=1$, then it is linearly stable.Note that $q_p=m$ is not an extremal limit, which instead corresponds to $\sqrt{N}\tilde{q}_p/\tilde{m}=1$. Since we are taking $\tilde{q}_p/\tilde{m}=\mathcal{O}(1/\sqrt{n})$ we are always far below this limit. That is, the regime we can access of $m<q_p\ll\sqrt{n}m$ is one of black branes with regular, non-extremal horizons, but stable ones.

Numerical evolution of the non-linear equations (2.71), (2.72) confirms that small perturbations of uniform black branes with $q_p<m$ grow and evolve until a static non-uniform solution is reached, while if $q_p>m$ the brane reverts back to the uniform state.

2.3.6 Static string solutions

The analysis of sec. 2.2.3 yields in this case the mechanics of a particle in the potential

$$U(\mathcal{P})=\mathcal{P}+\frac{m_0^2+q_p^2}{m_0}e^{-\mathcal{P}}-\frac{q_p^2}{2}e^{-2\mathcal{P}}\,, \tag{2.80}$$

with constant m_0. Now in order to have a minimum of the potential (where $e^{\mathcal{P}}=m_0$) we need $m_0>q_p$, which means that we are in the range where the uniform string

is unstable and tends to develop non-uniformities. In this case, the competition between the terms $+e^{-\mathcal{P}}$ and $-e^{-2\mathcal{P}}$ makes the oscillations of $\mathcal{P}$ take a longer time near its smallest values — that is, the neck of the non-uniform string, where it is thinner, becomes longer as q_p grows.

As in all subsequent chapters, the discussion of the conclusions of the preceding study are postponed until the final Conclusions in Chapter 8.

Chapter 3

Black strings at large D

In this chapter we use the large D formalism developed in Chapter 2 to analyze the thermodynamical properties of the different phases of neutral black strings at $D \geq 5$ and their stability. In this case, we do not restrict ourselves to the leading order in $1/D$ (as in equations (2.23) and (2.24)), but we go instead up to $1/D$. This allows us to extract the different behaviors of the string at different dimensions.

Quite surprisingly, this formalism gives good qualitative (and often quantitative) results even at low dimensions, and allows us to determine the critical dimension with remarkable accuracy. This chapter is based on the research published in [102].

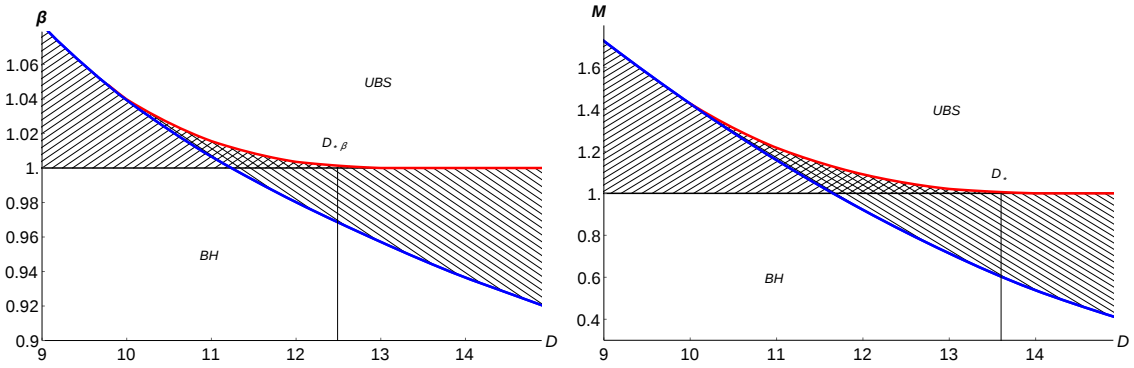

Figure 3.1: Range of existence (hatched) of non-uniform black strings in a compact circle of fixed length, as a function of the spacetime dimension D and the inverse temperature $\boldsymbol{\beta}$ or the mass $\mathbf{M}$ (results obtained numerically at 4NLO). The vertical axes are normalized relative to the value for a uniform black string at the threshold of the GL instability, so the lines $\boldsymbol{\beta}, \mathbf{M} = 1$ separate UBS into stable above the line, and unstable below the line. $D_* \simeq 13.6$ is Sorkin's critical dimension [29], which separates the dimensions in which weak non-uniformity makes $\mathbf{M}$ increase ($D < D_*$) or decrease ($D > D_*$). $D_{*\beta} \simeq 12.5$ plays a similar role for $\boldsymbol{\beta}$. The blue curve marks NUBS that reach zero tension, as a proxy to the transition to localized black holes (BH). The red curve indicates local maxima of $\boldsymbol{\beta}$ or $\mathbf{M}$, reached as the non-uniformity increases when $9 \lesssim D < D_{*\beta}, D_*$. The doubly-hatched region is a fold in phase space, where two NUBS phases coexist with the same $\boldsymbol{\beta}$ or the same $\mathbf{M}$, but differ in their entropies. For $D \lesssim 10$, NUBS branches terminate before any local maximum of $\boldsymbol{\beta}$ or $\mathbf{M}$ is reached. BH phases (not studied in this paper) coexist and can dominate thermodynamically over NUBS in regions of $\boldsymbol{\beta}, \mathbf{M} > 1$ at low D. The blue curves behave asymptotically at large D like $\boldsymbol{\beta} \sim D^{-1/4}$ and $\mathbf{M} \sim D^{-D/4}$.

Fig. 3.1 shows two diagrams for the expected range of existence of NUBS in a circle of fixed length, in the inverse temperature $\boldsymbol{\beta}$ (canonical ensemble) and in the mass $\mathbf{M}$ (microcanonical ensemble), as a function of the number of dimensions D. We normalize $\boldsymbol{\beta}$ and $\mathbf{M}$ relative to their values for a UBS at the threshold of the GL instability in the same circle. To get oriented, as the value of $\boldsymbol{\beta}$, or $\mathbf{M}$, decreases the UBS become thinner. UBS exist for all values of $\boldsymbol{\beta}$ and $\mathbf{M}$ in all $D \geq 5$, and are locally (GL) stable for $\boldsymbol{\beta}$, $\mathbf{M} > 1$ and unstable for $\boldsymbol{\beta}$, $\mathbf{M} < 1$.

In the diagram we include all NUBS phases, whether they are stable or not, either linearly, non-linearly, or thermodynamically. The blue line is a proxy for the transition of NUBS to localized black holes. This merger point is outside the applicability of the large-D approach to NUBS, so instead we estimate it as the point at which NUBS become so inhomogeneous that they develop negative tension. Therefore, the blue line should only be taken as a semiquantitative boundary. Up to this caveat, we expect Fig. 3.1 to capture qualitatively and quantitatively the properties of NUBS in dimensions around the critical value and higher. In particular, we expect that the asymptotic scaling that we find for the lower boundaries,

$$\boldsymbol{\beta}_{\rm min} \sim D^{-1/4}\,, \qquad \mathbf{M}_{\rm min} \sim D^{-D/4}\,, \tag{3.1}$$

is robust for very large D. In lower dimensions the quantitative accuracy worsens—hence we only extend the diagram down to $D \approx 9$—, but nevertheless the qualitative features do not seem to differ.

3.1 Thermodynamics of black strings

We expand the solution in the asymptotic region for $1 \ll \mathsf{R} \ll e^n$ [1]. We define functions $m(t,z)$ and $p(t,z)$ as the monopolar terms in A and C, *i.e.,*

$$\begin{aligned} A &= 1 - \frac{m(t,z) + \mathcal{O}\left(\ln \mathsf{R}/n\right)}{\mathsf{R}} + \mathcal{O}\left(\mathsf{R}^{-2}\right)\,, \\ C &= \frac{p(t,z) + \mathcal{O}\left(\ln \mathsf{R}/n\right)}{\mathsf{R}} + \mathcal{O}\left(\mathsf{R}^{-2}\right)\,. \end{aligned} \tag{3.2}$$

[1] The upper bound guarantees that the calculations remain within the large-n near-horizon zone [8]. The matching to the far-zone is explained in [14].

These are expanded in powers of $1/n$,

$$m(t,z) = \sum_{j=0}^{\infty} \frac{m_j(t,z)}{n^j}\,, \qquad p(t,z) = \sum_{j=0}^{\infty} \frac{p_j(t,z)}{n^j}\,. \tag{3.3}$$

It is now straightforward to compute the quasilocal stress-energy tensor in the asymptotic region,

$$T_{tt} = \frac{\Omega_{n+1}}{16\pi G}(n+1)\left(m(t,z) + \mathcal{O}\left(\frac{1}{n}\right)\right)\,, \tag{3.4}$$

$$T_{tz} = -\frac{\Omega_{n+1}}{16\pi G}\left(p(t,z) - \partial_z m(t,z) + \mathcal{O}\left(\frac{1}{n}\right)\right)\,, \tag{3.5}$$

$$T_{zz} = -\frac{\Omega_{n+1}}{16\pi G}\frac{1}{n}\left(m(t,z) - \frac{p^2(t,z)}{m(t,z)} + \partial_z p(t,z) - \partial_t m(t,z) + \mathcal{O}\left(\frac{1}{n}\right)\right)\,. \tag{3.6}$$

Note that the terms $\propto \ln \mathsf{R}/\mathsf{R}$ in the expansion (3.2) only contribute to the stress-energy tensor at order $1/n$ and higher.

For time-independent solutions we find convenient to define the mass density along the string (adequately rescaled to absorb n-dependent prefactors[2]),

$$\begin{aligned} M(z) &= -\frac{16\pi G}{(n+1)\Omega_{n+1}}\, T^t{}_t \\ &= m_0(z) + \mathcal{O}\left(\frac{1}{n}\right)\,, \end{aligned} \tag{3.7}$$

and the tension

$$\begin{aligned} \tau &= -\frac{16\pi G}{\Omega_{n+1}}\, T^z{}_z \\ &= m_0(z) - \frac{p_0^2(z)}{m_0(z)} + \partial_z p_0(z) + \mathcal{O}\left(\frac{1}{n}\right)\,. \end{aligned} \tag{3.8}$$

The tension τ is an intensive magnitude and in equilibrium configurations it must be uniform over the length of the string, *i.e.,* independent of z. This looks problematic, since τ in (3.8) does appear to depend on z. However, when there is no dependence on time eqs. (2.24) take the form

$$p_0(z) = m_0'(z)\,, \tag{3.9}$$

$$0 = \left(m_0''(z) + m_0(z) - \frac{(m_0'(z))^2}{m_0(z)}\right)'\,. \tag{3.10}$$

[2]Note that in M we factor out $(n+1)$, and not just n.

These imply that $\partial_z \tau = 0$. Indeed, this condition is also verified at higher orders in $1/n$. In our choice of units, for a UBS (of any length) the constant is $\tau = 1$ to all orders in $1/n$.

Note also that static solutions have zero momentum, $T_{tz} = 0$. This also happens, as expected, to all higher orders.

The horizon of the NUBS is at

$$\mathsf{R} = \mathsf{R}_h(z) = m_0(z) + \mathcal{O}\left(\frac{1}{n}\right) . \tag{3.11}$$

Bear in mind that the actual area-radius is

$$r_h = \mathsf{R}_h^{1/n} = 1 + \frac{\ln m_0}{n} + \mathcal{O}\left(n^{-2}\right) , \tag{3.12}$$

which shows that in the large-D approach the size of fluctuations of the horizon radius is $\mathcal{O}\left(1/n\right)$.

If $r_h(z)$ varies along the string between $r_h^{\min}$ and $r_h^{\max}$, a useful measure of the non-uniformity is [103]

$$\lambda = \frac{1}{2}\left(\frac{r_h^{\max}}{r_h^{\min}} - 1\right) . \tag{3.13}$$

Eq. (3.12) implies that $\lambda \sim 1/n$. Despite this limitation, in our study we will try to obtain large non-uniformities, approaching $O(1)$, by expanding to high orders in $1/n$.

We define a rescaled horizon entropy density, proportional to the area, as

$$\begin{aligned} S(z) &= \frac{\sqrt{n}}{\Omega_{n+1}} \mathrm{Area}(z, \mathsf{R}_h) \\ &= \sqrt{n G(z, \mathsf{R}_h)}\, \mathsf{R}_h^{\frac{n+1}{n}}(z) = m_0(z) + \mathcal{O}\left(\frac{1}{n}\right) . \end{aligned} \tag{3.14}$$

The densities $M(z)$ and $S(z)$ can be integrated over the length of the string L to obtain the total mass and entropy,

$$\mathbf{M} = \frac{L_{GL}^n}{L^{n+1}} \int_{-L/2}^{L/2} dz\, M(z) , \qquad \mathbf{S} = \frac{L_{GL}^{n+1}}{L^{n+2}} \int_{-L/2}^{L/2} dz\, S(z) , \tag{3.15}$$

where

$$L_{GL} = \frac{2\pi}{k_{GL}} \tag{3.16}$$

is the length of the uniform black string (of unit horizon radius) at the threshold of the GL instability. We have rescaled $\mathbf{M}$ and $\mathbf{S}$ by factors of $L^{-(n+1)}$ and $L^{-(n+2)}$, respectively, so as to render them invariant under changes of units. In other words, instead of having the units fixed by setting (as above) the horizon radius of the UBS equal to one, now the units are more sensibly set by the length of the compact circle L. In addition, we have introduced factors of powers of L_{GL} so that the non-uniform branches start out at $\mathbf{M}=1$, $\mathbf{S}=1$ at all n, since it is practical to normalize quantities so that their value for the UBS at the GL threshold is equal to one at all n.

A convenient measure of the tension that is invariant under changes of units is the so-called "relative binding energy" $\mathbf{n}$ (or tension per unit mass and length) introduced in [104, 105],

$$\mathbf{n}=\left(\frac{L_{GL}}{L}\right)^{n}\frac{\tau}{\mathbf{M}}\,. \tag{3.17}$$

Since the tension τ scales as (length)^n, the prefactor L^{-n} makes the relative binding energy $\mathbf{n}$ scale invariant, while L_{GL}^{n} normalizes it so that for the UBS at the GL threshold we have $\mathbf{n}=1$ at all n.

Finally, it is straightforward to compute the surface gravity at the horizon, κ, from which we define a rescaled surface gravity

$$\begin{aligned}\hat{\kappa}&=\frac{2}{n}\kappa\\&=1+\frac{1}{n}\left(\frac{1}{2}\left(\frac{m'(z)}{m(z)}\right)^{2}-\frac{m''(z)}{m(z)}-\ln m(z)\right)+\mathcal{O}\left(n^{-2}\right)\,.\end{aligned} \tag{3.18}$$

The zeroth law of black holes requires that when the static equations of motion are satisfied κ must be uniform over the length of the non-uniform black string. Since (3.8) and (3.18) satisfy

$$\partial_z\kappa=-\frac{1}{2m(z)}\partial_z\tau+\mathcal{O}\left(\frac{1}{n}\right) \tag{3.19}$$

and we have seen that $\partial_z\tau=0$ then the zeroth law is indeed verified at LO. It also holds at higher orders. For all UBS (of any length), the constant value is $\hat{\kappa}=1$ at all n.

The surface gravity is of course proportional to the temperature, and they both scale like an inverse length. We will find convenient to employ a scale-invariant

measure of the inverse temperature, which we take to be

$$\boldsymbol{\beta} = \frac{L_{GL}}{L}\,\hat{\kappa}^{-1}\,. \tag{3.20}$$

Again it is normalized so that $\boldsymbol{\beta} = 1$ for a UBS at the GL threshold.

Summarizing, the boldfaced quantities $\mathbf{M}$, $\mathbf{S}$, $\mathbf{n}$ and $\boldsymbol{\beta}$ are the mass, entropy, relative binding energy, and inverse temperature for the NUBS in a unit circle $z \sim z+1$, normalized relative to the values for the UBS at the GL threshold in that circle. Bearing in mind that the direction z has been rescaled by a factor $\sqrt{n}$, we recover the physical Mass, Entropy, Tension and Temperature of the NUBS on a circle of proper physical Length as

$$\textsc{Mass} = \mathbf{M}\,\frac{(n+1)\Omega_{n+1}}{16\pi G}\left(\frac{\sqrt{n}\,k_{GL}\,\textsc{Length}}{2\pi}\right)^{n}\textsc{Length}\,, \tag{3.21}$$

$$\textsc{Entropy} = \mathbf{S}\,\frac{\Omega_{n+1}}{4G}\left(\frac{\sqrt{n}\,k_{GL}\,\textsc{Length}}{2\pi}\right)^{n+1}\textsc{Length}\,, \tag{3.22}$$

$$\textsc{Tension} = \mathbf{n}\,\frac{\textsc{Mass}}{(n+1)\,\textsc{Length}}\,, \tag{3.23}$$

$$\textsc{Temperature} = \frac{\sqrt{n}}{2k_{GL}\,\textsc{Length}}\boldsymbol{\beta}^{-1}\,, \tag{3.24}$$

with k_{GL} given by (3.27). The non-uniformity parameter λ does not need any conversion to proper physical values.

3.2 Perturbative static solutions and static critical dimension

Our aim now is to construct non-linear NUBS solutions and study their thermodynamic and stability properties. In this section and in the next one we shall do this analytically in an expansion for small non-uniformity.

3.2.1 Perturbative NUBS

For now it is convenient to choose our length units so that the horizon is at $r = 1$ in the uniform black string solution—later we will set units differently. Now take this

solution, $m_0 = 1$, $p_0 = 0$, and perturb it slighty in the form

$$m_0 = 1 + \delta m\, e^{\Omega t + ikz}\,, \qquad p_0 = \delta p\, e^{\Omega t + ikz}\,. \tag{3.25}$$

Linearizing the equations (2.24) in δm and δp we obtain the spectrum

$$\Omega = \pm k(1 \mp k)\,. \tag{3.26}$$

We see that whenever $0 \leq |k| < 1$, the perturbation grows, $\Omega > 0$, so the black string is unstable. This is the Gregory-Laflamme instability in the large-D limit. The wavenumber $k_{GL} = 1$ corresponds to the threshold of the instability, where $\Omega = 0$. This critical wavenumber can be calculated to higher orders in $1/n$ using the effective equations. To 4NLO we find

$$k_{\rm GL} = 1 - \frac{1}{2n} + \frac{7}{8n^2} + \frac{-\frac{25}{16} + 2\zeta(3)}{n^3} + \frac{\frac{363}{128} - 5\zeta(3)}{n^4}\,. \tag{3.27}$$

This result was obtained earlier to NNLO using a linear perturbation analysis in [7], and then extended with similar methods to 4NLO in [106]. We extend now the linear perturbation analysis (3.25) of the static solution with $\Omega = 0$, $k = k_{GL}$, to higher non-linear order in the amplitude of the perturbation. To this effect, we expand the collective variables as Fourier series of the form

$$m(z) = 1 + \sum_{j=1}^{\infty} \mu_j(\epsilon)\epsilon^j \cos\left(jk(\epsilon)z\right), \qquad p(z) = \sum_{j=1}^{\infty} \nu_j(\epsilon)\epsilon^j \sin\left(jk(\epsilon)z\right)\,, \tag{3.28}$$

where we allow the length of the compact circle,

$$L(\epsilon) = \frac{2\pi}{k(\epsilon)}\,, \tag{3.29}$$

to vary with the non-uniformity perturbation parameter ϵ. This is necessary since, purely for calculational simplicity, we are arbitrarily fixing a length scale by setting the constant, z-independent Fourier mode in $m(z)$ to be 1 independently of ϵ. The boldfaced quantities in the previous section are insensitive to this choice.

At the lowest, linear order in ϵ, only the threshold static zero-mode, $j = 1$, is present. Then, at each higher order in ϵ a new higher harmonic enters with $j = 2, 3, \ldots$. At the same time, k is modified as ϵ grows, *i.e.,* the periodicity is

corrected. Therefore ϵ can be regarded as a mode-counting parameter. Bear in mind that besides the ϵ expansion, the functions m and p are also expanded in $1/n$. The calculations simplify slightly if we define ϵ so that

$$\mu_1 = 1 \tag{3.30}$$

for all values of n.

In order to illustrate the construction we solve the first few orders in the ϵ expansion for static solutions to leading order in $1/n$. Plugging the ansatz (3.28) in (3.10)[3] and successively solving the equations up to order ϵ^3 we obtain

$$\mu_2 = \frac{1}{6} + \mathcal{O}\left(\epsilon^2\right) , \qquad \mu_3 = \frac{1}{96} + \mathcal{O}\left(\epsilon^2\right) , \tag{3.31}$$

$$k = 1 - \frac{\epsilon^2}{24} + \mathcal{O}\left(\epsilon^4\right) . \tag{3.32}$$

Thus we obtain a static non-uniform black string solution with

$$m_0(z) = 1 + \epsilon \cos kz + \frac{\epsilon^2}{6}\cos 2kz + \frac{\epsilon^3}{96}\cos 3kz + \mathcal{O}\left(\epsilon^4\right) , \tag{3.33}$$

$$p_0(z) = -\epsilon\left(1 - \frac{\epsilon^2}{24}\right)\sin kz - \frac{\epsilon^2}{3}\sin 2kz - \frac{\epsilon^3}{32}\sin 3kz + \mathcal{O}\left(\epsilon^4\right) . \tag{3.34}$$

It is straightforward to extend these calculations to higher orders in ϵ. At the same time, using the higher order equations we can also include corrections in $1/n$. [4]

For solutions to leading order in $1/n$ we can immediately obtain the mass and entropy as[5]

$$\mathbf{M} = \mathbf{S} = 1 - \frac{n\epsilon^2}{24} + \mathcal{O}\left(\epsilon^4\right) , \tag{3.35}$$

[3]The second equation admits an obvious first integral, but this is not of much help for solving perturbatively the equations since the integration constant—the tension τ—is ϵ-dependent.

[4]We have found evidence that the power series in ϵ may have finite convergence radius. The ratio between successive values of the coefficients μ_i appears to be close to $1/2$, which would imply that the applicability of the expansion is limited to $\epsilon < \sqrt{2}$.

[5]Note that this expansion seems to require $\epsilon^2 \ll 1/n$, which originates in the factors $\sim (L_{GL}/L)^n$ in (3.15). This is not problematic, but instead we could equally well work with, *e.g.,* the mass-length $\mathbf{M}^{1/(n+1)}$ and entropy-length $\mathbf{S}^{1/(n+2)}$, which are equal to $1 - \epsilon^2/24 + \ldots$ and only require $\epsilon \ll 1$.

and the tension as

$$\tau = 1 - \frac{\epsilon^2}{2} + \mathcal{O}\left(\epsilon^4\right) . \tag{3.36}$$

With our choice of units, the rescaled surface gravity (3.18) is $\hat{\kappa} = 1$ to leading order in $1/n$ independently of the deformation.

The parameter ϵ is not a very physical measure of the non-uniformity. Instead we can employ λ in (3.13), which for our solution above is

$$\lambda = \frac{1}{2}\left(\left(\frac{m_0(0)}{m_0(\pi/k)}\right)^{1/n} - 1\right) = \frac{1}{n}\left(\epsilon + \frac{17}{92}\epsilon^3 + \mathcal{O}\left(\epsilon^4\right)\right) . \tag{3.37}$$

The results (3.35), (3.36), (3.37) completely characterize weakly non-uniform black strings to leading order at large-n. At this order the mass and entropy of a given NUBS are exactly equal, the temperature is independent of the deformation, and therefore the thermodynamics of NUBS is rather uninformative. However, the inclusion of $1/n$ corrections yields much more interesting results.

3.2.2 Static critical dimensions

With our definitions, a UBS with $\mathbf{M} = 1$ is at the threshold of the GL instability, while a UBS with $\mathbf{M} < 1$ is unstable, and one with $\mathbf{M} > 1$ is stable. Eq. (3.35) says that, to leading order at large n, weakly-non-uniform strings have $\mathbf{M} < 1$. Therefore, at sufficiently large n, for every weakly-unstable UBS there exists, nearby in solution space, a NUBS of the same mass. It is then possible that the UBS continuously evolves into a NUBS, in a smooth, second order transition between phases.

Finite n effects can modify this behavior. Including the NLO terms the mass of a weakly-NUBS is

$$\mathbf{M} = 1 - (n-8)\frac{\epsilon^2}{24} + \mathcal{O}\left(\epsilon^4\right) . \tag{3.38}$$

Therefore, if $n < n_* = 8$, *i.e.*, $D < D_* = 12$, the mass is larger than 1: nearby a weakly-unstable UBS there is no NUBS of the same mass that it could continuously evolve into, neither by fluctuating in the microcanonical ensemble, nor through dynamical evolution in which (by axial symmetry) no energy is radiated. The UBS must then transit in a non-smooth, first order manner to another phase further separated in solution space. We illustrate the two situations in Fig. 3.2.

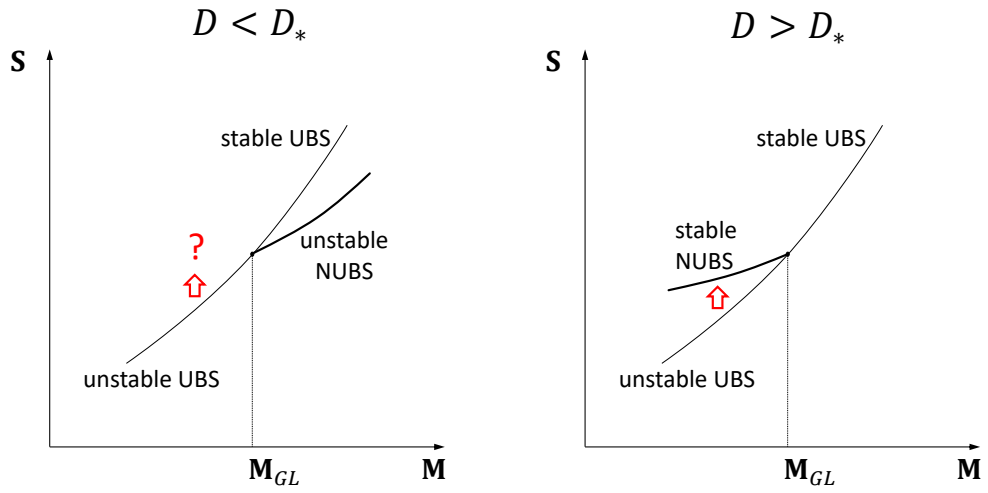

Figure 3.2: Eq. (3.38), and more accurately (3.39), shows that for $D < D_*$ there are no weakly non-uniform black strings with mass $\mathbf{M} < \mathbf{M}_{GL} = 1$ in the range of unstable uniform black strings, so the latter cannot evolve smoothly into any of the former (the transition is then of first order into a phase further away, possibly other NUBS or BH). For $D > D_*$ the mass correction is reversed, and there do exist NUBS with $\mathbf{M} < \mathbf{M}_{GL}$ that unstable UBS can smoothly evolve into. The calculation of the entropy in (3.43) shows that in $D > D_*$ this transition is consistent with the entropy law. Moreover, the analysis of sec. 3.3 explicitly shows that weakly NUBS are dynamically linearly stable when $D > D_*$, and unstable when $D < D_*$.

The value for the critical dimension can be improved by considering higher orders in $1/n$. For NUBS through 3NLO we obtain

$$\mathbf{M} = 1 - \frac{n\epsilon^2}{24}\left(1 - \frac{8}{n} - \frac{14}{n^2} + \frac{6 - 20\zeta(3)}{n^3}\right) + \mathcal{O}\left(\epsilon^4\right) . \tag{3.39}$$

Then, the change between $\mathbf{M}$ being smaller or larger than 1 at small non-uniformity occurs for

$$n_* = 9.65\,, \tag{3.40}$$

so that the smooth, continuous classical evolution of an unstable uniform black string to a weakly non-uniform one is only possible above the critical dimension

$$D_* = 13.65\,. \tag{3.41}$$

This agrees with remarkable accuracy with the numerical value $D_* \simeq 13.5$ obtained in [29].[6] In the large-n expansion it had been obtained earlier in [14] (in a slightly different calculation to NNLO).

We must verify that the black hole entropy law allows to transit from the weakly-unstable UBS to a nearby NUBS of the same mass in $D > D_*$. This calculation requires a higher order perturbation: the first law of black holes implies that, for equal masses, the entropies of the UBS and the nearby NUBS are equal to order ϵ^2 (in any D) [103][7]. Moreover, to leading order in $1/n$ the entropy of all the solutions is the same as their mass [15]. Therefore, in order to see the difference in the entropies we need the corrections at least at order ϵ^4/n. Furthermore, revealing the reversal in the difference in entropies at the critical dimension requires at least one higher order in $1/n$.

Bearing in mind that the entropy $\mathbf{S}$ of a UBS (not at the GL threshold!) with mass $\mathbf{M}$ is

$$\mathbf{S}_{\rm UBS} = \mathbf{M}^{\frac{n+1}{n}} \,, \tag{3.42}$$

we find that the relative entropy difference between NUBS and UBS of the same mass is

$$\begin{aligned} \frac{\Delta \mathbf{S}}{\mathbf{S}} &= \frac{\mathbf{S}}{\mathbf{S}_{\rm UBS}} - 1 \\ &= \left(1 - \frac{7}{n} - \frac{22}{n^2} - \frac{8(1+2\zeta(3))}{n^3}\right) \frac{\epsilon^4}{96n} + \mathcal{O}\left(\epsilon^5\right) \,. \end{aligned} \tag{3.43}$$

This changes sign at the critical dimension $n_* = 9.59$, *i.e.,*

$$D_* = 13.59 \,, \tag{3.44}$$

in good agreement with (3.41) to 3NLO accuracy. In fact, since it can be proven [29, 103] that the first law of black holes implies (for any n) that

$$\frac{\Delta \mathbf{S}}{\mathbf{S}} = \frac{n+1}{2n} \delta\mathbf{M} \left(\delta\boldsymbol{\beta} - \frac{1}{n}\delta\mathbf{M}\right) \,, \tag{3.45}$$

[6] Already the leading order result $n_* = 8$ provides a surprisingly good approximation. However, its calculation involves equating the LO and NLO in (3.39), which, strictly speaking, is not legitimate within perturbation theory. Nevertheless, these results for n_* (and others closely related to it, as we will see) seem to stand up because the coefficient of the term $1/n$ gives a value quite larger than the correction from the term $1/n^2$, *i.e.,* because $8 \gg 14/8$, and similarly at the next order. At present, all we can say is that this is a fortunate feature of the large-n expansion.

[7] More precisely, the leading-order variations satisfy $\delta\mathbf{S} = \frac{n+1}{n}\delta\mathbf{M}$.

where $\delta\boldsymbol{\beta}$ and $\delta\mathbf{M}$ are first-order variations (*i.e.,* here the corrections to $\mathcal{O}(\epsilon^2)$), then we see that D_* must be the same whether we obtain it from $\delta\mathbf{M} = 0$ or from $\Delta\mathbf{S}/\mathbf{S} = 0$. Note, however, that the sign of the entropy difference is not determined by this equation.

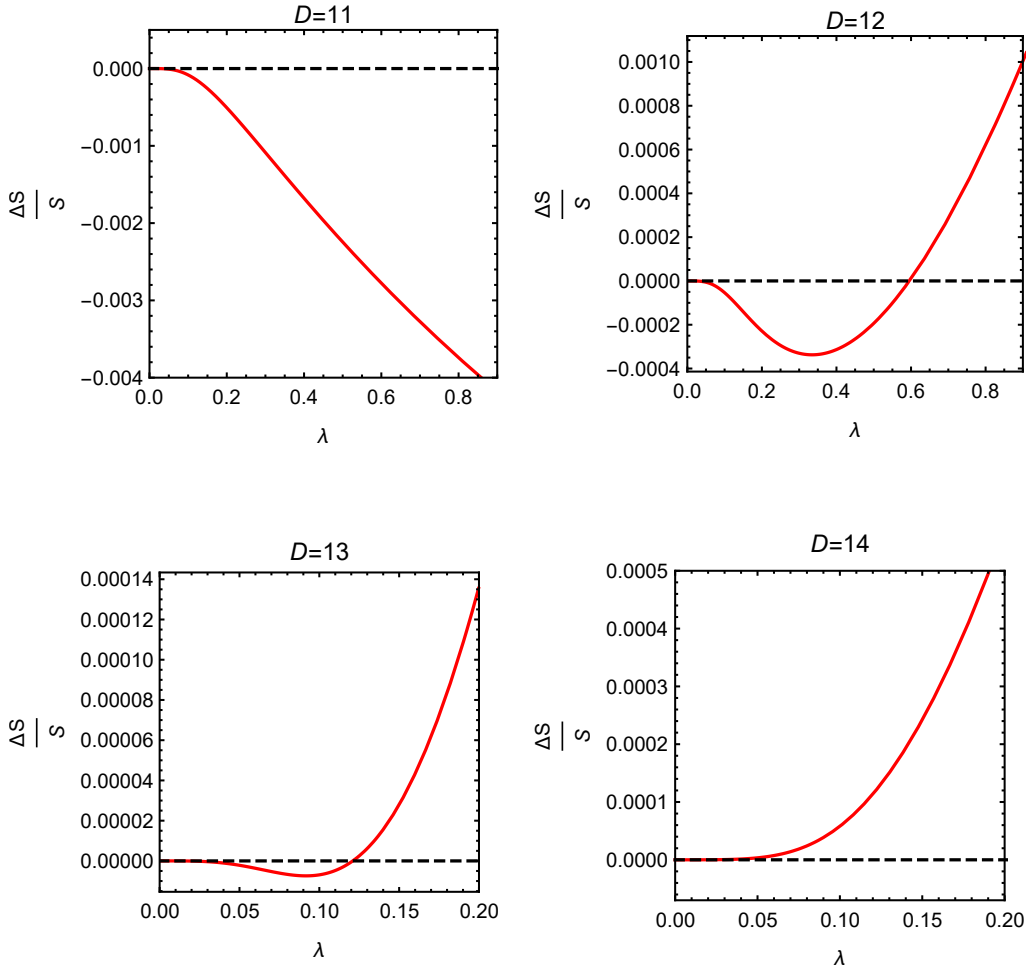

Figure 3.3: Entropy difference (3.43) between NUBS and UBS of the same mass as a function of non-uniformity λ (3.13). The NUBS in $D = 12, 13 < D_*$ with $\Delta\mathbf{S} > 0$ are thermodynamically stable even if they are below the critical dimension [23].

Thus the large-D expansion reproduces correctly all aspects of Sorkin's thermodynamic argument, including the precise value of D_*. As we will see in sec. 3.3.2,

the large-D expansion also allows to directly establish that the smooth evolution of unstable UBS to stable NUBS is *dynamically possible* above the critical dimension D_*.

We can further verify the presence of thermodynamically stable NUBS in $D = 11,\ 12$, which are below the critical dimension, as found in [23]. To this effect, in Fig. 3.3 we plot the entropy difference as a function of the deformation parameter λ. We observe that in $D = 12, 13 < D_*$, there appear NUBS at finite deformation with positive entropy difference. The resemblance to Fig. 7 of [23] (even fairly quantitatively) is remarkable.

3.2.3 Critical dimension for temperature

The value we obtain for the inverse temperature

$$\boldsymbol{\beta} = 1 - \frac{\epsilon^2}{24}\left(1 - \frac{8}{n} - \frac{2}{n^2} - \frac{20\zeta(3) - 6}{n^3}\right) + \mathcal{O}\left(\epsilon^4, n^{-4}\right) \tag{3.46}$$

is indeed such that (3.39), (3.43), (3.46) do satisfy (3.45).

Observe that there is a critical dimension

$$n_{*\beta} = 8.49 \quad i.e., \quad D_{*\beta} = 12.49 \tag{3.47}$$

at which the first order variation $\delta\boldsymbol{\beta}$ vanishes. If $D < D_{*\beta}$ then $\boldsymbol{\beta}$ increases as the non-uniformity appears, and it decreases if $D > D_{*\beta}$.

Notice that $D_{*\beta}$ is different than D_*, as required by (3.45). The numerical constructions of [23] exhibit the same change in the behavior of $\boldsymbol{\beta}$ between $D = 12$ and $D = 13$ (see their Fig. 4).

3.2.4 4NLO corrections and non-convergence of the $1/n$ expansion

Ref. [106] argued that the large-n expansion is not convergent, but only asymptotic. Non-perturbative effects that couple the near-horizon region to the far region turn out to limit the reliability of the perturbative expansion. The size of these effects is $\sim n^{-n/2}$, so they become comparable to perturbative corrections $1/n^k$ at order $k \sim n/2$. Therefore, when calculating the critical dimension $n_* \simeq 9$, we may expect

that terms from $1/n^4$ or $1/n^5$, *i.e.,* 4NLO or 5NLO corrections, begin to show poorer convergence.

We have found evidence of this. We have managed to extend our results for weakly-non-uniform black strings up to 4NLO, which adds to (3.39) the term

$$\delta^{(4)}\mathbf{M} = \frac{\epsilon^2}{18n^3}\left(21 + 2\pi^4 + 30\zeta(3)\right) . \tag{3.48}$$

Then the critical dimension for $\mathbf{M}$ is determined by requiring that

$$n_* = 8\left(1 + \frac{1.75}{n_*} + \frac{2.26}{n_*^2} + \frac{42.0}{n_*^3}\right) . \tag{3.49}$$

The coefficient of the last term is unusually large, with the effect that it corrects n_* by a larger amount than the previous term. More explicitly, at each successive order we get

$$n_* = 8 \;/\; 9.48 \;/\; 9.65 \;/\; 9.93\,, \tag{3.50}$$

which signals a loss of convergence in the last correction. The latter, then, should not be trusted.

The same breakdown of the expansion is observed, at the same order, in the calculation of $n_{*\beta}$. At 4NLO we get

$$\delta^{(4)}\boldsymbol{\beta} = -\frac{24}{n}\delta^{(4)}\mathbf{M}\,, \tag{3.51}$$

which yields

$$n_{*\beta} = 8 \;/\; 8.24 \;/\; 8.49 \;/\; 8.92\,. \tag{3.52}$$

Again, we deem the last value unreliable.

These results may be taken as suggesting that it would not be useful to try to obtain higher orders in the expansion. However, bear in mind that this can depend on the specific quantity that is computed. For instance, it was shown in [106] that while the 4NLO corrections do not uniformly improve the values for the quasinormal frequencies of UBS, they nevertheless yield the best approximation to k_{GL} even down to $D = 6$, where the accuracy is within 2.4%. We will find in sec. 3.4.1 that 4NLO results also give excellent agreement for $\mathbf{M}$ and $\mathbf{S}$ above but also below the critical dimension. Perhaps in these cases one needs to go to 5NLO to find evidence of non-convergence in these dimensions—our readers are invited to try their hand at such calculations.

3.3 Stability of NUBS and dynamical critical dimension

As far as we are aware, no dynamical study of the stability of non-uniform black strings has been performed yet in any finite number of dimensions.[8] The large-D expansion simplifies the task enormously, even allowing analytical investigation.

3.3.1 Quasinormal modes of NUBS

Let us consider a static solution $m_s(z)$, $p_s(z)$. We perturb it by adding time-dependent terms

$$m(t,z) = m_s(z) + e^{\Omega t}\delta m(z), \qquad p(t,z) = p_s(z) + e^{\Omega t}\delta p(z), \tag{3.53}$$

and expand the equations to linear order in δm and δp. If the initial solution is periodic over an interval of length $2\pi/k$, then the perturbation admits an expansion as Fourier series[9]

$$\begin{aligned} \delta m(z) &= \sum_{j=1}^{\infty} \delta m_j^{(+)} \cos(jkz) + \delta m_j^{(-)} \sin(jkz), \\ \delta p(z) &= \sum_{j=1}^{\infty} \delta p_j^{(+)} \sin(jkz) + \delta p_j^{(-)} \cos(jkz). \end{aligned} \tag{3.54}$$

We consider static solutions that have the symmetry $m_s(z) = m_s(-z)$, $p_s(z) = -p_s(-z)$, and then the spectrum can be split into even $(+)$ and odd $(-)$ modes.

Observe that Ω has dimensions of inverse length, so if we want to measure it, as we are doing for all other quantities, in units of the length L, then we must use the scale-invariant frequency

$$\mathbf{\Omega} = \frac{L}{L_{GL}}\Omega\,, \tag{3.55}$$

and the corresponding physical frequency will be

$$\textsc{Omega} = \frac{\mathbf{\Omega}}{\sqrt{n}\,k_{GL}\textsc{Length}}\,. \tag{3.56}$$

[8] The closest is the study in [23] using local Penrose inequalities.

[9] We exclude $j = 0$ since these are exact zero modes that can be absorbed in uniform rescalings and boosts.

When we take the static solution to be perturbative in ϵ and in $1/n$, the coefficients of the time-dependent fluctuation, $\delta m_j^{(\pm)}$ and $\delta p_j^{(\pm)}$, will also be power series of ϵ and $1/n$. At the lowest order in both expansions we are perturbing the uniform black string with $k = 1 + \mathcal{O}(\epsilon, 1/n)$. It is clear from our earlier result (3.26) that the modes with wavenumber $jk = j + \mathcal{O}(\epsilon, 1/n)$ have

$$\mathbf{\Omega} = -j(j \pm 1) + \mathcal{O}(\epsilon, 1/n) \ . \tag{3.57}$$

Therefore perturbation modes of a weakly-NUBS (small ϵ) with $j > 1$ will have $\Omega < 0$ and so these perturbations are stable. This was of course expected, since these 'overtones' all have wavelengths shorter than the 'fundamental' threshold mode $j = 1$. While it would be possible to compute corrections in ϵ and in $1/n$ to this result, there appears to be little motivation for it.

It then remains to study perturbations that are dominated by fundamental normal modes with $j = 1$, which, at small ϵ, lie near the stability threshold with $\mathbf{\Omega} = \mathcal{O}(\epsilon)$. It suffices to focus on even modes (odd ones are simply a translation of them), *i.e.*, $\delta m(z) = \cos kz + \mathcal{O}(\epsilon, 1/n)$, $\delta p(z) = -\sin kz + \mathcal{O}(\epsilon, 1/n)$.

We begin working at leading order in $1/n$, and perturb the static solution we found in section 3.2, with $m_s(z)$ and $p_s(z)$ given by (3.33) and (3.34), and k by (3.32). Solving for the coefficients $\delta m_j^{(\pm)}$, $\delta p_j^{(\pm)}$ perturbatively in ϵ up to cubic order we obtain

$$\delta m(z) = \cos kz + \epsilon \frac{1}{3} \cos 2kz + \epsilon^2 \frac{1}{32} \cos 3kz + \mathcal{O}\left(\epsilon^3\right) \ , \tag{3.58}$$

$$\delta p(z) = -\left(1 - \frac{\epsilon^2}{8}\right) \sin kz - \epsilon \frac{2}{3} \sin 2kz - \epsilon^2 \frac{3}{32} \sin 3kz + \mathcal{O}\left(\epsilon^3\right) \tag{3.59}$$

with

$$\mathbf{\Omega} = -\frac{\epsilon^2}{12} + \mathcal{O}\left(\epsilon^3\right) \ . \tag{3.60}$$

Since $\mathbf{\Omega} < 0$, we conclude that, to this order in small ϵ, and to leading order for $n \to \infty$, weakly non-uniform black strings are stable. This LO calculation can be readily carried over to two higher orders in ϵ, where we find

$$\mathbf{\Omega}(\epsilon) = -\frac{\epsilon^2}{12}\left(1 + \frac{7\epsilon^2}{16} + \frac{75497\epsilon^4}{414720}\right) + \mathcal{O}\left(\epsilon^8\right) , \tag{3.61}$$

so $\mathbf{\Omega}(\epsilon) < 0$ persists to this order. This analytical argument for the stability of NUBS when $D \to \infty$ is in perfect agreement with their numerically observed stability under dynamical evolution of the LO equations (2.24) [15].

3.3.2 Dynamical critical dimension

It becomes even more interesting when we add the first correction for finite n. In this case we obtain

$$\mathbf{\Omega} = -\frac{\epsilon^2}{12}\left(1-\frac{10}{n}\right)+\mathcal{O}\left(\epsilon^4\right)\,. \tag{3.62}$$

Here we see the appearance of a "dynamical critical dimension", $n_* = 10$, *i.e.*, $D_* = 14$, such that for $n < n_*$ weakly non-uniform black strings are dynamically unstable, while for $n > n_*$ they are stable.

This critical dimension is very close to the one we found from the thermodynamical analysis. The agreement improves with the 3NLO result

$$\mathbf{\Omega} = -\frac{\epsilon^2}{12}\left(1-\frac{10}{n}+\frac{6-2\zeta(2)}{n^2}-\frac{6-4\pi^2+20\zeta(3)}{n^3}\right)+\mathcal{O}\left(\epsilon^4\right), \tag{3.63}$$

so the critical value where $\mathbf{\Omega}$ changes sign is corrected to

$$n_* = 9.62\,, \tag{3.64}$$

i.e.,

$$D_* = 13.62\,. \tag{3.65}$$

Now this is the same result (well within the expected accuracy) as obtained in (3.41) and (3.44) from the thermodynamics of the phase space of *static* solutions. Going one order higher the expansion appears not to converge, but this might be expected from our discussion in sec. 3.2.4.[10]

The connection between the thermodynamic critical dimension of NUBS and the change in their dynamical quasinormal stability was expected on general grounds, but so far it had not been verified explicitly. The $1/D$ expansion has allowed us to establish it with excellent accuracy.

3.3.3 Quasinormal stability of NUBS and Poincaré turning points

We have extended the calculation of the lowest quasinormal frequencies of NUBS to higher orders in the non-uniformity. The most salient aspect of the result is to

[10] At 4NLO we find $\delta^{(4)}\mathbf{\Omega} = \epsilon^2(8+5\pi^2+49\pi^4/45)/(6n^4)$, which would yield $n_* = 9.96$.

show that large enough non-uniformity can change the stability of NUBS in some dimensions below the critical value.

In order to illustrate this phenomenon, let us keep only the next-to-leading-order terms in both ϵ and in $1/n$, and write them as

$$\mathbf{\Omega}(\epsilon) = -\frac{\epsilon^2}{12}\left(1+\frac{7\epsilon^2}{16}\right)\left(1-\frac{10}{n}\left(1-\frac{3\epsilon^2}{20}\right)\right) . \tag{3.66}$$

To leading order in the non-uniformity this is the same as (3.62), which showed that NUBS in $n < n_* = 10$ are unstable. However, when the next non-uniformity order, ϵ^4, is included, the instability gets weaker. More precisely, a NUBS with $\epsilon = \epsilon_0$, where

$$\epsilon_0 = \sqrt{\frac{2\,(n_*-n)}{3}} \simeq 0.82\sqrt{n_*-n}\,, \tag{3.67}$$

has a zero mode instead of a negative mode, and a NUBS with $\epsilon > \epsilon_0$ would be dynamically linearly stable even if it is below the critical dimension.

This finding ties in very well with the presence of a turning point at finite non-uniformity in the mass of NUBS in $n < n_*$.[11] To see the relation clearly, let us write the derivative of the mass with respect to non-uniformity as

$$\frac{\partial \mathbf{M}}{\partial \epsilon^2} = -\frac{n\mathbf{M}}{24}\left(1+\frac{83}{144}\epsilon^2\right)\left(1-\frac{8}{n}\left(1-\frac{23}{72}\epsilon^2\right)\right) . \tag{3.68}$$

The last term in brackets reveals that, below the (at this order, in this case) critical dimension $n_* = 8$, the mass reaches a turning point when the non-uniformity is $\epsilon = \epsilon_{tp}$, with

$$\epsilon_{tp} = \sqrt{\frac{9\,(n_*-n)}{23}} \simeq 0.63\sqrt{n_*-n}\,. \tag{3.69}$$

This result is very close to ϵ_0. Indeed, the two results are expected to coincide: Poincaré's turning-point method says that a solution at a turning point in phase space must have one zero mode (for at least one kind of perturbation). Although ϵ_0 and ϵ_{tp} are not exactly the same, they are sufficiently close, within the approximations we have made, to validate the conclusion that they conform to this argument.[12]

[11] This is related to, but not the same as the existence of stable NUBS below the critical dimension, discussed in [23] and in sec. 3.4.1.

[12] In order to make this agreement more precise we would need better accuracy in the non-uniformity than we have obtained, even more so if we are interested in turning points at integer

So, once again, we see that the large D expansion is an efficient means of establishing the links between local thermodynamical stability and linear dynamical stability that exist in this system.

3.4 Highly non-uniform black strings

In addition to the analytic expansions for small non-uniformity, we have explored numerically larger non-uniformity in strongly non-linear regimes. We have done this by finding highly deformed static NUBS, and by time evolution of UBS deep into a non-linear regime.

The effective large-D equations can be written and solved in two different ways. The first one is as a *sequential* set of $j+1$ equations, one equation for each term $m_j(t,z)$ of the pertubative expansion of $m(t,z)$, (3.3). The equation for $m_j(t,z)$ involves the solutions at lower orders, $m_i(t,z)$, $i=0,\ldots,j-1$.[13] Crucially, n does not appear anywhere in these equations: it only enters, as a free parameter, when we recombine the solutions $m_j(t,z)$ into a finite series in $1/D$ to recover the solution $m(t,z)$ up to jNLO. Thus, in this approach n remains a continuous, analytically tractable parameter, not only in the equations but also in the solutions.

The second approach consists of solving an *inclusive* equation for the total variable $m(t,z)$, (3.3), which includes at once all the corrections up to a given order. That is, to any order in the $1/n$ expansion we solve only one equation for $m(t,z)$, instead of $j+1$ equations for $m_j(t,z)$ in the sequential approach. The price to pay is that this single equation now involves n explicitly and therefore, if we want to integrate it numerically, we must assign a specific value to n. That is, in contrast to the sequential approach, the integration yields a solution for a specific value of n, and so we must solve the whole equation anew to obtain the solution for another value of n.

Both approaches should yield compatible results within a given order of the ex-

values of $n<n_*$, which lie far from the GL point. Calculations to higher non-uniformity than in (3.43) would also be needed to verify that around the turning point the solution with $\mathbf{\Omega}<0$ has larger entropy than the solution with the same mass and $\mathbf{\Omega}>0$, as required by Poincaré's method.

[13] If the equations were linear, the lower order solutions would yield sources for $m_j(t,z)$. Here the equations are non-linear, so $m_{i<j}(t,z)$ also appear as coefficients.

pansion, but we have found each one preferrable for a different problem.

The sequential approach can easily be applied to the solution of the ODEs of the static system, and this allows to efficiently scan the phase space of static solutions, including the unstable phases that would not be visible in a dynamical evolution. Once we obtain solutions for $m_0(z)$, $m_1(z)$, $m_2(z)$, $m_3(z)$ and $m_4(z)$, the complete solution $m(z)$ is known to 4NLO for any value of n. The dimensionality of the space of parameters that one needs to scan numerically is then reduced by one. This approach has the drawback that for some values of n the solutions are unphysical (for instance, with negative mass density or tension) and we must identify and remove them out of the space of static solutions.

The inclusive approach is more useful for the time evolution of the effective equations. We studied the endpoint of the dynamic evolution starting from a slightly perturbed unstable black string. We are able to verify stability beyond the linear analysis, but we find an apparent instability in a regime where the NUBS should presumably be stable, according to the static results. Already at NLO, there is a D-dependent limiting thickness, $\mathbf{M}_{\rm lim}(D)$, where the string becomes too inhomogeneous and the numerical code breaks down. This indicates the point at which the non-uniformity of the black string becomes so large that the effective equations of the $1/D$ expansion cease to be reliable. There is no true (finite-D) physics that corresponds to the phenomena that we observe there. Surprisingly, there seems to be a scaling behavior in the non-uniformity for the large-D breakdown, as $\mathbf{M}_{\rm lim}(D) \sim D^{-D/4}$, similar to the one encountered for the merger point.

To solve the equations we decomposed the functions $m_j(z)$ as (truncated) Fourier series. The Fourier coefficients were then fitted by a Levenberg-Marquardt algorithm in order to satisfy the effective equations. Additionally, the same results were computed independently up to NLO using a Chebyshev grid, and a Newton-Raphson relaxation.

3.4.1 Thermodynamic properties of NUBS branches

In our computations of static NUBS using the sequential approach we have chosen to terminate the branches, in each dimension, when the NUBS reach zero tension. Although this is an estimate and not an accurate determination of the actual merger

transition to the BH phase, we will see that it is remarkably close to the endpoints of the branches obtained through full-numerical solution of the Einstein equations.

In [14] an analytical approximation to the profile of zero-tension solutions was made. Their shape was found to be fairly close to what one would expect for a BH. The NNLO horizon position in this case is

$$\mathsf{R}_h(z) \sim e^{-z^2/2}\left(1-\frac{z^4}{n}+\frac{3z^8-16}{96n^2}\right)\,, \tag{3.70}$$

which indicates that when the BH fills up the length of the compact circle, this length will scale as $L \sim \Delta z \sim n^{1/4}$. From this one can readily estimate that the (static) merger transition between NUBS and BH occurs for values that scale as

$$\mathbf{M}^{1/(n+1)},\, \boldsymbol{\beta} \sim n^{-1/4}\,, \tag{3.71}$$

since both these quantities are defined to be inversely proportional to L (see (3.15) and (3.20)).

Our numerical results clearly confirm this scaling behavior, exhibiting its onset already at dimensions as low as $n \approx 8$, *i.e.,* $D \approx 12$, see Fig. 3.4. We denote the zero-tension values of the NUBS mass as

$$\mathbf{M} = \mathbf{M}_{\rm min}(D) \sim D^{-D/4}\,. \tag{3.72}$$

These are the curves shown in blue in figs. 3.1 and 3.4.

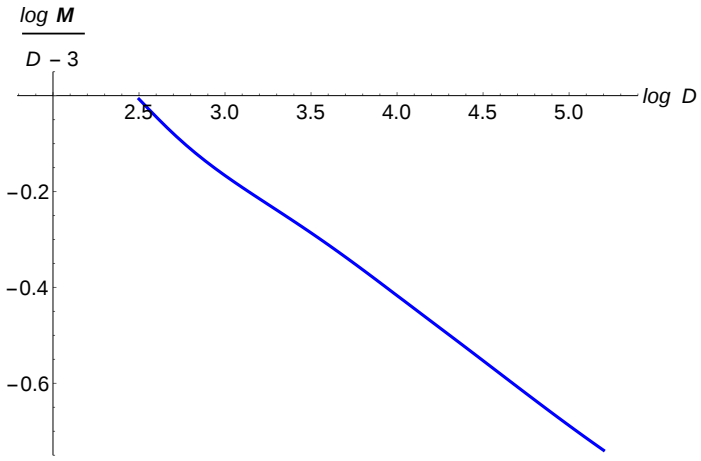

Figure 3.4: Scaling behavior of the zero-tension curve $\mathbf{M}_{\rm min}(D)$ that we take as a proxy for the merger transition between static NUBS and BH phases. The curve (obtained at 4NLO) falls off as $D^{-1/4}$, in excellent agreement with the analytical estimate (3.71).

The following figures 3.5, 3.6, 3.7, 3.8, show our numerically computed branches of NUBS that are extended until they reach zero tension. We also present the results of our analytical calculations in the expansion in ϵ which, as we could expect, are accurate only as long we do not depart too far from the beginning of the branch. Furthermore, we include a comparison with the results obtained in [23] in $D = 13$ and $D = 14$ (just below and above D_*) through full numerical solution of the Einstein equations.

Figs. 3.5 and 3.6 show the total mass and entropy of NUBS as functions of the inverse temperature. We are not presenting diagrams of $\mathbf{S}$ vs. $\mathbf{M}$ since (as is indeed apparent by comparing these diagrams) the difference between them is very small and the curves for NUBS are too close to the curves for UBS to give a useful image.

The figures show that our 4NLO results for the mass and entropy provide an excellent match to the calculations in [23]. We emphasize that there is no free parameter in this comparison. The quantitative agreement is remarkable not only at the GL point but also further along the branches. This is strong evidence that the large-D expansion, with higher order corrections included, can work well even for inhomogeneities of order one despite its apparent limitation to inhomogeneities $\sim 1/D$. We are particularly surprised by how well the zero-tension condition for the

termination of the branches appears to agree with the limits found in [23]. This is presumably due to the fact, already observed in [14], that the zero-tension solution (3.70) appears to capture well the geometry near the equator of a BH (but not near the axis where $\mathsf{R}_h \to 0$). Then the solution (3.70) reproduces correctly the mass and area of the BH since at large-D these quantities are dominated by their values near the equatorial bulge.

The curves for the relative binding energy $\mathbf{n}$ in Fig. 3.7 reproduce the main qualitative features previously found for NUBS. However, they end at $\mathbf{n} = 0$ (zero tension) while the actual curves for NUBS branches terminate at positive, non-zero tension, where, at least in $D = 5, 6$, they merge with black hole phases in a spiralling way [21, 24, 25]. These spirals are a feature controlled by the critical self-similar solution at the static merger transition [107], which does not seem to be captured by the large-D effective equations for black strings. It may be visible, though, in large-D studies aimed closer to the self-similar solution.

Overall, these diagrams exhibit the main qualitative features of the NUBS branches of static solutions, both above and below the critical dimension $D_* = 13.6$. The quantitative accuracy is excellent at $D = 13$ and higher, but worsens as D gets smaller. Nevertheless, the position of the GL point in all these diagrams is excellently reproduced even down to $D = 6$ [106].

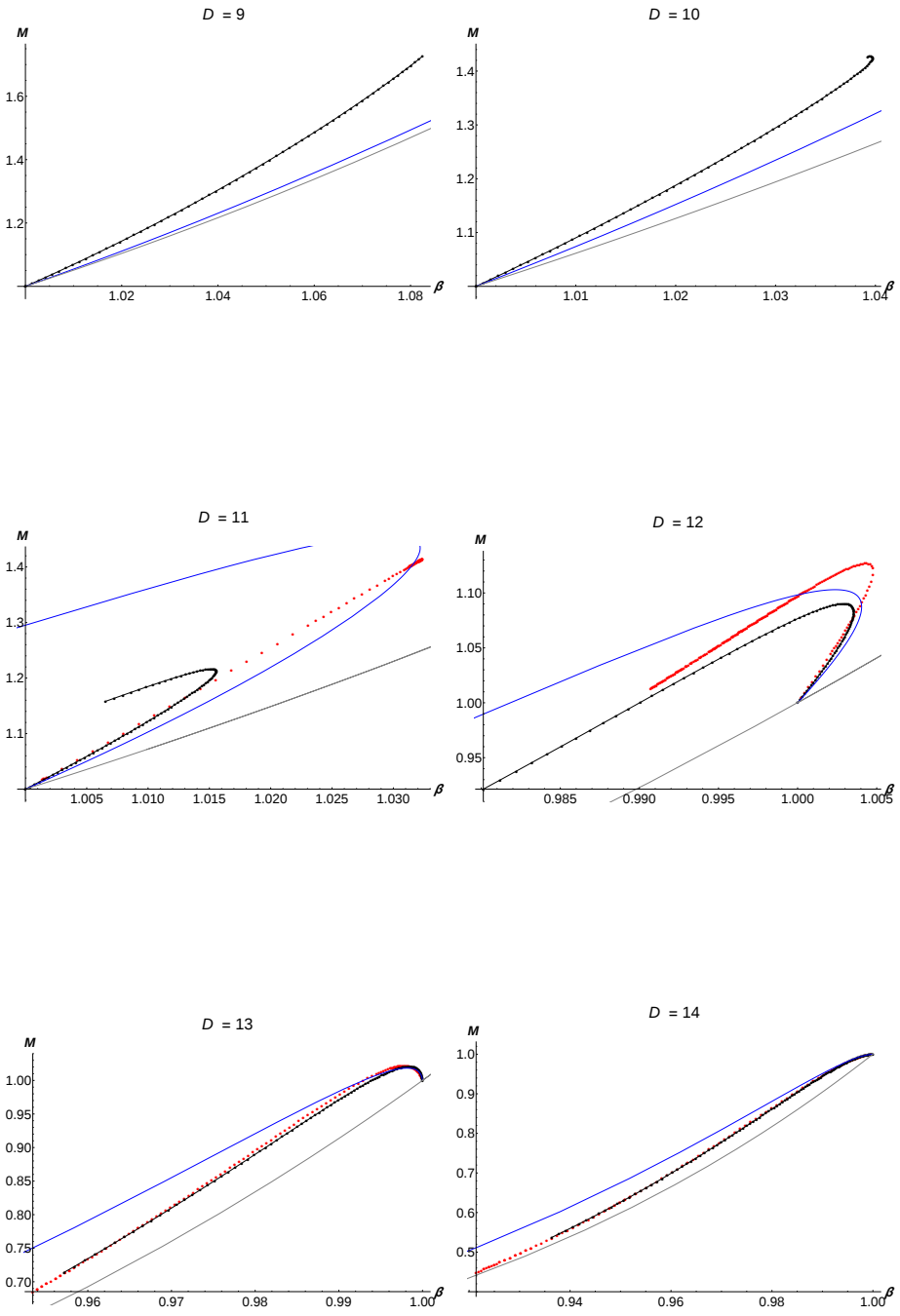

Figure 3.5: Mass $\mathbf{M}$ vs. inverse temperature $\boldsymbol{\beta}$. Black dots: large-D numerical results for NUBS. Blue solid: large-D perturbative solution for NUBS. Red dots: finite-D full-numerical NUBS in [23]. Gray solid: uniform black string ($\mathbf{M}_{\rm UBS} = \boldsymbol{\beta}^n$). From the branching point at $\mathbf{M} = \boldsymbol{\beta} = 1$, we see that $\boldsymbol{\beta}$ increases when $D < 12.5$ and decreases when $D > 12.5$, while $\mathbf{M}$ increases when $D < 13.6$ and decreases when $D > 13.6$.

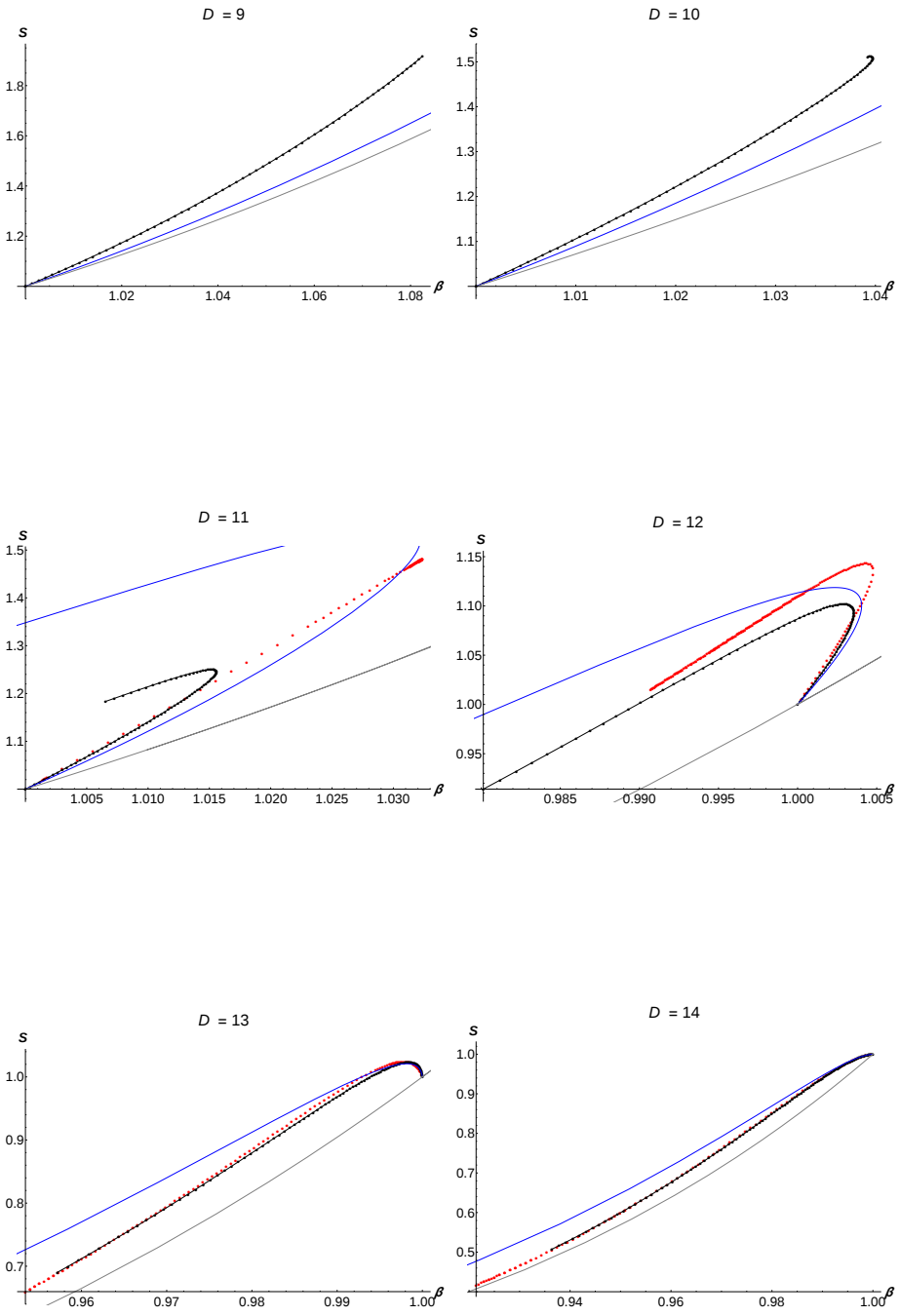

Figure 3.6: Entropy $\mathbf{S}$ vs. inverse temperature $\boldsymbol{\beta}$. Black dots: large-D numerical results for NUBS. Blue solid: large-D perturbative solution for NUBS. Red dots: finite-D full-numerical NUBS in [23]. Gray solid: uniform black string ($\mathbf{S}_{\rm UBS} = \boldsymbol{\beta}^{n+1}$). From the branching point at $\mathbf{S} = \boldsymbol{\beta} = 1$, we see that $\mathbf{S}$ increases when $D < 13.6$ and decreases when $D > 13.6$.

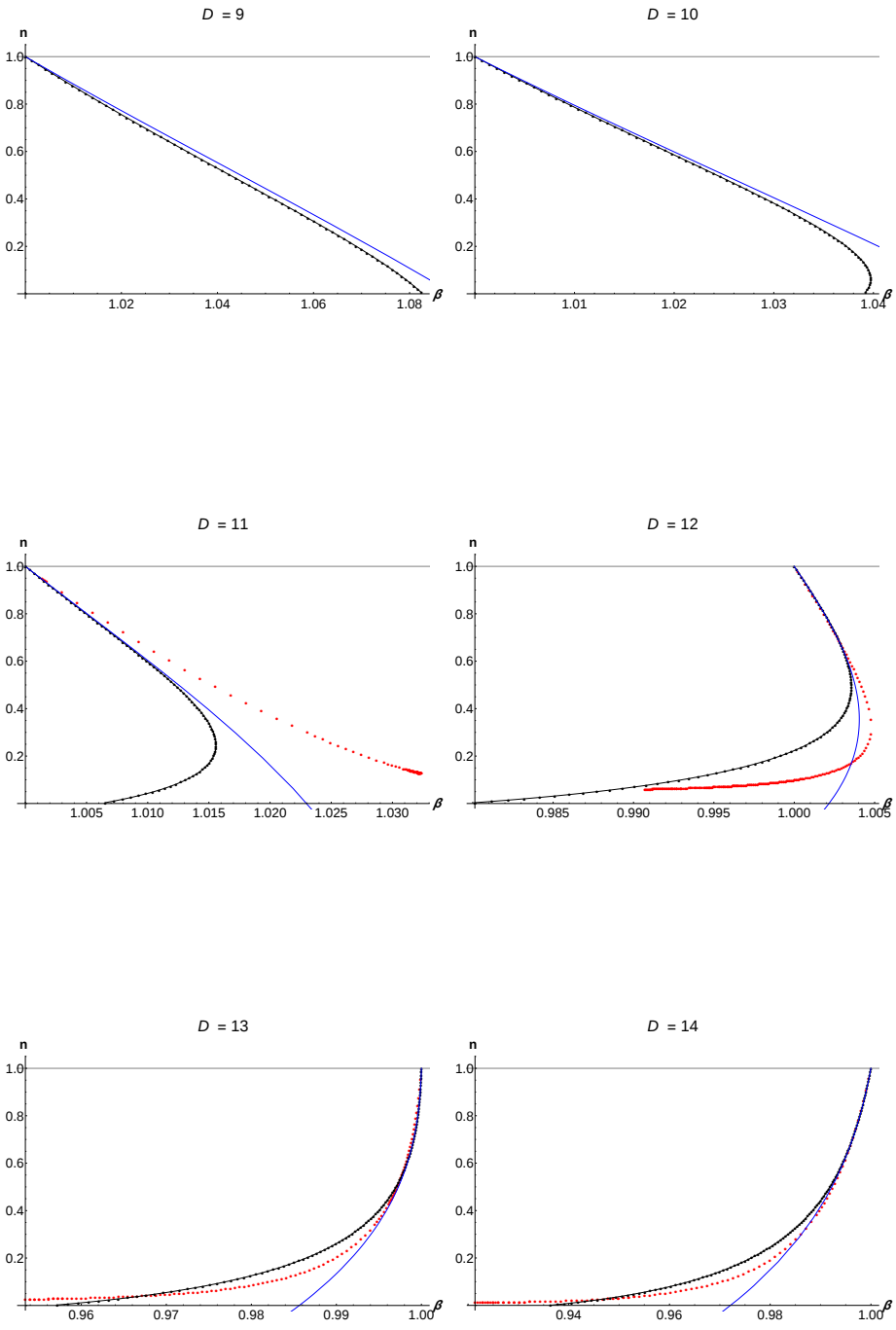

Figure 3.7: Relative binding energy $\mathbf{n}$ (tension per unit mass and length) vs. inverse temperature $\boldsymbol{\beta}$. Black dots: large-D numerical results for NUBS. Blue solid: large-D perturbative solution for NUBS. Red dots: finite-D full-numerical NUBS in [23]. The line $\mathbf{n}_{\rm UBS} = 1$ corresponds to uniform black strings.

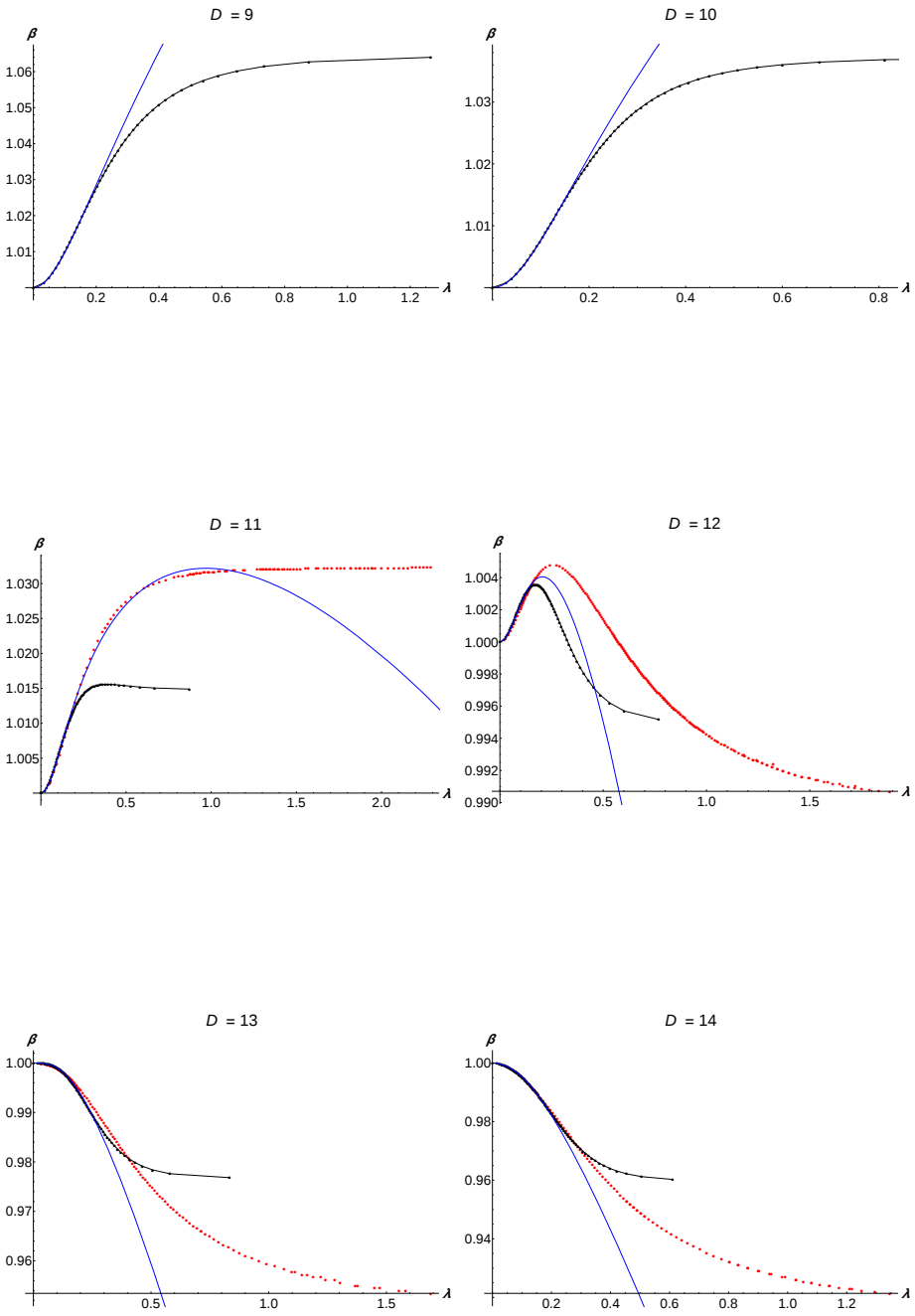

Figure 3.8: Inverse temperature β vs. deformation parameter λ. Black dots: large-D numerical results for NUBS. Blue solid: large-D perturbative solution for NUBS. Red dots: finite-D full-numerical NUBS in [23]

3.4.2 Dynamics

Ref. [15] exhibited numerical simulations of the evolution of unstable black strings in the limit $D \to \infty$. They showed that evolution following the LO equations always ends at stable NUBS. When we incorporate NLO corrections (using the inclusive approach) the outcome of the evolution depends on the thickness of the initial uniform black string.

Black strings with $\mathbf{M}$ not much below the GL instability proceed directly towards stable NUBS with the same value of $\mathbf{M}$. However, when we consider lighter strings, they develop larger inhomogeneity until the evolution breaks down. It would be appealing to attribute this breakdown to a singular pinch-down to zero size of the black string horizon, which would be naturally followed by a (non-classical) transition to a BH configuration. However, we cannot distinguish this effect from a more banal breakdown of the large-D expansion as the inhomogeneity grows too large. Indeed, we expect that this is the reason that the evolutions break down when the mass of the black string is in a range $\mathbf{M} > \mathbf{M}_{\rm min}(D)$, where there exist stable NUBS that are natural endpoints.

Observe that the breakdown can happen only in the inclusive approach; the sequential method cannot lead to any such breakdown, only to the appearance of unphysical solutions that would have negative tension, such as we have constructed above. That is, time evolution in the sequential approach can be regarded as a particular relaxation approach to obtain static solutions.

We conclude that the numerical time evolution of black strings in the large-D expansion can be useful to verify the stability of NUBS when these are not too light. However, the (inclusive) large-D approach breaks down when the mass $\mathbf{M}$ of the black strings becomes small enough, even within the range of existence of stable NUBS.

Chapter 4

Black holes as blobs on a brane: Collisions and violation of Cosmic Censorship

The large D effective equations introduced in Chapter 2 have been shown to have an unexpected application to the description of localized black holes. In the approach of [43] to the physics of large-D black holes, these appear as spheroidal blobs on the horizon of a thin black brane. These blobs not only account correctly for the mass, entropy, and angular momentum of stationary Myers-Perry (MP) black holes in the limit $D \to \infty$: they can also be set in linear motion by a boost, and when perturbed, their vibrations reproduce with accuracy the quasinormal modes of the black hole, axisymmetric or not. The presence of the thin black brane does not affect these properties of single black holes, but acts as a regulator when two black holes either touch or split apart: the horizons never actually merge nor break up, but are always continuously joined by the thin black brane. This feature allows us to follow the entire evolution of the system. This chapter is based on the research published in [5].

These black-hole blobs evolve according to the equations for the large-D effective dynamics of a neutral black brane. As shown in [15, 97], any solution of

$$\partial_t m + \nabla_i (m v^i) = 0, \qquad \partial_t (m v^i) + \nabla_j \tau^{ij} = 0\,, \tag{4.1}$$

where

$$\tau_{ij} = m(v_i v_j - \delta_{ij} - 2\nabla_{(i} v_{j)} - \nabla_i \nabla_j \ln m)\,, \tag{4.2}$$

yields a solution of the Einstein equations to leading order in $1/D$ describing a (possibly dynamical) configuration of a black brane horizon. Here $m(t, x^j)$ and $v^i(t, x^j)$ are the mass (and area) density and the velocity along the brane. Throughout this chapter we fix the units in the effective theory by normalizing the total (conserved) mass to $M = \int d^2x\, m = 1$.

MP black holes correspond to gaussian profiles for m, which become broader as their spin increases (a gaussian describes the area density of a large-dimensional sphere, see [43]). At low spin all the quasinormal modes of the solutions are stable, but when the spin reaches a critical value, a 'bar-mode' instability appears, similar to those present in neutron stars, in which the horizon lengthens along one axis and shrinks along the transverse one. Ref. [43] found an exact non-linear solution of (4.1) for a stationary rotating black bar (which, as we remarked, does not radiate

when $D \to \infty$). It also identified zero-mode perturbations of black bars which are Gregory-Laflamme threshold modes of black strings when the bars are long.

Figure 4.1 shows these stationary phases in the plane of angular velocity Ω vs. angular momentum J. MP black holes exist for all J but are bar-mode unstable for $J > 2$, where black bars exist. With the effective-theory mass $M = 1$, the dimensionless ratio of physical spin $\mathbf{J}$ to physical mass $\mathbf{M}$ is obtained as

$$\frac{\mathbf{J}}{\mathbf{M}^{\frac{D-2}{D-3}}} \simeq \frac{J}{\sqrt{2\pi e D}} \tag{4.3}$$

(we set $16\pi G = 1$). Bear in mind that this expression is only asymptotically valid at large D, and not very accurate for moderate D, even for MP black holes.

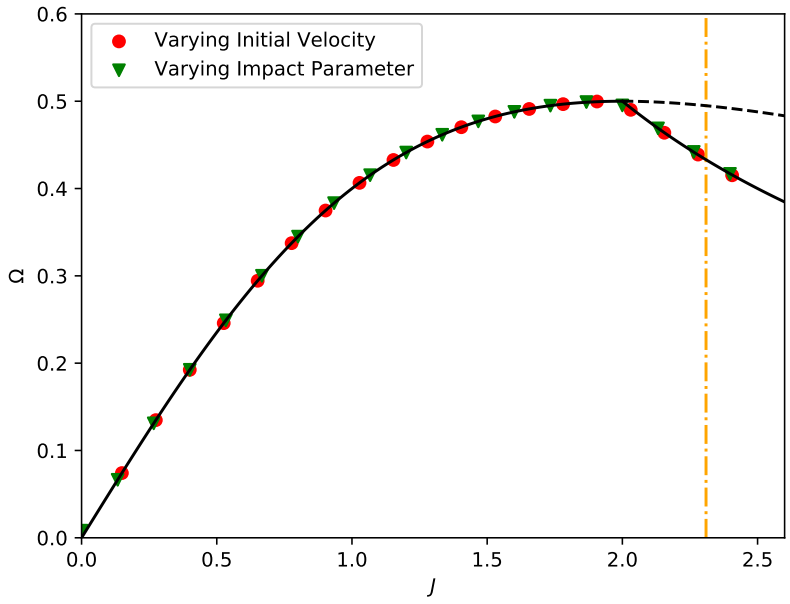

Figure 4.1: Phase diagram for MP black holes and black bars [43] (dashed and continuous lines), and final states of the numerical evolution of a collision after $t = 10$ (circles and triangles). The vertical axis is the angular velocity of the horizon, the horizontal axis the total angular momentum for fixed mass. The orange dash-dotted line at $J = 4/\sqrt{3}$ marks the stability limit for black bars. For $J \gtrsim 2.43$ the intermediate bar configuration breaks, so we omit these values in this plot.

4.1 Colliding black holes at large D

We set up two gaussian blobs (black holes) on a 2-brane in a collision course, and follow their evolution by numerically solving (4.1). For simplicity we consider black holes with equal masses, zero spin, and equal but oppositely oriented velocities.

Before describing our results, let us review some aspects of black hole collisions at large D [8]. First, whenever $D > 4$ it is well known that there are no bounded stable Keplerian orbits; hence there is no inspiral phase. The short range of the gravitational interaction at large D then requires that the two black holes are aimed at one another with a sufficiently small impact parameter. This is not a problem for our purposes since we require J of order one in (4.3), so the angular momenta and impact parameters are indeed small (in physical mass units). When the two black holes are within a distance $\mathcal{O}(r_0/D)$ of each other (where r_0 is a characteristic length of the black hole), their horizons are expected to quickly merge on a time scale $\mathcal{O}(r_0/D)$, presumably forming a tube of size $\mathcal{O}(r_0/D)$ between them. At this point they will emit a burst of gravitational radiation of frequency $\omega = \mathcal{O}(D/r_0)$. The horizon then evolves quickly until it enters a regime of slower evolution, on time scales $\mathcal{O}(r_0)$ controlled by (4.1).

When we evolve the entire collision using (4.1), all the fast dynamics on time scales $\mathcal{O}(r_0/D)$ is smoothed out. Since the thin black brane regulates the collision, there is properly never an instant in which the black holes merge, and the initial sharp outburst of high-frequency radiation is not visible. Missing this first part of the process is not an important shortcoming: we expect that this quick evolution is almost featureless, as indicated already by the universal nature of quasinormal modes of high frequencies $\mathcal{O}(D/r_0)$ [10, 108]. The most interesting part of the dynamics is the one accurately captured by eqns. (4.1) (which provide the non-linear theory of the "featureful" quasinormal modes of frequency $\mathcal{O}(1/r_0)$), *i.e.,* the evolution of the merged horizon.

We solve numerically the evolution equations by discretizing the spatial directions in a square domain with periodic boundary conditions. We have used two independent codes, with equivalent results: one is written in the *Julia* language [109] and the other one in *Mathematica*. The *Julia* code uses a two-dimensional Fourier grid with FFT differentiation in the spatial directions, and the *DifferentialEquations.jl*

package [110] for time integration. The *Mathematica* code uses finite-difference differentiation in the spatial directions and a fourth-order Runge-Kutta method in the time direction.

4.2 Results

We have performed numerical simulations of collisions with different initial velocities and impact parameters for the colliding black holes. Since there is no gravitational radiation, the total angular momentum J is conserved throughout the evolution, which we have checked in our numerics. We have found that, for a large range of initial velocities and impact parameters, the value of J is enough to predict the final state of the system, according to the stationary configurations that exist with that J: rotating MP black hole or black bar, stable or unstable. This is shown in Figs. 4.1 and 4.2.

That is, for collisions with $J < 2$ we obtain final states that correspond to MP black holes, which are the only stationary and stable phases in this range. For larger J the MP black holes are unstable to bar formation and correspondingly we do not find these anymore as final states in our simulations. Instead, for $2 < J < J_c = 4/\sqrt{3} \approx 2.31$ the final states are stable black bars. The critical value J_c is given by the reflection-symmetric marginal mode of the bars found in [43], which marks the beginning of the unstable region for the black bars that can be formed in our simulations. For values of J slightly larger than J_c the bars are long-lived, and we do not observe their breaking in our numerics. However, for J sufficiently high, the bars do split—more specifically, we observe this for $J \gtrsim 2.43$ for running times of order $t \sim 10$ (in units of $M = 1$). These bars break after two turns or less, and the intermediate configurations can resemble more an evolving dumbbell, whose life-time decreases with J, than a quasi-stationary bar.

In Fig. 4.3 we show snapshots of the time evolution of a collision that yields CC violation. After the breaking, the two pieces of the bar fly apart and quickly settle into boosted MP black holes. Going to their rest frame, we observe that their approach to equilibrium is governed by the lowest-lying quasinormal mode computed in [43]. The final black holes have the same mass as the initial ones, and non-zero

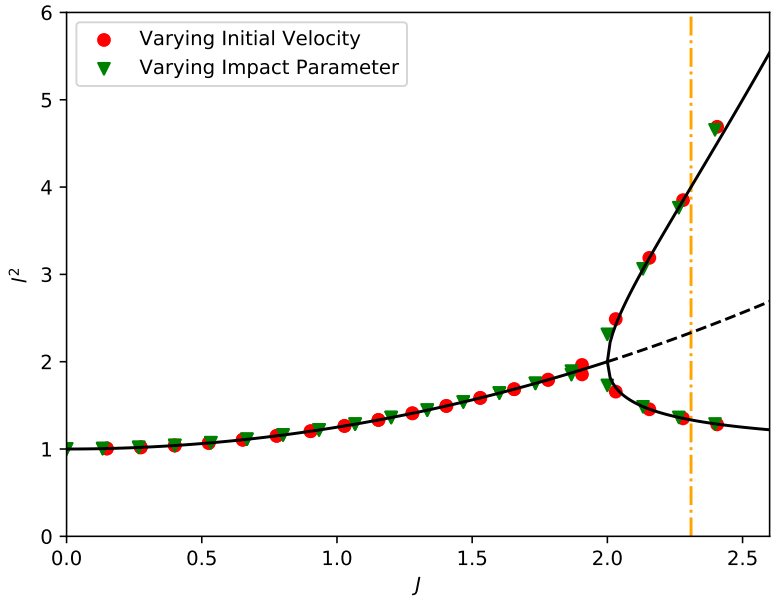

Figure 4.2: Longitudinal and transverse (squared) axial lengths $\ell_{\parallel}^2$ and $\ell_{\perp}^2$ of the final states of the numerical evolution of a collision after $t = 10$ (circles and triangles). The axial lengths $\ell_{\parallel}^2$ and $\ell_{\perp}^2$ for MP black holes and black bars, as defined in [43], are shown by the continuous and dashed lines.

spin, but the total horizon area does not decrease in the process since when $D \to \infty$ the black hole area is not affected by its spin. Let us also note that putting non-zero intrinsic spin on the initial black holes allows to demonstrate the formation of the long-lived bar and its subsequent instability in collisions with very small impact parameter [111].

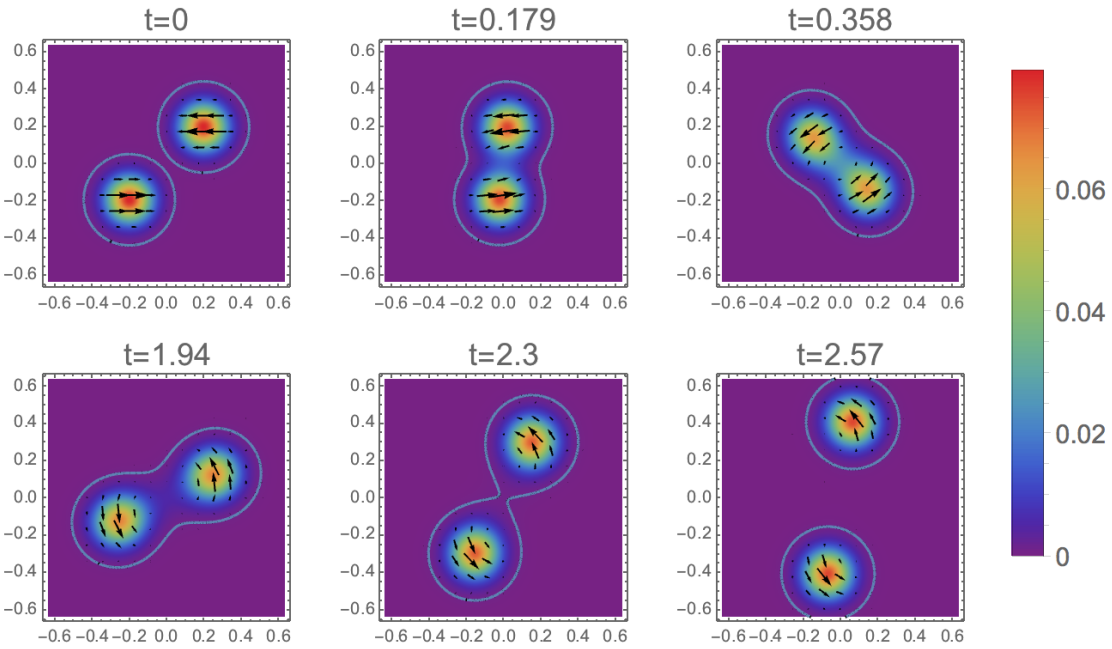

Figure 4.3: Snapshots of the time evolution of a collision for $J = 2.43$. The density plots show the energy density m, while the arrows depict mv_i. Contour lines corresponding to $m = 8 \times 10^{-4}$ are drawn to guide the eye. After the black holes merge, they form a (deformed) bar that lasts for a time of order $\Delta t \approx 2.3$, until it breaks apart.

Chapter 5

Strong Cosmic Censorship

This chapter takes a first glance at the fully nonlinear behavior of asymptotically de Sitter charged black holes close to extremality. All results included here are restricted to spherical symmetry. The simulations seem to be compatible to the prediction of [51], *i.e.,* that Penrose's Strong Cosmic Censorship could be violated in these extreme spacetimes.

The first part of the chapter is devoted to the description of the numerical scheme that we have used to perform the simulations (*Double Null Through Spectral methods*, or DoNuTS) codeThis procedure takes a different approach to previous codes by introducing spectral methods, thus reducing drastically both the computational requirements that are needed and the running time. In the second part the main results are summarized. This chapter is based on the research published in [112].

We consider here an evolving, electrically charged spacetime, modelled by the Einstein-Maxwell action with a cosmological constant Λ, minimally coupled to a massive scalar field Φ with mass parameter μ,

$$S = \int d^4x\sqrt{-g}\left(R - 2\Lambda - F^2 - 2\Phi_{,\alpha}\Phi^{,\alpha} - 2\mu^2\Phi^2\right) ,$$

where $F^2 = F_{\alpha\beta}F^{\alpha\beta}$ and $F_{\alpha\beta}$ is the Maxwell tensor. The equations of motion reduce to

$$\begin{aligned} G_{\mu\nu} + \Lambda g_{\mu\nu} &= 2F_{\mu\alpha}F_{\nu}{}^{\alpha} - \frac{1}{2}g_{\mu\nu}F^2 \\ &\quad + 2\Phi_{,\mu}\Phi_{,\nu} - g_{\mu\nu}\left(\Phi_{,\alpha}\Phi^{,\alpha} + \mu^2\Phi^2\right) , \qquad (5.1) \\ \Box\Phi &= \mu^2\Phi\,, \qquad dF = d\star F = 0\,, \qquad (5.2) \end{aligned}$$

where $\star$ is the Hodge dual.

We focus on spherically symmetric spacetimes, written in double null coordinates as

$$\begin{aligned} ds^2 &= -2e^{2\sigma(u,v)}dudv + r^2(u,v)d\Omega^2\,, \qquad (5.3) \\ F &= F_{uv}(u,v)du\wedge dv\,, \qquad \Phi = \Phi(u,v)\,, \qquad (5.4) \end{aligned}$$

where u and v are ingoing and outgoing coordinates, respectively. In this framework, Maxwell's equations decouple and imply that

$$F_{uv}r^2e^{-2\sigma} = \text{constant} = Q\,, \qquad (5.5)$$

with Q a conserved (electric) charge.

5.1 Numerical evolutions

To numerically evolve the field equations we specify initial conditions along two null segments, $u = u_i$ and $v = v_i$. We fix the residual gauge freedom as follows:

$$r(u_i, v) = v\,, \qquad r(u, v_i) = r_0 + u r_{u0}\,, \tag{5.6}$$

where r_{u0} is a constant and $r_0 = v_i$. The profile of the scalar field is set as purely ingoing

$$\Phi(u_i, v) = A e^{-\left(\frac{v-v_c}{w}\right)^2}\,, \tag{5.7}$$

with the outgoing flux being set to zero, $\Phi_{,u}(u, v_i) = 0$.

To interpret our results it will be convenient to consider the following alternative outgoing null coordinates: $\mathring{v}$, an Eddington-Finkelstein type coordinate, defined by integrating

$$\left(1 - \frac{2M}{r} + \frac{Q^2}{r^2} - \frac{\Lambda}{3} r^2\right) d\mathring{v} = r_{,v}\, dv \tag{5.8}$$

along the event horizon (EH), and t, the affine parameter of an outgoing null geodesic, obtained by integrating

$$\left(1 - \frac{2M}{r} + \frac{Q^2}{r^2} - \frac{\Lambda}{3} r^2\right) dt = -r_{,u} r_{,v}\, dv \tag{5.9}$$

along a constant u line. In these expressions M stands for the Misner-Sharp mass function, which we also closely monitor during the integration, given by

$$M(u, v) = \frac{r}{2}\left(1 + \frac{Q^2}{r^2} - \frac{\Lambda}{3} r^2 + 2 e^{-2\sigma} r_{,u} r_{,v}\right)\,. \tag{5.10}$$

The constant r_{u0} is thus related to the initial BH mass, $M_0 \equiv M(u_i, v_i)$. Recall that the blow-up of this scalar signals the breakdown of the field equations [113] (compare with [114, 115]).

To estimate the curvature we compute the Kretschmann scalar K computed from the field equations (see 5.2; a direct evaluation of this scalar in terms of the metric was found to lead to important round-off error-related problems).

According to the results in Refs. [48, 51], concerning the massless case, we expect the curvature to blow up for all non-trivial initial data throughout the entire subextremal parameter range. Although it is a potentially interesting nonlinear effect,

we recall that the blow-up of K, per se, is of little significance: it implies neither the breakdown of the field equations [116] nor the destruction of macroscopic observers [117]. Recall that the results in Refs. [52,53] suggest that the introduction of scalar mass could lead, for appropriate choices of BH parameters, to solutions with bounded curvature. As we will see below, our results contradict this expectation.

5.2 Numerical procedure

5.2.1 Algorithm

Our equations of motion have the form

$$r_{,uv} + \frac{r_{,u}r_{,v}}{r} + \frac{e^{2\sigma}}{2r}\left[1 - \frac{Q^2}{r^2} - \left(\Lambda + \mu^2\Phi^2\right) r^2\right] = 0\,, \tag{5.11}$$

$$\sigma_{,uv} - \frac{r_{,u}r_{,v}}{r^2} - \frac{e^{2\sigma}}{2r^2}\left(1 - 2\frac{Q^2}{r^2}\right) + \Phi_{,u}\Phi_{,v} = 0\,, \tag{5.12}$$

$$\Phi_{,uv} + \frac{1}{r}\left(\Phi_{,u}r_{,v} + \Phi_{,v}r_{,u}\right) + \frac{e^{2\sigma}}{2}\mu^2\Phi = 0\,, \tag{5.13}$$

and are subjected to the following constraints

$$r_{,uu} - 2r_{,u}\sigma_{,u} + r\left(\Phi_{,u}\right)^2 = 0\,, \tag{5.14}$$

$$r_{,vv} - 2r_{,v}\sigma_{,v} + r\left(\Phi_{,v}\right)^2 = 0\,. \tag{5.15}$$

These equations must be satisfied by the initial data. Then, by virtue of the Bianchi identities, they will be satisfied in the whole computational domain provided that the dynamical equations are accurately satisfied.

To integrate these equations, we start by transforming them into a system of ODEs. Our procedure is as follows. Let $h(u,v)$ be any evolved quantity $r(u,v)$, $\sigma(u,v)$ and $\Phi(u,v)$. Defining $f(v) = \partial_u h(u,v)$, all dynamical equations, *for fixed* u, have the form

$$f'(v) + f(v)p(v) = g(v)\,, \tag{5.16}$$

where $'$ denotes the derivative with respect to v. These equations can be solved by introducing the integrating factor

$$\lambda(v) = \exp\left(\int_{v_i}^{v} p(v')\,dv'\right), \qquad \lambda'(v) = p(v)\lambda(v)\,.$$

Multiplying Eq. (5.16) by $\lambda(v)$, we get

$$f'(v)\lambda(v) + f(v)\lambda'(v) = [f(v)\lambda(v)]' = g(v)\lambda(v)$$
$$\Leftrightarrow f(v) \equiv \partial_u h(v) = \frac{1}{\lambda(v)}\left[f(v_i) + \int_{v_i}^{v} g(v')\lambda(v')\,dv'\right],$$

which are ODEs in u for all values of v. Given initial conditions in the two null segments $u = u_i$, $h(u_i, v)$ $\forall v$ and $v = v_i$, $f(v_i) \equiv \partial_u h(u, v_i)$ $\forall u$, we can integrate the equations in a rectangular region $u_i < u < u_f$ and $v_i < v < v_f$.

For our three functions in Eqs. (5.11), (5.12) and (5.13), $p(v)$ and $g(v)$ are the following:

$$\begin{aligned}
p_r(v) &= \frac{r_{,v}}{r}\,,\\
g_r(v) &= -\frac{e^{2\sigma}}{2r}\left[1 - \frac{Q^2}{r^2} - \left(\Lambda + \mu^2\Phi^2\right) r^2\right],\\
p_\Phi(v) &= \frac{r_{,v}}{r}\,,\\
g_\Phi(v) &= -\frac{r_{,u}\Phi_{,v}}{r} - \frac{e^{2\sigma}}{2}\mu^2\Phi\,,\\
p_\sigma(v) &= 0\,,\\
g_\sigma(v) &= \frac{r_{,u}r_{,v}}{r^2} + \frac{e^{2\sigma}}{2r^2}\left(1 - 2\frac{Q^2}{r^2}\right) - \Phi_{,u}\Phi_{,v}\,.
\end{aligned}$$

We integrate these equations using the *Double Null Through Spectral methods* (DoNuTS) code written in Julia [109]. To integrate the system within DoNuTS, all functions are expanded in a Chebyshev basis in the v direction (where all v derivatives and integrations can be readily performed), and the remaining ODEs in the u direction are integrated using an adaptive step integrator through the DifferentialEquations.jl Julia package [110].

To avoid round-off errors we use the expression for the Kretschmann scalar in [118] (adapted to include a scalar field mass), instead of computing it directly in terms of the metric:

$$
\begin{aligned}
K \equiv R_{\alpha\beta\gamma\delta}R^{\alpha\beta\gamma\delta} = \frac{16}{r^6}\left[\left(M-\frac{3Q^2}{2r}+\frac{\Lambda}{6}r^3\right)+\frac{r}{2}\left(1-\frac{2M}{r}+\frac{Q^2}{r^2}-\frac{\Lambda}{3}r^2\right)\left(\frac{r\Phi_{,u}}{r_{,u}}\right)\left(\frac{r\Phi_{,v}}{r_{,v}}\right)\right]^2 \\
+\frac{16}{r^6}\left(M-\frac{Q^2}{2r}+\frac{\Lambda}{6}r^3\right)^2+\frac{16}{r^6}\left(M-\frac{Q^2}{r}-\frac{r^3}{3}\left(\Lambda+\mu^2\Phi^2\right)\right)^2 \\
+\frac{4}{r^4}\left(1-\frac{2M}{r}+\frac{Q^2}{r^2}-\frac{\Lambda}{3}r^2\right)^2\left(\frac{r\Phi_{,u}}{r_{,u}}\right)^2\left(\frac{r\Phi_{,v}}{r_{,v}}\right)^2,
\end{aligned}
$$

where M is the Misner-Sharp mass.

5.2.2 Adaptive gauge

When using the initial gauge, $r_{,u}$ becomes extremely large around the apparent horizon for large v. Therefore, in order to explore the near-horizon region at late times, it is convenient to use an adaptive gauge in u during the numerical evolution.

Since the change $u \to \tilde{u}(u)$ together with $\sigma \to \sigma - \frac{1}{2}\log\left(\frac{d\tilde{u}}{du}\right)$ leaves the equations invariant, we can change the gauge in u along the integration by choosing appropriately the initial condition $\sigma_{,u}(u, v_i)$ at each value of u.

To explore the near-horizon geometry, we can choose an Eddington-like gauge for u, *i.e.,* a gauge that brings the event horizon to $u \to \infty$. A good way to do so, as described in [119], is to set $\sigma(u, v_f) = \log\left(2r_{,v}(u, v_f)\right) + C$, where C can be any constant. In the DoNuTS code, this is achieved by picking the initial condition for $\sigma_{,u}(u, v_i)$

$$
\sigma_{,u}(u, v_i) = -\left[\sigma(u, v_f) - \log\left(2r_{,v}(u, v_f)\right) + \frac{3}{2}\log 2\right]. \tag{5.17}
$$

The term $\frac{3}{2}\log 2$ is chosen so that $\sigma_{,u}(u_i, v_i)$ is small when $\sigma(u_i, v_f) \approx -\frac{1}{2}\log 2$. With this condition, $\sigma(u, v_f)$ is damped towards the desired value $\log\left(2r_{,v}(u, v_f)\right) - \frac{3}{2}\log 2$ along the evolution in u. Additionally, in order to satisfy the constraint equation (5.14), we must introduce an additional ODE for the initial condition $r_{,u}(u, v_i)$ at $v = v_i$,

$$
r_{,uu}(u, v_i) = 2r_{,u}(u, v_i)\sigma_{,u}(u, v_i) \tag{5.18}
$$

with $r_{,u}(u_i, v_i) = r_{u0}$ obtained using the expression (5.10) for the Misner-Sharp mass. By solving this ODE along with all the others, we get the initial conditions at $v = v_i$ at each value of u along the integration.

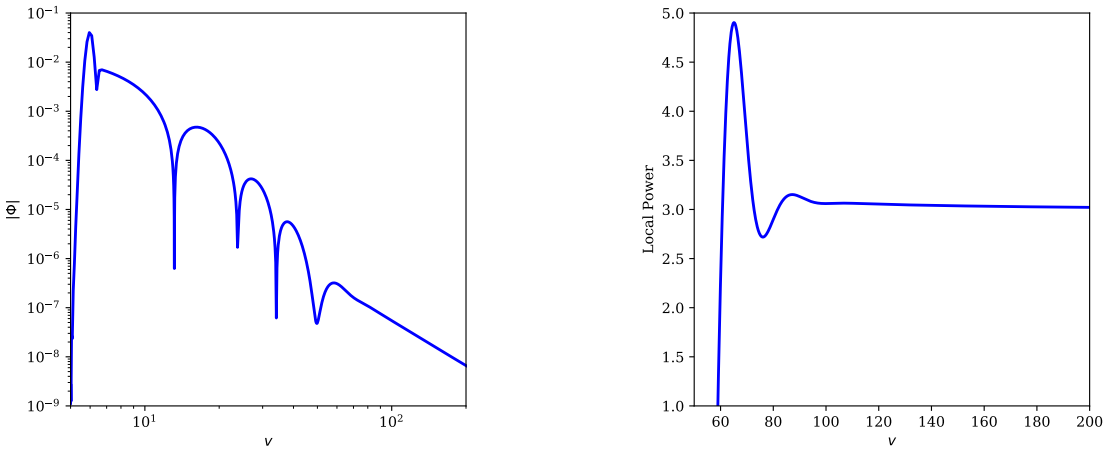

Figure 5.1: Massless scalar field along the event horizon with corresponding "local power" for a configuration with $M_0 = 1.0$, $Q = 0.95$, $\Lambda = 0$, $\mu = 0$, $A = 0.01$, $v_c = 6.0$ and $w = 0.25$. The power-law decay $\Phi \sim v^{-3}$ matches to a very good precision the one expected from linearized analysis [47], and reproduces well previous nonlinear results [120].

5.2.3 Code tests

As a test of our numerical implementation we have reproduced the late-time decay of an asymptotically flat configuration with a massless scalar field. For this, it was crucial to employ the gauge conditions (5.17), (5.18). We also compute the "local power" of the scalar field decay, defined as $-v\Phi_{,v}/\Phi$. These are shown in Fig. 5.1 and are consistent with expected results.

To further test the code, we have analyzed its convergence properties. We thus evaluate the quantity

$$\delta_{n,m}(F) \equiv \max |1 - F_n/F_m| \tag{5.19}$$

for a given function F_N obtained with resolution N at a fixed u coordinate, and where the maximum is evaluated for all values of v. Here, the index m refers to a reference solution obtained using a large number m of grid points while n denotes test solutions using a coarser resolution, $n < m$.

In Fig. 5.2 we show the convergence properties of the Kretschmann scalar for

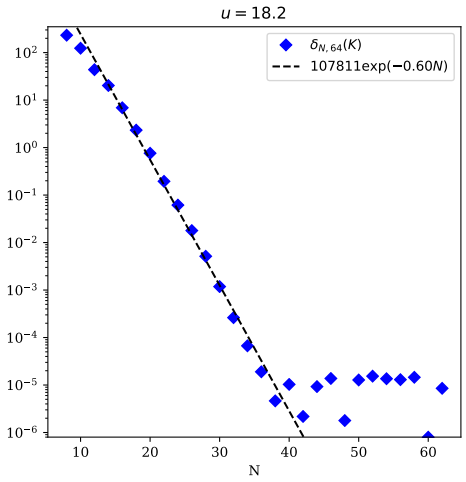

Figure 5.2: $\delta_{N,64}(K)$ at $u = 18.2$ for configuration **B1**. 20 domains were employed in the v direction, where each domain has N points. The plot clearly shows exponential convergence until $N \approx 40$.

configurations **B1**. The plots show exponential convergence up to $N \approx 40$.

Finally, since we use a free-evolution scheme, we have checked that the constraint equations (5.14) and (5.15) remain satisfied throughout our evolution. We show typical plots for the corresponding constraint violation in Fig. 5.3.

5.3 Initial conditions

The physical problem is then fully determined upon specifying Q, Λ, μ, M_0, A, v_c and w. Since our purpose here is to determine whether the linearized predictions of Refs. [51, 52] hold in the full nonlinear regime, we focus on $M_0 = 1$, $\Lambda = 0.06$ and use the following configurations:

A: $Q = 0.9000$, $\mu = 0$, corresponding to $Q = 0.890 Q_{\rm max}$. In this case, the results in Ref. [51] (lower left panel of Fig. 3) predict *mass inflation*.

B: $Q = 1.0068$, $\mu = 0$, corresponding to $Q = 0.996 Q_{\rm max}$. Linearized studies provide evidence in favor of a *no mass inflation* scenario [51].

C: $Q = 1.0068$, $\mu = 1.0$. The results of Ref. [51] together with those of Ref. [52] –

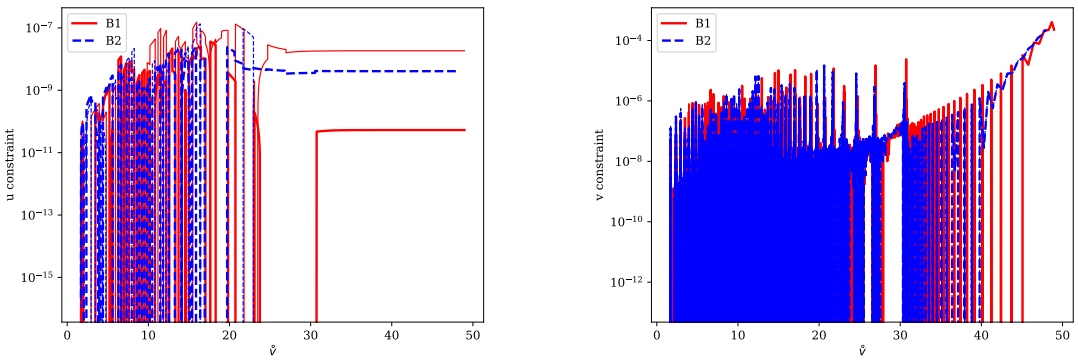

Figure 5.3: Constraint violations during our evolutions of configurations **B**.

see Fig. 2 – also provide evidence in favor of a *no mass inflation* scenario. Here we are considering the superposition of both neutral massless scalar perturbations [51] and charged massive scalar perturbations [52] as being the most predictive of the full non-linear evolution. If we just take into account massive scalar perturbations, then the results in Ref. [52] (see Fig. 2]) and [53] (page 22) suggest that curvature might also be bounded.

To test the dependence of our results on initial data, we use the following initial profiles for the scalar field:

1: $A = 0.04$, $w = 0.1$ and $v_c = 3.0$;

2: $A = 0.08$, $w = 0.5$ and $v_c = 3.0$.

We have evolved the relevant system of equations using the DoNuTS code, described briefly in Section 5.2. It is based on the formulation presented in Refs. [120–122], but the integration technique makes it spectrally accurate in the v-direction and, correspondingly, runs with trivial memory requirements and orders of magnitude faster than previously reported codes.

5.4 Results

It is important to start by noticing that, as widely expected [48, 123], our numerics show that all solutions contain a non-empty CH in their BH interior. This can be attested by monitoring the radius function – shown in Fig. 5.4 – along null lines

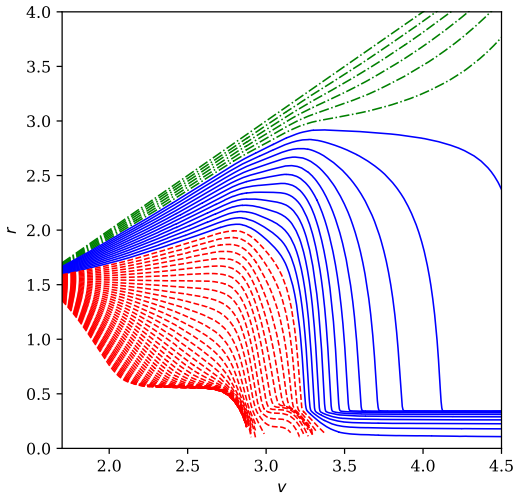

Figure 5.4: Radius function for constant-u slices in a configuration with $M_0 = 1.0$, $Q = 0.9$, $\Lambda = 0.06$, $\mu = 0$, $A = 0.4$, $v_c = 3.0$ and $w = 0.25$. Dashed-dotted green lines reach infinity, full blue lines hit the CH and red dashed lines hit the singularity at $r = 0$.

$u = u_1$, for $u_1 > u_{\rm EH}$, where $u = u_{\rm EH}$ is the event horizon. In fact, for u_1 larger but close to $u_{\rm EH}$, the radius converges, in v, to a non-vanishing constant. It is also interesting to note that, for some initial configurations and large enough u_1, the radius does converge to zero, signaling (in that region) a singularity beyond which the metric cannot be extended [124].

As is well known the behavior of the scalar field along the event horizon is of great significance for the structure of the BH interior region. The first noteworthy feature of our results is that, as expected, the field decays exponentially (in $\mathring{v}$), as shown in Fig. 5.6. More surprisingly, we also clearly observe an oscillatory profile; this might seem odd at first, since it is in contrast with what happens for $\Lambda = 0$ and with the expectation created by the study of sufficiently sub-extremal BHs with $0 < M^2\Lambda \ll 1$ [125]. However, it turns out that such behavior should be expected from the linearized analysis of Refs. [51, 52], where it is shown that, for a configuration resembling our configuration **B**, there are two modes which dominate the response: a non-oscillatory "near extremal" (NE) mode with characteristic fre-

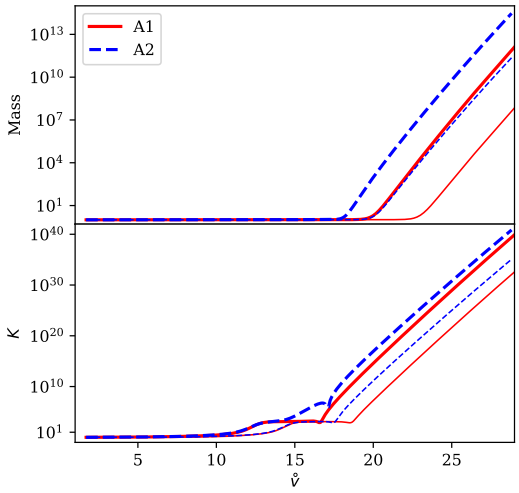

Figure 5.5: Mass function (5.10) and Kretschmann scalar as functions of $\mathring{v}$ for configurations **A1** (red solid line) and **A2** (blue dashed line). Thin lines are evaluated at $u = u_{\rm EH} + 1$ and thick lines are evaluated at $u = u_{\rm EH} + 2$. These results are consistent with the existence of mass inflation leading to a weak singularity.

quency $\omega_{\rm NE} \sim -0.081i$, *and* a "photon sphere" (PS) mode with $\omega_{\rm PS} \sim 0.096 - 0.095i$ (these numbers are given in the units and time-coordinate of Ref. [51]). Here we find very good agreement with the PS mode (when translated to our $\mathring{v}$ coordinate) which is oscillatory in nature. Similar agreement can be found for the remaining configurations **A** and **C**. We also recall that, according to the results in [51], in the $M^2\Lambda \ll 1$ case, the dominant mode is a non-oscillatory "de Sitter" mode, in agreement with [125].

Our main results (concerning mass and curvature) are summarized in Figs. 5.5-5.8. Fig. 5.5 shows the evolution of the mass function and the Kretschmann scalar for configurations **A**: in these cases mass inflation occurs, and, consequently, the curvature invariant K diverges. Note that an observer crossing one such region will be subjected to physical *deformations* which are not necessarily infinite (see discussion below). Nonetheless, because there is mass inflation, the singularity is strong enough to deserve the classification of *terminal boundary*, since it corresponds to a locus where the field equations cease to make sense. These conclusions are

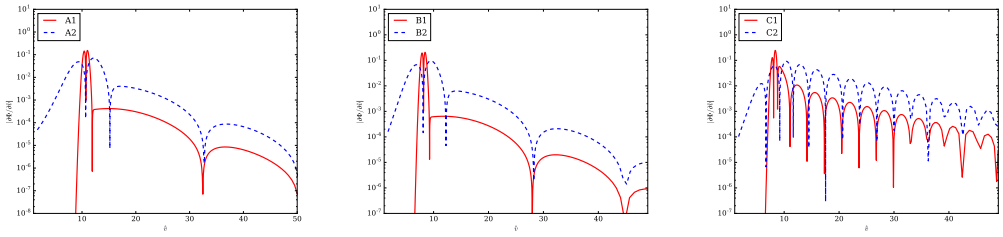

Figure 5.6: Scalar field derivative $\partial\Phi/\partial\mathring{v}$ as a function of $\mathring{v}$ for configurations **A** (left plot), **B** (middle plot), **C** (right plot) with initial profiles 1 (red solid lines) and 2 (blue dashed lines). $\partial\Phi/\partial\mathring{v}$ evaluated at $u = u_{\rm EH}$.

consistent with the linear results in [51] and the nonlinear results in [48].

The main result of this work concerns Fig. 5.7: we find configurations for which no mass inflation occurs in the simulation computational domain. This does not necessarily imply that mass inflation will not appear at later times. In fact, as a consequence of the "accretion" of the ingoing scalar field pulse, the final parameters of the black hole are slightly outside the region where (according to [51]) there should be no mass inflation at all. Clearly, then, the results are still inconclusive. However, we do observe that the timescale where mass inflation would appear has increased drastically with respect to configuration **A**, making these results compatible with the SCC violation hypothesis. Moreover, as recently predicted [48, 51], the CH remains a curvature singularity, since the curvature scalar K diverges. However, the lack of mass inflation would make the singularity so "mild" that, in principle, one should be able to continue the evolution of the space-time metric across it, by solving the Einstein field equations!

A somewhat unexpected feature (of configuration **B**) is the oscillatory way in which the curvature scalar diverges. In hindsight, such behavior could be expected from the previously discussed oscillatory behavior of the scalar field along the event horizon. Note that in a no mass inflation situation it is the blow up of $\Phi_{,v}/r_{,v}$ that dominates the behavior of K. This should be contrasted with what happens when mass inflation occurs: then it is the *monotone* divergence of the mass that controls the Kretschmann; this last fact provides an explanation for the non-oscillatory behavior observed for configuration **A**.

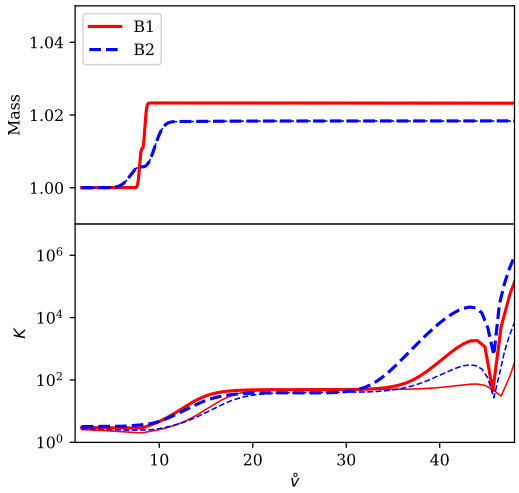

Figure 5.7: Mass function (5.10) and Kretschmann scalar as functions of $\mathring{v}$ for configurations **B1** (red solid line) and **B2** (blue dashed line). Thin lines are evaluated at $u = u_{\rm EH} + 1$ and thick lines are evaluated at $u = u_{\rm EH} + 2$.

Concerning massive scalars, the results presented in Fig. 5.8 identify configuration **C** as another configuration not reaching mass inflation in the computational timescale. Once again we find that the corresponding CH is a "weak" curvature singularity. In fact, the presence of scalar mass seems to have no attenuation effect on the growth of K, in contrast with what might be expected from linear analysis [52] and [53].

We finish this section with some further remarks concerning the blow up of curvature. In configuration **A**, our results indicate that the Kretschmann scalar blows up as t^{-2} (possibly modulated by logarithmic terms), where t is the affine parameter defined in (5.9) with the Cauchy horizon located at $t = 0$. This might suggest that the curvature blows up as t^{-1}, but, as noted in [46,117], there are curvature components that may blow up even faster. In fact, the quantities that determine the blow-up of the Kretschmann scalar are the square of the (Misner-Sharp) mass M and the square of the gradient of Φ, which is dominated by $(\Phi_{,v}/r_{,v})^2$. However, all curvature components are controlled by M and $(\Phi_{,v}/r_{,v})^2$ (the origin of the last term can be traced to the energy-momentum tensor). From the behavior of the Kretschmann

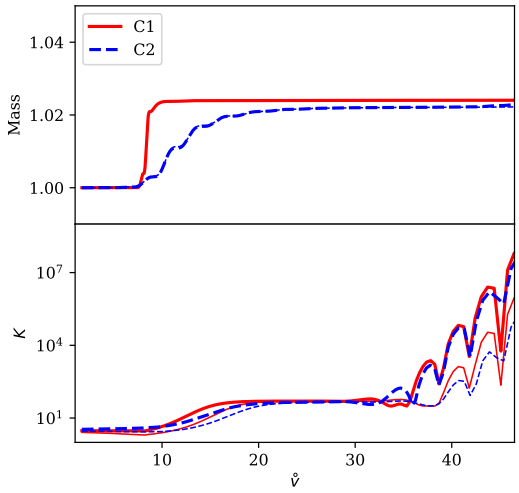

Figure 5.8: Same as Fig. 5.7, for configurations **C1** (red solid) and **C2** (blue dashed).

scalar we can then conclude that the components of the curvature blow up at most as t^{-2}; we also expect inverse logarithmic powers [114, 115, 117] that are hard to detect numerically. Although divergent, these curvature components should yield (with the help of the logarithmic terms) a finite "tidal deformation" when integrated twice with respect to t, in agreement with the picture in [117].

From the equation (see Ref. [118])

$$M_{,v} = \frac{1}{2}\left(1 - \frac{2M}{r} + \frac{Q^2}{r^2} - \frac{\Lambda}{3}r^2\right)\left(\frac{\Phi_{,v}}{r_{,v}}\right)^2 r_{,v} \tag{5.20}$$

we conclude that no mass inflation would be essentially equivalent to the integrability of $(\Phi_{,v}/r_{,v})^2$, with respect to t[1]. Moreover, when both occur we immediately see that the curvature can only give rise to finite "tidal deformations".

[1]In fact, there is a mathematical equivalence under the reasonable, in principle generic, assumption that the quantity $1 - \frac{2M}{r} + \frac{Q^2}{r^2} - \frac{\Lambda}{3}r^2$ does not vanish at the Cauchy horizon.

Chapter 6

Plasma polarization and Love numbers of AdS black branes

In this chapter we use black branes in the context of holographic dualities, generally known as *AdS/CFT* correspondences, to compute the behavior of plasma states of quantum field theories in curved geometries. By defining a (conformally invariant) quantum theory on the boundary of AdS, we can then extract information about it from gravitation in the bulk. The deformations of the boundary will act as an external tidal potential that will alter the geometry in the bulk, whose response we parametrize in terms of the Love numbers. This way, by computing the Love numbers we can derive the reaction of the CFT to the geometry of the spacetime it is embedded in. sThis chapter is based on the research published in [126].

6.1 Black branes in AdS

The solution for a neutral black brane in AdS_{n+1} with cosmological constant $\Lambda = -\frac{n(n-1)}{2R^2}$ is

$$\frac{ds^2}{R^2} = \frac{dv^2}{v^2 f} + \frac{1}{v^2}\left(\eta_{\alpha\beta} + (1-f)u_\alpha u_\beta\right) dx^\alpha dx^\beta \,, \tag{6.1}$$

where $\alpha, \beta = 1, \ldots, n$ label the field theory directions, u_α is a timelike vector with $u_\alpha u_\beta \eta^{\alpha\beta} = -1$, and

$$f = 1 - \mu v^n \,. \tag{6.2}$$

We denote the bulk radial coordinate as v, such that $v = 0$ corresponds to the AdS boundary and $v = \mu^{-1/n}$ to the black brane horizon. The parameter μ determines the temperature T of the configuration through

$$\mu = \left(\frac{4\pi T}{n}\right)^n \,. \tag{6.3}$$

When $\mu \neq 0$ one can set $\mu = 1$ without loss of generality. However, for the most part we will keep μ explicitly in our equations so we can easily recover the AdS vacuum by setting $\mu = 0$.

The renormalized boundary metric

$$\gamma_{\alpha\beta} = \lim_{v\to 0} \frac{v^2}{R^2} g_{\alpha\beta} \tag{6.4}$$

in which the dual field theory lives is the flat Minkowski metric $\eta_{\alpha\beta}$. We want to study the response of the field theory to a small deformation of this geometry, which

we decompose into plane waves,

$$\gamma_{\alpha\beta} = \eta_{\alpha\beta} + \bar{h}_{\alpha\beta} e^{ik_\alpha x^\alpha} \,. \tag{6.5}$$

The $\bar{h}_{\alpha\beta}$ are constant numbers that characterize the relative amplitudes of the different metric deformations. We study time-independent perturbations, *i.e.,* with zero frequency

$$u^\alpha k_\alpha = 0 \,. \tag{6.6}$$

This means that the perturbations are stationary, but not necessarily static since we allow non-zero components $u^\alpha \bar{h}_{\alpha\beta}$, which include momentum. We also allow non-zero gravitational potentials $u^\alpha u^\beta \bar{h}_{\alpha\beta}$.

Henceforth we partially fix the frame by choosing a time direction t and aligning k_α with a direction z, *i.e.,*

$$u^\alpha = \delta^\alpha{}_t \,, \qquad k_\alpha = k\, \delta_{\alpha z} \,. \tag{6.7}$$

where k is the wavenumber of the perturbation.

In the gravitational problem we study small deformations of the black brane geometry that satisfy the Einstein-AdS equations. Fixing a radial gauge where g_{vv} and $g_{v\alpha}$ remain unchanged,[1] the metric is perturbed as

$$\frac{ds^2}{R^2} = \frac{dv^2}{v^2 f} + \frac{1}{v^2}\left(-f dt^2 + dz^2 + \delta_{ij} dx^i dx^j + h_{\alpha\beta}(v) e^{ikz} dx^\alpha dx^\beta\right) \,, \tag{6.8}$$

where $i, j = 1, \ldots, n-2$ label the coordinates x^i orthogonal to z.

Near the asymptotic boundary we require that (6.5) holds, so

$$\lim_{v\to 0} h_{\alpha\beta}(v) = \bar{h}_{\alpha\beta} \,. \tag{6.9}$$

Then the $\bar{h}_{\alpha\beta}$ are interpreted as asymptotic gravitational potentials acting on the black brane.

[1] With this, after requiring regularity of the geometry, the horizon position remains at the pole of g_{vv} at $v = \mu^{-1/n}$.

6.2 Holographic stress tensor

The Brown-York stress-energy tensor $\hat{T}_{\alpha\beta}$ is computed in the AdS boundary with regularized metric $\hat{g}_{\alpha\beta}$ at constant, small v. The renormalized metric is (6.4) and the renormalized stress-energy tensor is

$$T_{\alpha\beta} = \lim_{v\to 0}\left(\frac{R}{v}\right)^{n-2}\hat{T}_{\alpha\beta}\,. \tag{6.10}$$

We compute it using counterterm subtraction in AdS_4 and AdS_5 ($n = 3,\, 4$) [127], in which

$$8\pi G\,\hat{T}_{\alpha\beta} = K_{\alpha\beta} - K\hat{g}_{\alpha\beta} - \frac{n-1}{R}\hat{g}_{\alpha\beta} + \frac{R}{n-2}\hat{G}_{\alpha\beta} - \frac{R^3}{12}\left(H^1_{\alpha\beta} - 3H^2_{\alpha\beta}\right)\log(ve^b), \tag{6.11}$$

where $G_{\alpha\beta}$ is the Einstein tensor of the boundary metric $\hat{g}_{\alpha\beta}$, and the last two terms, which enter only in AdS_5 due to the conformal anomaly, are

$$H^1_{\alpha\beta} = \frac{1}{\sqrt{-\hat{g}}}\frac{\delta(\sqrt{-\hat{g}}\hat{R}^2)}{\delta\hat{g}^{\alpha\beta}} = 2\nabla_\alpha\nabla_\beta\hat{R} - 2\hat{g}_{\alpha\beta}\nabla_\rho\nabla^\rho\hat{R} - \frac{1}{2}\hat{g}_{\alpha\beta}\hat{R}^2 + 2\hat{R}\hat{R}_{\alpha\beta}, \tag{6.12}$$

$$\begin{aligned} H^2_{\alpha\beta} = \frac{1}{\sqrt{-\hat{g}}}\frac{\delta(\sqrt{-\hat{g}}\hat{R}_{\rho\sigma}\hat{R}^{\rho\sigma})}{\delta\hat{g}^{\alpha\beta}} =& 2\nabla_\rho\nabla_\beta\hat{R}^\rho_\alpha - \nabla_\rho\nabla^\rho\hat{R}_{\alpha\beta} - \frac{1}{2}\hat{g}_{\alpha\beta}\nabla_\rho\nabla^\rho\hat{R} \\ & - \frac{1}{2}\hat{g}_{\alpha\beta}\hat{R}_{\rho\sigma}\hat{R}^{\rho\sigma} + 2\hat{R}^\rho_\alpha\hat{R}_{\rho\beta}. \end{aligned} \tag{6.13}$$

Here all geometric quantities refer to the metric $\hat{g}_{\alpha\beta}$. The constant b in (6.11) is arbitrary and reflects a renormalization scheme dependence.[2] This ambiguity could be fixed by *e.g.,* imposing supersymmetry on the boundary [128], but this is not particularly well motivated in our set up.

6.3 Gauge invariant perturbation analysis

Following [64] we decompose the perturbations into scalars, vectors and tensors with respect to the group $O(n-2)$ of rotations orthogonal to the z axis (the boost symmetries are broken at finite temperature). In each of these channels one can find

[2] Actually one can include finite contributions to the stress tensor (6.11) (and (6.42)) from H^1 and H^2 with separate coefficients. For simplicity we do not do it, and our choice above is such that the stress tensor is traceless.

master variables $Z_{S,V,T}(v)$, in terms of which all the other metric components can be recovered, up to gauge transformations of the form $h_{\alpha\beta} \to h_{\alpha\beta} - 2\nabla_{(\alpha}\xi_{\beta)}$, with $\xi_\alpha = \xi_\alpha(v)e^{ikz}$, which leave the Z invariant. Since the equations are linear and we want the perturbation to be non-zero at the boundary we can fix the normalization to

$$Z_{S,V,T}(0) = 1\,. \tag{6.14}$$

For tensors and vectors the metric perturbations and the master variables are simply related,

$$h_{ij}(v) = \bar{h}^T_{ij}\, Z_T(v)\,, \tag{6.15}$$

$$h_{ti}(v) = \bar{h}_{ti}\, Z_V(v)\ , \tag{6.16}$$

with $\bar{h}^T_{ij}$ a constant symmetric traceless tensor and $\bar{h}_{ti}$ a constant vector. For scalars the relation is

$$h_{tt}(v) + \frac{1}{2}\left(\frac{n}{n-2} - f\right) h(v) = \bar{H} Z_S(v)\,, \tag{6.17}$$

where

$$h(v) = \delta^{ij} h_{ij}(v)\,. \tag{6.18}$$

At the boundary, (6.17) gives

$$\bar{H} = \bar{h}_{tt} + \frac{1}{n-2}\bar{h}\,. \tag{6.19}$$

The tensor perturbations correspond to shearing deformations of the background geometry in planes orthogonal to z, which then induce shear in the plasma. The vectors create a stationary motion in the background, which will drag with it the black brane and impart momentum to the dual plasma[3]. The scalars introduce gravitational wells $\bar{h}_{tt}$ and averaged external pressures $\delta^{ij}\bar{h}_{ij}$, which cause inhomogeneities in the energy density and local pressure of the plasma.

From the Einstein equations in the bulk we derive the equations for the master tensor variable,[4]

$$Z''_T(v) - \frac{n-f}{fv} Z'_T(v) - \frac{k^2}{f} Z_T(v) = 0\,, \tag{6.20}$$

[3]This motion creates vorticity in the plane (x^i, z).

[4]For $n = 4$ these are the zero-frequency limit of the equations presented in [64].

vector,

$$Z_V''(v) - \frac{n-1}{v} Z_V'(v) - \frac{k^2}{f} Z_V(v) = 0\,, \tag{6.21}$$

and scalar,

$$\begin{aligned} Z_S''(v) + \frac{1}{v}\left(1 - n\frac{(2f-1)(n-2)f+n}{((n-2)f+n)f}\right) Z_S'(v) \\ + \frac{1}{f}\left(\frac{(1-f)^2(n-2)n^2}{((n-2)f+n)v^2} - k^2\right) Z_S(v) = 0. \end{aligned} \tag{6.22}$$

Once Z_S is obtained, the metric components in the scalar sector can be recovered using (6.17) and solving the first-order constraint equations

$$h'(v) = \frac{n(1-f)}{2f^2 v} h_{tt}(v) + \frac{1}{f} h_{tt}'(v), \tag{6.23}$$

and

$$\begin{aligned} h_{zz}'(v) =& \frac{n(1-f)((3n-2)f-n) + 4fk^2v^2}{2f^2v((n-2)f+n)} h_{tt}(v) \\ &+ \frac{n(f-1)}{((n-2)f+n)f} h_{tt}'(v) - \frac{2k^2 v}{(n-2)f+n} h(v). \end{aligned} \tag{6.24}$$

All the components of the metric perturbation that do not appear here can be gauge-fixed to zero. The component $h_{zz}(v)$ is partly constrained by the choice of radial gauge, but since the constraint (6.24) contains h_{zz}' but not h_{zz} there remains gauge freedom to always set

$$\bar{h}_{zz} = 0\,. \tag{6.25}$$

In the boundary geometry this is simply achieved by changing $z \to z + c_z\, e^{ikz}$ with a suitable constant $c_z = O(\bar{h}_{\alpha\beta})$.

Of all the other boundary values in the scalar sector, only $\bar{H}$ (6.19) is physically meaningful, while $\bar{h}_{tt}$ and $\bar{h}$ separately are not. A Weyl transformation of the boundary geometry leaves $\bar{H}$ invariant, but changes $\bar{h}_{tt}$ and $\bar{h}$ separately. Thus the dual conformal field theory is only sensitive to $\bar{H}$.

This can also be understood from the bulk viewpoint. The functions $h_{tt}(v)$ and $h(v)$ are modified by bulk coordinate changes. In particular, a residual radial gauge transformation of the form

$$v \to v\left(1 + \frac{c_v}{2} e^{ikz}\sqrt{1-\mu v^n}\right) \tag{6.26}$$

with constant c_v preserves the radial gauge condition at all v, and transforms

$$\begin{aligned} h_{tt}(v) &\to h_{tt}(v) + \frac{c_v}{2}\left(n-(n-2)f\right)\sqrt{1-\mu v^n}\,, \\ h(v) &\to h(v) - c_v(n-2)\sqrt{1-\mu v^n}\,, \end{aligned} \tag{6.27}$$

while $Z_S(v)$ and $\bar{H}$ remain invariant.[5] One can now choose c_v so that only $\bar{H}$, and not $\bar{h}$ nor $\bar{h}_{tt}$ separately, appears in the perturbed metric. This reflects the fact that changes in bulk radial gauge result into Weyl transformations at the boundary.

In this manner we can get rid of $\bar{h}_{tt}$ or $\bar{h}$ (insofar as they do not enter through $\bar{H}$), but one should be aware that the transformation (6.26) is not analytic near the horizon and generates terms in the metric of the form $\sim\sqrt{1-\mu v^n}$. A gauge where the metric components $h_{\alpha\beta}(v)$ are analytic on the horizon may be preferable over other gauges. In our subsequent calculations we will compute the values of $\bar{h}$ and $\bar{h}_{tt}$ that correspond to this analytic gauge. How this is done will be well illustrated with the hydrodynamic solution to the equations that we present in 6.6. Bear in mind, however, that this is just a convenience: choosing the analytic gauge does not confer any separate invariant meaning to $\bar{h}_{tt}$ nor $\bar{h}$.

6.4 Linear response

When submitted to these external forces, the reaction of the black brane (and the dual field theory state) is expected to show up in the holographic stress-energy tensor: in the tensor channel as an induced shear T_{ij}; in the vector channel as a momentum flow T_{ti} due to the dragging by the geometry; and in the scalar channel as local fluctuations in the energy density T_{tt} and averaged pressure $\delta^{ij}T_{ij}$ of the dual plasma.

6.4.1 Love numbers

The gauge-invariant content of the response can be readily extracted from the solutions to the master equations using the standard AdS/CFT dictionary. In all three

[5] $h_{zz}(v)$ also changes, and keeping $h_{zv}=0$ requires an additional transformation $z\to z+\xi_z(v)e^{ikz}$.

channels, the indices of the differential equation for the variables $Z(v)$ near $v = 0$ are 0 and n. Therefore, near the boundary the solutions are expanded as

$$Z(v) = A(1 + \dots) + B(v^n + \dots)\,. \tag{6.28}$$

A and B are the coefficients of the non-normalizable and normalizable solutions of the metric perturbation. They depend on k, and as is standard in AdS/CFT they correspond, respectively, to the external source acting on the system, and to the expectation value of the operator that the source couples to. In the present case, a non-zero value of A sources a boundary metric deformation $\bar{h}_{\alpha\beta}$ in the corresponding channel, while B determines the response of the system, *i.e.,* the expectation value of the field theory stress-energy tensor, $\delta T_{\alpha\beta}$, generated by the perturbation.

We define the dimensionless Love numbers $\lambda_{T,V,S}$ for each channel as

$$\lambda = R^n \frac{B}{A}\,. \tag{6.29}$$

With our normalization (6.14) this is simply $\lambda = BR^n$.

This definition of the Love numbers is in complete analogy to their introduction in the context of asymptotically flat black holes in [61]. We can make this more manifest if we change to a radial variable

$$r = \frac{R^2}{v}, \tag{6.30}$$

and consider, for instance, a tensor perturbation. Then the corresponding metric component is

$$\frac{R^2}{r^2} g_{ij}(r, z) = \delta_{ij} + \bar{h}^T_{ij} e^{ikz} \left(1 + \dots + \lambda_T \frac{R^n}{r^n} + O\left(r^{-n-1}\right)\right), \tag{6.31}$$

which can be compared to Eq. (1.1) of [61].

6.4.2 From Love numbers to stress tensor

One of the basic entries of the AdS/CFT dictionary (as explained in this context in [64], see also [129]) is that knowledge of the λ is tantamount to knowledge of the expectation values of the two-point correlation functions of the stress-energy tensor $T_{\alpha\beta}$. Both are obtained from the terms of order v^n in the series around $v = 0$

of the metric coefficients. However the relationship between them is not a simple proportionality. The stress-energy tensor contains contributions besides λ that are independent of the boundary condition in the bulk, *i.e.,* of the specific state of the theory. These contributions are renormalization-scheme dependent. We could, for instance, subtract the vacuum stress-energy out of them, but instead we shall keep these vacuum terms in the counterterm subtraction method. This allows us to retain the effects of vacuum polarization.

Note also that in contrast to the calculation in [64], which focused on the quasinormal poles of $\langle T_{\alpha\beta}T_{\rho\sigma}\rangle$, we are not setting the source A to zero. Furthermore, we only consider zero-frequency perturbations. Therefore we are investigating properties of the correlation functions $\langle T_{\alpha\beta}T_{\rho\sigma}\rangle$ that do not show up in quasinormal mode analyses.

The correlators $\langle T_{\alpha\beta}T_{\rho\sigma}\rangle$ can be obtained if we know the one-point function $\langle T_{\alpha\beta}\rangle$ as a function of the source, *i.e.,* of the metric perturbation $\delta\gamma_{\rho\sigma}$, since

$$\langle T_{\alpha\beta}T_{\rho\sigma}\rangle = -\frac{2}{\sqrt{-\gamma}}\frac{\delta\langle T_{\alpha\beta}\rangle}{\delta\gamma^{\rho\sigma}}\,. \tag{6.32}$$

In the gravitational set up $\langle T_{\alpha\beta}\rangle$ is the renormalized holographic stress-energy tensor. For reference, we give its definition in 6.2. In our case the stress-energy tensor takes the form (henceforth omitting the brackets $\langle\cdots\rangle$)

$$T_{\alpha\beta} = T^0_{\alpha\beta} + \delta T_{\alpha\beta}\,, \tag{6.33}$$

where the first term is the stress-energy tensor of the unperturbed, homogeneous black brane,

$$T^0_{tt} = \frac{n-1}{16\pi G}\mu\,, \qquad T^0_{ij} = \frac{1}{16\pi G}\mu\,\delta_{ij}\,, \tag{6.34}$$

and the second term $\delta T_{\alpha\beta}$ contains the inhomogeneities linearly induced by the metric deformations $\delta\gamma_{\alpha\beta} = \bar{h}_{\alpha\beta}e^{ikz}$. Here the bulk Newton constant G is related to the dual theory gauge group's rank N as

$$N^2 \sim GR^{-3} \quad \text{in } \mathrm{AdS}_5\,, \qquad N^{3/2} \sim GR^{-2} \quad \text{in } \mathrm{AdS}_4\,, \tag{6.35}$$

with numerical factors that depend on the specific realization of the duality (*e.g.,* the volume of the compact space transverse to AdS).

Once we compute $\delta T_{\alpha\beta}$ the two-point function can be obtained as

$$\langle T_{\alpha\beta} T_{\rho\sigma} \rangle = -2 \frac{\partial T_{\alpha\beta}}{\partial \bar{h}^{\rho\sigma}} e^{-ikz} \,. \tag{6.36}$$

In the following we give the perturbation solutions in a boundary expansion up to order v^n, and the form of the stress-energy tensor in terms of λ. The latter will be computed in later sections.

It is possible to obtain explicit solutions for any n, but the expressions are cumbersome so we only give them for AdS_5 and AdS_4.

Boundary expansion and stress-energy tensor in AdS_5

In AdS_5 in the tensor sector there are two independent polarizations of the shear, which can be taken to be $h_\times = h_{xy}$, and $h_+ = h_{xx} = -h_{yy}$. For perturbations in the scalar sector we have $h_{xx} = h_{yy} = h/2$. The field theory metric is then

$$\begin{aligned} ds^2 = \gamma_{\alpha\beta} dx^\alpha dx^\beta = \eta_{\alpha\beta} dx^\alpha dx^\beta + \bar{h}_{tt} e^{ikz} dt^2 + \frac{\bar{h}}{2} e^{ikz} (dx^2 + dy^2) \\ + 2\bar{h}_{ti} e^{ikz} dt dx^i + \bar{h}_+ e^{ikz} (dx^2 - dy^2) + 2\bar{h}_\times e^{ikz} dx dy \,. \end{aligned} \tag{6.37}$$

The boundary expansion of Z in the three sectors is the same up to order v^4,

$$Z_{T,S,V}(v) = 1 - \frac{k^2 v^2}{4} + \left(\frac{\lambda_{T,S,V}}{R^4} - \frac{k^4}{16} \log v \right) v^4 + O\left(v^6\right) . \tag{6.38}$$

The metric components in the tensor and vector channels are obtained from $Z_{T,V}$ using (6.15) and (6.16), while for the scalars they are obtained from Z_S and from the solutions of the constraints (6.23), (6.24). We find

$$h_{tt}(v) = \bar{h}_{tt} \left(1 + \frac{\mu}{2} v^4\right) + \frac{\bar{H}}{6} \left(-k^2 v^2 + \left(\frac{4\lambda_S}{R^4} - 4\mu - \frac{k^4}{4} \log v \right) v^4 \right) + O\left(v^6\right) , \tag{6.39}$$

$$h(v) = \bar{h} \left(1 - \frac{\mu}{2} v^4\right) + \frac{\bar{H}}{6} \left(-k^2 v^2 + \left(\frac{4\lambda_S}{R^4} + 2\mu - \frac{k^4}{4} \log v \right) v^4 \right) + O\left(v^6\right) , \tag{6.40}$$

$$h_{zz}(v) = \bar{h}_{zz} + \left(\frac{\bar{h}_{tt}}{2} - \frac{\bar{H}}{3} \right) k^2 v^2 + \frac{\bar{h}_{tt}}{2} \mu v^4 + O\left(v^6\right) . \tag{6.41}$$

The stress-energy tensor is

$$\begin{aligned}
8\pi G\, T_{\alpha\beta}\, dx^\alpha dx^\beta = {} & \left(3dt^2 + dx^2 + dy^2 + dz^2\right) \frac{\mu}{2} \left(1 + \bar{h}_{tt} e^{ikz}\right) \\
& + \left(2\bar{h}_\times\, dx\, dy + \bar{h}_+ (dx^2 - dy^2)\right) e^{ikz} \left(\frac{2\lambda_T}{R^4} + \frac{\mu}{2} - \frac{3k^4}{32}\right) \\
& + 2\bar{h}_{ti}\, dt\, dx^i\, e^{ikz} \left(\frac{2\lambda_V}{R^4} + \frac{\mu}{2} - \frac{3k^4}{32}\right) \\
& + \bar{H} dt^2 e^{ikz} \left(\frac{4}{3}\left(\frac{\lambda_S}{R^4} - \mu\right) - \frac{k^4}{16}\right) \\
& + \bar{H} \left(dx^2 + dy^2\right) e^{ikz} \left(\frac{2\lambda_S}{3R^4} - \frac{\mu}{6} - \frac{k^4}{32}\right) \\
& + dz^2\, \frac{\mu}{2} \bar{h}_{tt} e^{ikz} \,.
\end{aligned} \tag{6.42}$$

The k^4 terms here are renormalization-scheme dependent, and in general are modified to $k^4 \to k^4(1 - 4b/3)$, where the arbitrary constant b is the coefficient of the finite counterterms in (6.11). In the following we fix $b = 0$ for simplicity, but the existence of this ambiguity should be borne in mind.

The gauge-invariant boundary scalar is

$$\bar{H} = \bar{h}_{tt} + \frac{\bar{h}}{2} \,. \tag{6.43}$$

As we discussed in the previous section, in the scalar sector only this parameter is physically meaningful, while $\bar{h}_{tt}$ and $\bar{h}$ separately are not: the coordinate transformations (6.26) change them. Consistently with this, observe that if we rescale

$$\mu \to \mu \left(1 - \bar{h}_{tt} e^{ikz}\right) \,, \tag{6.44}$$

and also perform a rescaling of z (which makes $\bar{h}_{zz} \neq 0$), then we can make $\bar{h}_{tt}$ disappear from (6.42). In other words, the apparent spatial dependence of the plasma temperature does not have any invariant meaning for a CFT. Even if (6.44) suggests that the perturbation makes the horizon position z-dependent, this is a gauge effect. In particular it is easy to see that the surface gravity remains uniform over the horizon, as required by the zeroth law.

We can also write the stress-energy tensor in a way that separates its different contributions and connects more directly to the hydrodynamic expansion at small

k. Define a boundary velocity field u^α as

$$u^t = 1 + \frac{e^{ikz}}{2}\bar{h}_{tt}, \qquad u^i = -\left(\frac{\lambda_V}{R^4\mu} + 1 - \frac{3k^4}{64\mu}\right) e^{ikz}\bar{h}_{ti}\,, \tag{6.45}$$

which is unit-normalized, $\gamma^{\alpha\beta}u_\alpha u_\beta = -1$, and choose

$$\bar{h}_{tt} = -\bar{H}\left(\frac{4}{9}\left(\frac{\lambda_S}{R^4\mu} - 1\right) - \frac{k^4}{48\mu}\right)\,. \tag{6.46}$$

Then the stress-energy tensor takes a 'Landau frame' form

$$T_{\alpha\beta} = \frac{\mu}{16\pi G}\left(\gamma_{\alpha\beta} + 4u_\alpha u_\beta\right) + T^{(1)}_{\alpha\beta}\,, \tag{6.47}$$

in which the first term has the form of a perfect-fluid stress-energy tensor (with conformal equation of state) and the second term is purely spatial, orthogonal to u^α,

$$u^\alpha T^{(1)}_{\alpha\beta} = 0\,. \tag{6.48}$$

It is given by

$$\begin{aligned} 8\pi G\, T^{(1)}_{\alpha\beta}\, dx^\alpha dx^\beta = {} & \left(2\bar{h}_\times\, dx\, dy + \bar{h}_+(dx^2 - dy^2)\right) e^{ikz}\left(\frac{2\lambda_T}{R^4} - \frac{3k^4}{32}\right) \\ & + \bar{H}\left(dx^2 + dy^2 - 2dz^2\right) e^{ikz}\left(\frac{2}{9}\left(\frac{\lambda_S}{R^4} - \mu\right) - \frac{k^4}{96}\right)\,. \end{aligned} \tag{6.49}$$

When the stress-energy tensor is written in this way, the first part can be regarded as capturing how the plasma adapts to the deformed geometry $\gamma_{\alpha\beta}$ and to a velocity flow u_α while maintaining its perfect-fluid form. The choice of u and of $\bar{h}_{tt}$ is indeed such that the vector-channel polarization, and the scalar-channel polarization in the tt direction, are all encoded in this term. The second term, $T^{(1)}_{\alpha\beta}$, measures the polarization effects away from the perfect-fluid form. Bear in mind, though, that both terms in (6.47) contain physical polarizations of the uniform plasma.

We will see that when $k \to 0$ we have

$$\lambda_T \to 0, \qquad \lambda_V \to -\mu R^4, \qquad \lambda_S \to \mu R^4\,. \tag{6.50}$$

This implies that in the limit that the perturbation is homogeneous we have $u^\alpha \to \delta^\alpha{}_t$ and $T^{(1)}_{\mu\nu} \to 0$, and hence there does not remain any physical polarization effect.

Boundary expansion and stress-energy tensor in AdS_4

In AdS_4 there are no tensor perturbations. In the scalar sector, $h(v) = h_{xx}(v)$. The field theory metric is

$$ds^2 = \gamma_{\alpha\beta}dx^\alpha dx^\beta = \eta_{\alpha\beta}dx^\alpha dx^\beta + \bar{h}_{tt}e^{ikz}dt^2 + 2\bar{h}_{tx}e^{ikz}dtdx + \bar{h}_{xx}e^{ikz}dx^2\,. \quad (6.51)$$

The boundary expansion for Z is

$$Z_{V,S}(v) = 1 - \frac{k^2v^2}{2} + \frac{\lambda_{V,S}}{R^3}v^3 + O\left(v^4\right), \quad (6.52)$$

and the stress tensor

$$\begin{aligned} 8\pi G\, T_{\alpha\beta}dx^\alpha dx^\beta = &\left(2dt^2 + dx^2 + dz^2\right)\frac{\mu}{2}\left(1 + \frac{\bar{h}_{tt}}{2}e^{ikz}\right) \\ &+ 2\bar{h}_{ti}\,dt\,dx^i\,e^{ikz}\frac{3}{2}\left(\frac{\lambda_V}{R^3} + \frac{\mu}{3}\right) \\ &+ \bar{H}dt^2e^{ikz}\frac{3}{4}\left(\frac{\lambda_S}{R^3} - \frac{\mu}{2}\right) \\ &+ \bar{H}dx^2e^{ikz}\frac{3}{4}\left(\frac{\lambda_S}{R^3} + \frac{\mu}{6}\right) \\ &+ dz^2\,\frac{\mu}{2}\bar{h}_{tt}e^{ikz}\,. \end{aligned} \quad (6.53)$$

Now the gauge-invariant boundary scalar is

$$\bar{H} = \bar{h}_{tt} + \bar{h}_{xx}\,, \quad (6.54)$$

and the metric functions are

$$h_{xx}(v) = \bar{h}_{xx}\left(1 - \frac{\mu}{2}v^3\right) + \frac{\bar{H}}{4}\left(-k^2v^2 + \left(\frac{2\lambda_S}{R^3} + \mu\right)v^3\right) + O\left(v^4\right), \quad (6.55)$$

$$h_{tt}(v) = \bar{h}_{tt} + \frac{\bar{H}}{4}\left(-k^2v^2 + \left(\frac{2\lambda_S}{R^3} - \mu\right)v^3\right) + O\left(v^4\right), \quad (6.56)$$

$$h_{zz}(v) = \bar{h}_{zz} + \left(\frac{\bar{h}_{tt}}{2} - \frac{\bar{H}}{4}\right)k^2v^2 + \frac{\bar{h}_{tt}}{2}\,\mu v^3 + O\left(v^4\right). \quad (6.57)$$

Similar remarks as in AdS_5 apply about the elimination of $\bar{h}_{tt}$.

The 'Landau frame' expression of the stress-energy tensor is

$$T_{\alpha\beta} = \frac{\mu}{16\pi G}\left(\gamma_{\alpha\beta} + 3u_\alpha u_\beta\right) + T^{(1)}_{\alpha\beta}\,, \quad (6.58)$$

with

$$u^t = 1 + \frac{e^{ikz}}{2}\bar{h}_{tt}, \qquad u^i = -\left(\frac{\lambda_V}{R^3\mu} + 1\right) e^{ikz}\bar{h}_{ti}\,, \tag{6.59}$$

$$\bar{h}_{tt} = -\frac{\bar{H}}{2}\left(\frac{\lambda_S}{R^3\mu} - \frac{1}{2}\right)\,, \tag{6.60}$$

and

$$8\pi G\, T^{(1)}_{\alpha\beta}\, dx^\alpha dx^\beta = \frac{3\bar{H}}{8}(dx^2 - dz^2)e^{ikz}\left(\frac{\lambda_S}{R^3} - \frac{\mu}{2}\right)\,. \tag{6.61}$$

Again, when $k \to 0$ we will find

$$\lambda_V \to -\mu R^3, \qquad \lambda_S \to \frac{\mu R^3}{2}\,, \tag{6.62}$$

which cancel the zero-momentum offsets in u^α and $T^{(1)}_{\mu\nu}$.

6.5 Vacuum polarization

Let us now turn to the explicit calculation of the Love numbers.

It is instructive to begin with the polarization of the vacuum, since it can be solved exactly in all channels, for all k, and in all dimensions. These Love numbers can be regarded as representing Casimir-like stress-energies of the field theory vacuum.

In the vacuum state, with $\mu = 0$, the equations in the three channels become the same,

$$Z''(v) - \frac{n-1}{v}Z'(v) - k^2 Z(v) = 0. \tag{6.63}$$

This equation is solved in terms of modified Bessel functions. The solution that remains finite at the Poincaré horizon, $v \to \infty$, is

$$Z(v) = v^{n/2}K_{n/2}(kv)\,. \tag{6.64}$$

Expanding this solution in series around $v = 0$ we obtain the vacuum Love numbers,

$$\lambda_{\rm vac}(k) = \begin{cases} \left(H_{n/2} - 2\gamma - 2\log\left(\frac{kR}{2}\right)\right)\dfrac{(-1)^{n/2}}{(n/2-1)!\,(n/2)!\,2^n}\,(kR)^n & n \text{ even} \\ \dfrac{\Gamma(-n/2)}{\Gamma(n/2)\,2^n}\,(kR)^n & n \text{ odd} \end{cases} \tag{6.65}$$

where γ is the Euler-Mascheroni constant and $H_n = \sum_{p=1}^{n} p^{-1}$ are the harmonic numbers.

Observe that: (i) the dependence $\sim (kR)^n$ is the one expected for the vacuum energy density of a conformal field theory in n dimensions; (ii) the logarithmic term in even n comes from the conformal anomaly and makes the terms $H_{n/2} - 2\gamma$ scheme dependent; (iii) the sign of the Love numbers (at large enough k) alternates as $n \to n+2$. This dimension-dependence of the sign of the polarization response is the same as for the Casimir energy on a spherical space [130].

In the specific cases of interest to us here,

$$\lambda_{\rm vac}(k) = \frac{(kR)^3}{3} \quad \text{in } \mathrm{AdS}_4\,, \tag{6.66}$$

$$\lambda_{\rm vac}(k) = -\frac{(kR)^4}{16}\left(\log\left(\frac{kR}{2}\right) + \gamma - \frac{3}{4}\right) \quad \text{in } \mathrm{AdS}_5\,. \tag{6.67}$$

For large k the perturbations probe the ultraviolet, short-distance structure of the field theory and the results should be asymptotically independent of whether the state is at finite or zero temperature. In other words, for $k \gg T$ the perturbations concentrate in the bulk around $0 \leq v \lesssim 1/k$ and are largely insensitive to the presence or absence of the brane. It then follows that the Love numbers at large k should always asymptote to their conformal vacuum values, and in particular

$$\lambda(k) \sim (-1)^{\lfloor n/2 \rfloor + 1}(kR)^n\,. \tag{6.68}$$

Finally, note that when $\mu = 0$ the gauge transformations (6.26) do not introduce any non-analytic behavior in the bulk. The gauge is analytic for any arbitrary choice of $\bar{h}_{tt}$.

6.6 Polarization of the finite-temperature plasma

At finite temperature the perturbation equations do not admit exact solutions. We solve them in two ways: in a long-wavelength, hydrodynamic expansion for small k, and numerically for a range of k, up until the large-k asymptotic behavior (6.68) is established.

6.6.1 Long-wavelength expansion: AdS_5

The following are the solutions obtained in a power series expansion in k. They are valid for all $0 < v \leq 1$. We set for simplicity $\mu = 1$. For the case of AdS_5, we have

$$\begin{aligned} Z_T(v) =& 1 - \frac{1}{4}\log\left(1+v^2\right)k^2 + \frac{1}{128}\left(\pi^2 - 4(\log 2)^2 + 8\log\left(\frac{2}{1-v^2}\right)\log\left(1+v^2\right)\right. \\ &\left. + 8\log 2\log\left(1-v^4\right) - 8\mathrm{Li}_2\left(\frac{1+v^2}{2}\right) - 2\mathrm{Li}_2\left(1-v^4\right)\right)k^4 + O\left(k^6\right) , \end{aligned} \tag{6.69}$$

$$\begin{aligned} Z_V(v) =& 1 - v^4 - \frac{1}{4}v^2\left(1-v^2\right)k^2 \\ &+ \frac{1}{32}\left(v^2(1-v^2) - 2v^4\log v - \left(1-v^4\right)\log\left(1+v^2\right)\right)k^4 + O\left(k^6\right) , \end{aligned} \tag{6.70}$$

$$Z_S(v) = 1 + v^4 + \frac{1}{12}\left(-4v^2\left(1+v^2\right) + \left(1+v^4\right)\log\left(1+v^2\right)\right)k^2 + O\left(k^4\right) . \tag{6.71}$$

These are all finite and indeed analytic functions at $v = 1$.

The solutions of the constraint equations are

$$h_{tt}(v) = C\sqrt{1-v^4}\left(1+v^4\right) + \frac{\bar{H}}{6}\left(1-v^2\right)\left(1-v^4\right)k^2 + O\left(k^4\right) \tag{6.72}$$

$$h(v) = 2\bar{H} - 2C\sqrt{1-v^4} + \frac{\bar{H}}{6}\left(\log\left(1+v^2\right) - 2\left(1+v^2\right)\right)k^2 + O\left(k^4\right) \tag{6.73}$$

$$\begin{aligned} h_{zz}(v) =& \bar{h}_{zz} + C\left(1-\sqrt{1-v^4}\right) \\ &- \frac{\bar{H}}{6}\left(v^2 + \log\left(1+v^2\right) - 6C\arcsin(v^2)\right)k^2 + O\left(k^4\right) . \end{aligned} \tag{6.74}$$

Observe here the presence of an integration constant C, which corresponds to

$$C = \bar{h}_{tt} - \frac{\bar{H}}{6}k^2 + O\left(k^4\right) . \tag{6.75}$$

This constant corresponds to the gauge freedom discussed in (6.26), (6.27). The gauge-invariant function $Z_S(v)$ is independent of it, but when $C \neq 0$ the metric functions h_{tt}, h, h_{zz} are not analytic at the horizon position $v = 1$. Therefore if we choose a gauge where the metric is analytic on the horizon, this implies that (restoring now μ, and adding the next order in k)

$$\bar{h}_{tt} = \frac{\bar{H}}{6}\left(\frac{k^2}{\sqrt{\mu}} + \frac{k^4}{24\mu}\left(\pi - 12 + 6\log 2\right)\right) + O\left(k^6\right) . \tag{6.76}$$

The Love numbers that we find are

$$\frac{\lambda_T(k)}{R^4} = \frac{k^2\sqrt{\mu}}{8} + \frac{k^4}{64}\left(3 - 4\log 2\right) - \frac{k^6}{768\sqrt{\mu}}\left(\pi^2 - 12\left(\log 2\right)^2\right) + O(k^8), \tag{6.77}$$

$$\frac{\lambda_V(k)}{R^4} = -\mu + \frac{k^2\sqrt{\mu}}{4} - \frac{k^4}{64} + \frac{k^6}{128\sqrt{\mu}}\left(1 - 2\log 2\right) - \frac{k^8}{6144\mu}\left(\pi^2 + 6 - 24\log 2\right) + O(k^{10}), \tag{6.78}$$

$$\frac{\lambda_S(k)}{R^4} = \mu - \frac{3k^2\sqrt{\mu}}{8} + \frac{k^4}{64}\left(11 - 4\log 2\right) + O(k^6). \tag{6.79}$$

6.6.2 Long-wavelength expansion: $\mathbf{AdS}_4$

Similarly, for AdS_4 (again, setting momentarily $\mu = 1$), we have

$$\begin{aligned} Z_V(v) =& 1 - v^3 - \frac{1}{2}(1-v)v^2k^2 \\ &- \frac{1}{108}\left(9v(1-v)(2+v) + 2\sqrt{3}\left(1-v^3\right)\left(\pi - 6\arctan\left(\frac{1+2v}{\sqrt{3}}\right)\right)\right)k^4 + O\left(k^6\right) \end{aligned} \tag{6.80}$$

$$\begin{aligned} Z_S(v) = 1 + \frac{v^3}{2} - \frac{v^2k^2}{2} + \frac{1}{216}\Bigg(& 36v\left(1+v^2\right) + \sqrt{3}\left(2+v^3\right)\left(\pi - 6\arctan\left(\frac{1+2v}{\sqrt{3}}\right)\right) \\ &- 9\left(2+v^3\right)\log\left(1+v+v^2\right)\Bigg)k^4 + O(k^6)\,, \end{aligned} \tag{6.81}$$

with metric functions

$$\begin{aligned} h_{tt}(v) = \frac{\bar{H}}{24}k^2\Bigg(& -4v^2(1-v^3) + \frac{\left(2+v^3\right)\sqrt{\pi(1-v^3)}\,\Gamma\left(\frac{5}{3}\right)}{\Gamma\left(\frac{7}{6}\right)} \\ &+ v^2\left(-2+v^3+v^6\right)\,{}_2F_1\left(1,\frac{7}{6};\frac{5}{3};v^3\right)\Bigg) + O\left(k^4\right)\,, \end{aligned} \tag{6.82}$$

$$h_{xx}(v) = \bar{H}\left(1 - \frac{k^2}{12}\left(\frac{\sqrt{\pi(1-v^3)}\,\Gamma\left(\frac{5}{3}\right)}{\Gamma\left(\frac{7}{6}\right)} + v^2\left(4 - \left(1-v^3\right)\,{}_2F_1\left(1,\frac{7}{6};\frac{5}{3};v^3\right)\right)\right)\right) + O\left(k^4\right)\,, \tag{6.83}$$

$$h_{zz}(v)=\bar{h}_{zz}+\bar{H}\left(\frac{\sqrt{\pi}\left(1-\sqrt{1-v^3}\right)\,\Gamma\left(\frac{5}{3}\right)}{12\Gamma\left(\frac{7}{6}\right)}-\frac{1}{40}v^2\left(10+v^3\,{}_2F_1\left(1,\frac{7}{6};\frac{8}{3};v^3\right)\right)\right)k^2+O\left(k^4\right)\,. \tag{6.84}$$

Since the expressions are cumbersome, here we have already chosen the analytic gauge, which determines (now with μ restored)

$$\bar{h}_{tt}(k)=\bar{H}\left(\frac{k^2}{\mu^{2/3}}\frac{\sqrt{\pi}\,\Gamma\left(\frac{5}{3}\right)}{12\Gamma\left(\frac{7}{6}\right)}-\frac{k^4}{9\mu^{4/3}}\left(1-\frac{\sqrt{3}\pi^{3/2}}{9\Gamma\left(\frac{2}{3}\right)\Gamma\left(\frac{5}{6}\right)}\right)\right)+O(k^6). \tag{6.85}$$

The Love numbers are, then

$$\frac{\lambda_V(k)}{R^3}=-\mu+\frac{k^2\mu^{1/3}}{2}+\frac{k^4}{12\mu^{1/3}}+\frac{k^6}{72\mu}\left(\sqrt{3}\pi-9+3\log 3\right)+O(k^8), \tag{6.86}$$

$$\frac{\lambda_S(k)}{R^3}=\frac{\mu}{2}+\frac{2k^4}{9\mu^{1/3}}-\frac{k^6}{27\mu}+O(k^8). \tag{6.87}$$

Some comments are in order. First, observe that since this is a small k expansion in $k/T\sim k/\mu^{1/n}\ll 1$, we do not expect to recover the large-k asymptotic behavior (6.68) of the vacuum.

Second, as anticipated in (6.50) and (6.62), we find non-zero values of the vector and scalar Love numbers at very long wavelengths, $k\to 0$. These are such that the physical polarization effects vanish in this limit.

Finally, let us compare these results with those in [65, 66] for the gravitational forcing on the AdS black brane in the hydrodynamic limit. Refs. [65, 66] give

$$T_{\alpha\beta}=\frac{\mu}{16\pi G}\left(\gamma_{\alpha\beta}+nu_\alpha u_\beta\right)+\frac{\mu^{\frac{n-2}{n}}}{8\pi G}C_{\alpha\gamma\beta\delta}u^\gamma u^\delta\,. \tag{6.88}$$

Here $C_{\alpha\mu\beta\nu}$ is the Weyl tensor of the field theory metric $\gamma_{\alpha\beta}$, and the velocity vector u^α is chosen in the Landau frame. This result is valid to two-derivative order in the boundary theory, hence to order k^2 in the linearized approximation. It is straightforward to compare the Weyl term against our result (6.49) up to this order, and verify the agreement between the two calculations in AdS_5. In AdS_4 the boundary Weyl tensor is identically zero, so $T^{(1)}_{\alpha\beta}$ vanishes at order k^2. This is in agreement with the absence of a k^2 term in λ_S in (6.87).[6]

[6]Refs. [65, 66] work in Eddington-Finkelstein coordinates which are regular at the horizon. In

6.6.3 Numerical results

Now we solve the equations by numerical integration. After setting, without loss of generality, $\mu = 1$, we impose regularity on the horizon at $v = 1$ by demanding that the gauge invariant function $Z(v)$ is analytic there. Then we solve the equations in powers of $(1 - v)$ to a high order (without any arbitrary constants other than the overall normalization of Z), and proceed to integrate them numerically towards the boundary, where we extract the Love numbers (6.29). We do the integrations with the `NDSolve` function from MATHEMATICA, which uses a fourth-order Runge-Kutta procedure with adaptive step. The equations are very well behaved so the calculation is unproblematic.

The results are shown in figs. 6.1, 6.2, where we compare them with the hydrodynamic expansion at small k and with the large-k vacuum limit. In 6.8 we give the values of $\bar{h}_{tt}(k)$ that result when we choose a gauge in which $h_{tt}(v)$ (and then also $h(v)$ and $h_{zz}(v)$) is analytic at the horizon.

Overall, we see that the small-k hydrodynamic expansion and the large-k values from the vacuum provide together a good approximation to the numerical calculations. It seems likely that Padé approximants can interpolate efficiently at intermediate values of k, but we have not attempted this.

Observe that the Love numbers can change sign as k increases, *i.e.,* the plasma appears to polarize in opposite ways at small and large wavelengths. This must be interpreted with care, given that the zero-momentum offsets in λ, (6.50) and (6.62), disappear in the stress-energy tensor in Landau frame. The latter may be more appropriate to study the sign of the response. Then we see, for instance, that the anisotropic, transverse pressure induced in the scalar channel, $T^{(1)}_{xx} + T^{(1)}_{yy}$, is negative for all k in AdS_5, and positive for all k in AdS_4. The (gauge-dependent) term $\bar{h}_{tt}$ which, in Landau frame, reflects the perfect-fluid response in the scalar sector, has opposite signs in AdS_5 and AdS_4, but in each case it retains the same sign for all k. On the other hand, the vector-channel velocity u^i induced in AdS_5 changes sign as k is increased, while in AdS_4 it keeps the same orientation at all k.

---

our calculations, in AdS_5 the analytic gauge choice (6.76) coincides up to order k^2 with the Landau gauge (6.46). In AdS_4 the Landau gauge (6.60) does not coincide with the analytic gauge (6.85) at order k^2. However, it seems that this could be remedied if in (6.58) we redefined $\mu \to \mu(1 + c\, e^{ikz})$ with suitably chosen $c = O(\bar{h}_{\alpha\beta}, k^2)$.

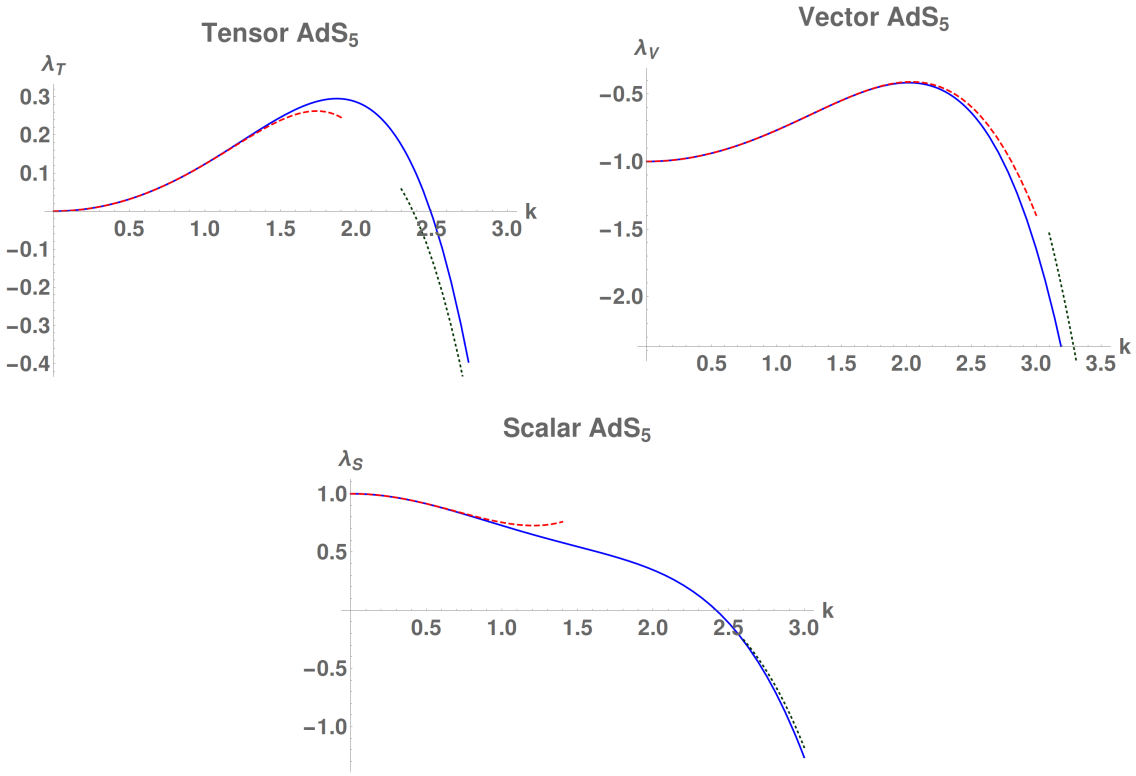

Figure 6.1: Love numbers $\lambda_{T,V,S}$ for black branes in AdS_5 as a function of the wavenumber k. Solid blue: numerical results. Dashed red: perturbative expansions in powers of k, eqs. (6.77), (6.78), (6.79). Dotted green: large-k limit (6.67). We set $R = 1$, the Love numbers $\lambda_{T,V,S}$ are dimensionless, and k is measured in units of $\mu^{1/4} = \pi T$.

Perhaps the most salient feature is that the response coefficients in AdS_4 show a mostly featureless monotonicity in k, while in AdS_5 the behavior differs significantly at large and small k. This occurs even for the vacuum polarization, (6.67), but in this case it is the $\log k$ in the Love number, and not a power of k, that effects the change.

As is familiar from the Casimir effect, the sign of quantum polarization effects is often difficult to anticipate on intuitive grounds. Nevertheless, it may be interesting to investigate further the possible meaning of these results. The exploration of further models might hint at universal features of the geometric polarization.

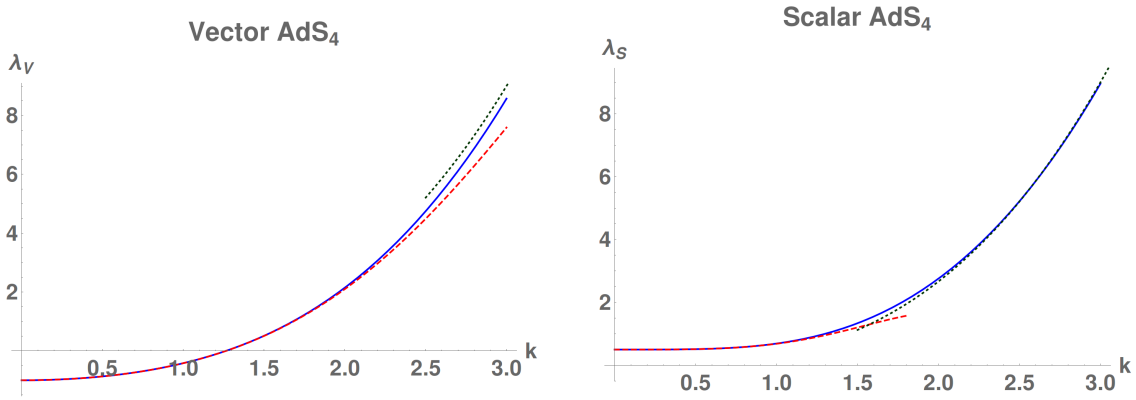

Figure 6.2: Love numbers $\lambda_{V,S}$ for black branes in AdS_4 as a function of the wavenumber k, in units $\mu = 1$. Solid blue: numerical results. Dashed red: perturbative expansions in powers of k, eqs. (6.86), (6.87). Dotted green: large-k limit (6.66). The Love numbers $\lambda_{V,S}$ are dimensionless and k is measured in units of $\mu^{1/3} = 4\pi T/3$.

6.7 Electric polarization

Now we consider the polarizing effect on the black brane of a small static electric field in the z direction, with electric potential $A_t(v)e^{ikz}$. The dual plasma, initially neutral, polarizes into an inhomogeneous distribution of positive and negative charge densities due to the presence of an external chemical potential. We denote the amplitude of the chemical potential by

$$\bar{A}_t = A_t(0)\,, \tag{6.89}$$

and, like in our previous analysis, we introduce the variable Z_E by

$$A_t(v) = \bar{A}_t\, Z_E(v)\,. \tag{6.90}$$

6.7.1 Linear response theory

The Maxwell equations in the black brane background are

$$Z_E''(v) - \frac{n-3}{v} Z_E'(v) - \frac{k^2}{f} Z_E(v) = 0\,. \tag{6.91}$$

The boundary expansion of the solutions takes the form

$$Z_E(v) = A(1 + \dots) + B(v^{n-2} + \dots)\,, \tag{6.92}$$

and the polarization response is determined by the coefficient

$$\lambda_E = R^{n-2}\frac{B}{A}\,. \tag{6.93}$$

This coefficient determines the expectation value of the charge density J^t. In order to find the precise relation, following the standard AdS/CFT prescription we differentiate the Maxwell action with respect to the boundary electric potential to get

$$\langle J^t\rangle = -\frac{1}{2}\sqrt{-\hat{g}}\,n_\mu F^{\mu t}\,, \tag{6.94}$$

where n_μ is the unit normal to the boundary at small v with induced metric $\hat{g}_{\alpha\beta}$. The charge density at the boundary is then given by the electric field in the normal direction.

In AdS_4 the boundary expansion of the solution to (6.91) is

$$Z_E(v) = 1 + \frac{\lambda_E}{R}v + O(v^2) \tag{6.95}$$

which yields

$$\langle J^t\rangle = \bar{A}_t e^{ikz}\frac{\lambda_E}{2R}\,. \tag{6.96}$$

In AdS_5 there is a logarithmic term

$$Z_E(v) = 1 + \left(\frac{\lambda_E}{R^2} + \frac{k^2}{2}\log v\right)v^2 + O(v^3)\,. \tag{6.97}$$

This results in a divergence that is cancelled by adding a boundary counterterm to the action of the form $I_{ct} \sim \log v \int d^4x\sqrt{-\hat{g}}F_{\alpha\beta}F^{\alpha\beta}$. Then

$$\langle J^t\rangle = \bar{A}_t e^{ikz}\left(\frac{\lambda_E}{R^2} + \frac{k^2}{4}\right) \tag{6.98}$$

(again, the term k^2 is renormalization-scheme dependent).

The two-point correlation function is obtained as

$$\langle J^t J^t\rangle = \frac{\delta\langle J^t\rangle}{\delta\bar{A}_t}e^{-ikz}\,. \tag{6.99}$$

6.7.2 Polarization coefficients

In the zero-temperature vacuum, $\mu = 0$, Eq. (6.91) becomes

$$Z_E''(v) - \frac{n-3}{v} Z_E'(v) - k^2 Z_E(v) = 0, \tag{6.100}$$

which is the same as the one for gravitational perturbations if we change $n \to n-2$. Therefore, the electric polarization of the vacuum can be determined from the gravitational vacuum Love numbers as

$$\lambda_{E,\text{vac}}^{(n)}(k) = \lambda_{\text{vac}}^{(n-2)}(k) \tag{6.101}$$

and the latter were computed in (6.65). This gives

$$\begin{aligned} \lambda_{E,\text{vac}} &= -\,kR \quad \text{in } \mathrm{AdS}_4\,, \\ \lambda_{E,\text{vac}} &= -\,\frac{(kR)^2}{2}\left(\log\left(\frac{kR}{2}\right) + \gamma - \frac{1}{2}\right) \quad \text{in } \mathrm{AdS}_5\,. \end{aligned} \tag{6.102}$$

At finite temperature, the long-wavelength hydrodynamic expansion yields

$$Z_E(v) = 1 - v^2 + \frac{1}{4}\left(2v^2 \log(2v) - \left(1+v^2\right)\log\left(1+v^2\right)\right)k^2 + O\left(k^6\right)\,,$$

$$\frac{\lambda_E(k)}{R^2} = -\sqrt{\mu} + \frac{k^2}{4}(2\log 2 - 1) + \frac{k^4}{96\sqrt{\mu}}\left(\pi^2 - 12(\log 2)^2\right) + O(k^6) \quad \text{in } \mathrm{AdS}_5\,, \tag{6.103}$$

and

$$Z_E(v) = 1 - v + \frac{k^2}{2}\left(\frac{2(2v+1)}{\sqrt{3}}\arctan\left(\frac{2v+1}{\sqrt{3}}\right) - \frac{\pi(5v+1)}{3\sqrt{3}} + v\log 3 - \log\left(v^2+v+1\right)\right) + O(k^4)\,,$$

$$\frac{\lambda_E(k)}{R} = -\mu^{1/3} + \frac{k^2}{6\mu^{1/3}}\left(3\log 3 - \sqrt{3}\pi\right) + O(k^4) \quad \text{in } \mathrm{AdS}_4\,. \tag{6.104}$$

The results of the numerical and hydrodynamic evaluations of $\lambda_E(k)$ are presented in Fig. 6.3.

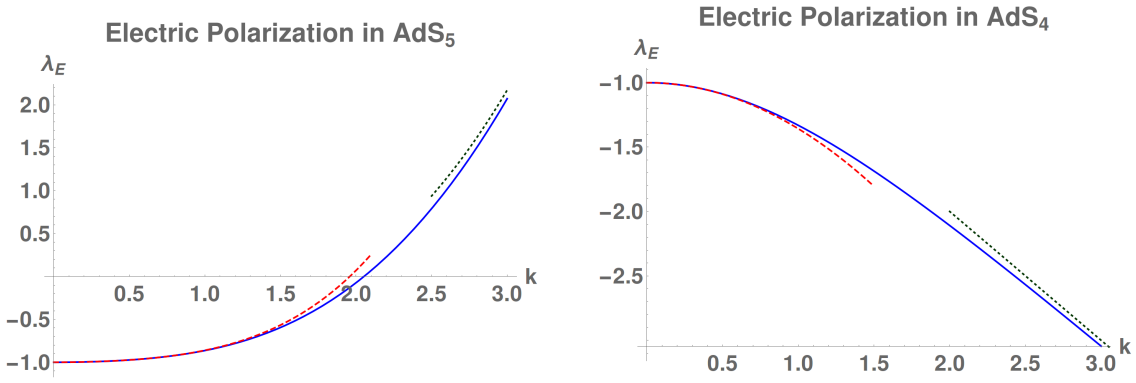

Figure 6.3: Electric polarization response of black branes in AdS_5 and AdS_4 as a function of wavenumber k, in units $\mu = 1$. Solid blue: numerical results. Dashed red: perturbative expansions in powers of k, eqs. (6.103), (6.104). Dotted green: large-k limit (6.102).

Observe that as $k \to 0$ the electric polarization λ_E and the charge density $\langle J^t \rangle$ take non-zero values. This is indeed expected: this is a uniform perturbation of the black brane that adds a uniform charge distribution to it. What we then have is the Reissner-Nordstrom AdS black brane in the limit of small, linearized charge density (which does not backreact on the geometry).

Of course this uniform charge is not a polarization effect. The way to remove it is simple. Rather than a charge density induced by an electric potential, the actual polarization effect is the charge separation in the neutral plasma, *i.e.,* the appearance of a dipole distribution

$$D_z = \partial_z J^t = \mathrm{Re}(ikJ^t) \tag{6.105}$$

induced as a response to an external electric field

$$E_z = \partial_z A_t = \mathrm{Re}(ikA_t)\,. \tag{6.106}$$

Then when $k \to 0$ the dipole polarization vanishes.

Notice that a similar remark could be applied to the geometric polarization: like in the Casimir effect, the measurable effect of the polarization is not so much the energy itself but the force that arises when the geometrical set up varies.

6.8 Analytic gauge

We have discussed that certain choices of the radial coordinate v lead to metric functions $h_{tt}(v)$, $h(v)$, $h_{zz}(v)$ that behave like $\sim \sqrt{1-\mu v^n}$ near the horizon at $v = \mu^{-1/n}$. This non-analyticity is inconvenient for showing that the horizon is regular. For instance, if one changes $(t, v) \to (x^+, v)$ where the latter are ingoing Eddington-Finkelstein coordinates, then if the v-gauge is not analytic the metric in these coordinates is singular at the horizon. Proving horizon regularity requires to first perform a change of the type (6.26) to an analytic radial gauge. Nevertheless, invariants such as the surface gravity can be computed in any radial gauge.

The transformations (6.26) alter $\bar{h}_{tt}$. Fig. 6.4 gives the values of $\bar{h}_{tt}(k)$ that result when taking the analytic gauge. We compare them with the hydrodynamic calculations of 6.6.

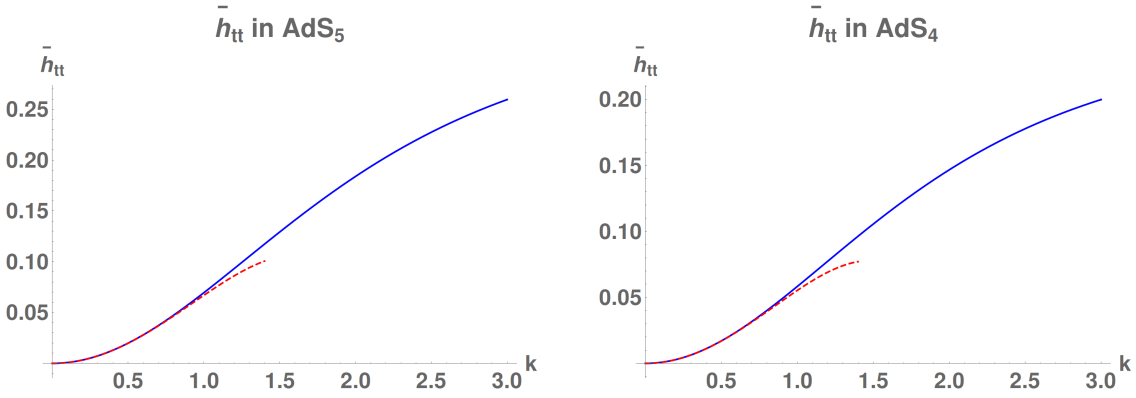

Figure 6.4: Values of $\bar{h}_{tt}(k)$ in the analytic gauge, for AdS$_5$ and AdS$_4$. Solid blue: numerical results. Dashed red: perturbative expansions in powers of k, eqs. (6.76), (6.85).

Chapter 7

Horndeski's Theory

This chapter explores some mathematical properties of Horndeski's theories as extensions of General relativity. Namely, the *well-psedness* of the equations of motion and the existence and uniqueness of global solutions. We do so by focusing on the subset of Horndeski's theories that are known to lead to symmetric hyperbolic equations of motion in a generalized harmonic gauge. We analyze, in some examples, the advantages of using the Einstein frame for the action. We use fully numerical time evolutions of one particular subclass of theories to exemplify some of the pathologies that may arise. This chapter is based on the research published in [131].

Horndeski's theories describe gravitational interactions in terms of a metric tensor g_{ab} and a scalar field ϕ. Their equations of motion are determined from the action,

$$S = \frac{1}{16\pi G}\int d^4x\sqrt{-g}(\Sigma_{i=1}^{5}\,\mathcal{L}_i) \tag{7.1}$$

where,

$$\mathcal{L}_1 = R + X - V(\phi)\,, \tag{7.2}$$
$$\mathcal{L}_2 = \mathcal{G}_2(\phi, X)\,, \tag{7.3}$$
$$\mathcal{L}_3 = \mathcal{G}_3(\phi, X)\Box\phi\,, \tag{7.4}$$
$$\mathcal{L}_4 = \mathcal{G}_4(\phi, X)R + \partial_X\mathcal{G}_4(\phi, X)\delta^{ac}_{bd}\nabla_a\nabla^b\phi\nabla_c\nabla^d\phi\,, \tag{7.5}$$
$$\mathcal{L}_5 = \mathcal{G}_5(\phi, X)G_{ab}\nabla^a\nabla^b\phi - \frac{1}{6}\partial_X\mathcal{G}_5(\phi, X)\delta^{ace}_{bdf}\nabla_a\nabla^b\phi\nabla_c\nabla^d\phi\nabla_e\nabla^g\phi\,. \tag{7.6}$$

with $X = -1/2\nabla_a\phi\nabla^a\phi$, G_{ab} the Einstein tensor, $\mathcal{G}_i$ are functions of the scalars $\{\phi, X\}$, V is a potential and $\delta^{b_1..b_n}_{a_1..a_n}$ is the generalized Kronecker delta symbol.

A thorough analysis of hyperbolicity properties of the resulting equations of motion, given the complexity of the PDE system, is naturally a difficult task. One such study has been presented recently in [93] (see also [94]). Here, following steps taken to establish local well posedness of Einstein equations [132], –whereby the introduction of harmonic coordinates renders Einstein equations manifestly symmetric hyperbolic– a judicious coordinate choice is found to guarantee strong hyperbolicity. Within this context, it is shown that only a special subset of Horndeski's theories leads to strong hyperbolicity in harmonic gauge in the nonlinear regime.

This subset is given by the action,

$$S = \frac{1}{16\pi}\int d^4x\sqrt{-g}\left[(1+\mathcal{G}_4(\phi))R + X - V(\phi) + \mathcal{G}_2(\phi,X)\right] \ , \tag{7.7}$$

Notice the action above corresponds to the so called Jordan frame (as the Ricci scalar appears multiplied by a non-trivial function of ϕ). The equations of motion obtained from this action can be found in [93]. A conformal transformation, of the form $\tilde{g}_{ab} = \Omega^2 g_{ab}$ with $\Omega = \sqrt{1+\mathcal{G}_4(\phi))}$, can be exploited to obtain the equations in the Einstein frame. We assume that the conformal factor Ω never vanishes, which ensures that the transformation is well-defined and the two formulations of the theory are equivalent. It allows one to rewrite the above action as,

$$S = \frac{1}{16\pi}\int d^4x\sqrt{-\tilde{g}}\Bigg\{\tilde{R} + \frac{1}{(1+\mathcal{G}_4(\phi))^2}\Big[\left(3[\mathcal{G}_4'(\phi)]^2 + 1 + \mathcal{G}_4(\phi)\right)\tilde{X} \\ -V(\phi) + \mathcal{G}_2\left(\phi, (1+\mathcal{G}_4(\phi))\tilde{X}\right)\Big]\Bigg\} \ , \tag{7.8}$$

where $\tilde{X} = -1/2\tilde{\nabla}_c\phi\,\tilde{\nabla}^c\phi$. From this action, the equations of motion are

$$\tilde{G}_{ab} = \left[\frac{3[\mathcal{G}_4'(\phi)]^2 + 1 + \mathcal{G}_4(\phi)}{2(1+\mathcal{G}_4(\phi))^2}\,\tilde{X} + \frac{-V(\phi)+\mathcal{G}_2(\phi,X)}{2(1+\mathcal{G}_4(\phi))^2}\right]\tilde{g}_{ab} \\ + \left[\frac{3[\mathcal{G}_4'(\phi)]^2}{2(1+\mathcal{G}_4(\phi))^2} + \frac{1+\partial_X\mathcal{G}_2(\phi,X)}{2(1+\mathcal{G}_4(\phi))}\right]\tilde{\nabla}_a\phi\tilde{\nabla}_b\phi \ , \tag{7.9}$$

$$\left[\tilde{g}^{ab} - \frac{(1+\mathcal{G}_4(\phi))^2\partial^2_{XX}\mathcal{G}_2(\phi,X)}{3[\mathcal{G}_4'(\phi)]^2 + (1+\mathcal{G}_4(\phi))(1+\partial_X\mathcal{G}_2(\phi,X))}\tilde{\nabla}^a\phi\tilde{\nabla}^b\phi\right]\tilde{\nabla}_a\tilde{\nabla}_b\phi \\ = \frac{1}{3[\mathcal{G}_4'(\phi)]^2 + (1+\mathcal{G}_4(\phi))(1+\partial_X\mathcal{G}_2(\phi,X))}\Bigg\{V'(\phi) - \partial_\phi\mathcal{G}_2(\phi,X) - 2\,\mathcal{G}_4'(\phi)\frac{V(\phi)-\mathcal{G}_2(\phi,X)}{1+\mathcal{G}_4(\phi)} \\ + \left[2(1+\mathcal{G}_4(\phi))\partial^2_{\phi X}\mathcal{G}_2(\phi,X) + \mathcal{G}_4'(\phi)\Big(6\mathcal{G}_4''(\phi) - 1 - 3\partial_X\mathcal{G}_2(\phi,X) - 6\frac{[\mathcal{G}_4'(\phi)]^2}{1+\mathcal{G}_4(\phi)}\Big)\right]\tilde{X} \\ + 2\mathcal{G}_4'(\phi)(1+\mathcal{G}_4(\phi))\partial^2_{XX}\mathcal{G}_2(\phi,X)\tilde{X}^2\Bigg\} \ . \tag{7.10}$$

In order to write the scalar field equation in the convenient form (7.10), we have divided it by the overall factor $3[\mathcal{G}_4'(\phi)]^2 + (1+\mathcal{G}_4(\phi))(1+\partial_X\mathcal{G}_2(\phi,X))\,(1+\mathcal{G}_4(\phi))^{-2}$. In the following, we will assume that this factor is non-zero. Notice that neither

of the right hand sides in eqns (7.9)-(7.10) involve second order derivatives of the relevant fields (metric or scalar), and, the hyperbolic properties of the system can be assessed independently for g_{ab} and ϕ. In the case of the metric tensor, such properties only depend on the metric tensor itself and we can draw from the vast knowledge about properties of Einstein equations (see e.g. [133]). In particular, we recall that they can be straightforwardly rendered into symmetric hyperbolic form. Indeed, following again [132], one can introduce harmonic coordinates ($\tilde{\Gamma}_a = 0$), and equation (7.9) becomes symmetric hyperbolic. Further, we recall the speed of propagation of perturbations is *independent of the metric tensor itself* (thus the equation is linearly degenerate and no shocks can arise from smooth initial data). Importantly, the observations above with regards to well posedness (at least locally) and linear degeneracy are certainly valid for other gauges. As we shall discuss below, regardless of the gauge choice, the scalar field equation has particular 'worrisome' properties.

The principal part of the scalar field equation depends on $\{g_{ab}, \phi, \partial_a\phi\}$. Indeed, the principal part of the equation for ϕ, equation (7.10), is given by a wave equation of a modified metric

$$\gamma^{ab} = \tilde{g}^{ab} - \frac{(1+\mathcal{G}_4(\phi))^2\partial^2_{XX}\mathcal{G}_2(\phi,X)}{3[\mathcal{G}_4'(\phi)]^2 + (1+\mathcal{G}_4(\phi))(1+\partial_X\mathcal{G}_2(\phi,X))}\tilde{\nabla}^a\phi\tilde{\nabla}^b\phi\,. \tag{7.11}$$

Thus, propagation speeds of scalar field perturbations depend on the state of the field and its gradient. As a consequence, shocks can develop from smooth initial data, at which point uniqueness of the solution is lost and with it, well posedness [1]. Another potential problem is that the equation itself might change character pointwise in the spacetime. Indeed the character of this equation, *i.e.,* hyperbolic, elliptic or parabolic, is determined by the eigenvalues of γ^{ab}. Namely, if no eigenvalue is zero, and the sign of only one of them is opposite to the others the equation is hyperbolic [2] (with + signature it would be one negative). If all signs are the same the equation is elliptic and if at least one eigenvalue is zero parabolic. For a well defined initial value problem describing a small departure from General Relativity, the equation would be hyperbolic. Notice that at the linear level, equation (7.10) is symmetric hyperbolic, linearly degenerate and the scalar field perturbations propagate at the

[1] To recover it, further conditions would need to be imposed, see discussions in [134, 135].

[2] If more than one is of opposite sign, the equation would be ultra-hyperbolic in character.

speed of light of the metric $\tilde{g}_{ab}$. However, at the non-linear level –even with smooth initial data– if dispersion does not win and gradients grow (assuming $\partial_{XX}\mathcal{G}_2 \neq 0$) the character of the equation can change and, by continuity, it would do so by turning –locally– to parabolic and then elliptic. Thus either through a change of character, or by loss of uniqueness due to shocks well posedness could be lost.

Interestingly, a change in character in spherically symmetric non-linear studies in subclasses of Horndeski's theories has been identified, for instance in k-essence [136] and Einstein-Dilaton-Gauss-Bonnet [137]. The theories studied in these references are seemingly different from Eq. (7.7), but they can be linked to a Horndeski theory through the following mappings. In the former case, only the kinetic term $\mathcal{G}_2(X)$ is present, while in the latter we only have $\mathcal{G}_5(\phi, X) = -\lambda \ln|X|$ where λ is the coupling constant [3].

Notice however that the potential change in character or the development of shocks might be absent in special cases. To assess this, consider the following transformation for the scalar field

$$\tilde{\phi} = \int \frac{3[\mathcal{G}_4'(\phi)]^2 + (1+\mathcal{G}_4(\phi))(1+\partial_X\mathcal{G}_2(\phi,X))}{(1+\mathcal{G}_4(\phi))^2}\,\mathrm{d}\phi\,. \tag{7.12}$$

The scalar equation of motion becomes

$$\tilde{g}^{ab}\tilde{\nabla}_a\tilde{\nabla}_b\tilde{\phi} = \frac{1}{(1+\mathcal{G}_4(\phi))^2}\Bigg\{V'(\phi) - \partial_\phi\mathcal{G}_2(\phi,X) - 2\,\mathcal{G}_4'(\phi)\frac{V(\phi)-\mathcal{G}_2(\phi,X)}{1+\mathcal{G}_4(\phi)} \\ - \mathcal{G}_4'(\phi)\left[6\mathcal{G}_4''(\phi) - 1 + \partial_X\mathcal{G}_2(\phi,X) - 6\frac{[\mathcal{G}_4'(\phi)]^2}{1+\mathcal{G}_4(\phi)}\right]\tilde{X}\Bigg\}\,, \tag{7.13}$$

where ϕ is to be understood as a function of $\tilde{\phi}$: $\phi(\tilde{\phi})$, provided the relation (7.12) is invertible. Then, the scalar field $\tilde{\phi}$ obeys a wave equation of the original metric $\tilde{g}_{ab}$, and no pathologies would arise (unless $\tilde{g}^{ab}$ itself becomes singular). However, the equivalence between the new scalar field and the old one is a nontrivial question, as the transformation (7.12) may not always be well defined. In particular, the requirement that the newly defined scalar field should verify $\tilde{\nabla}_{[\mu}\tilde{\nabla}_{\nu]}\tilde{\phi} = 0$ further

[3] Although such a function $\mathcal{G}_5$ is not smooth at $X = 0$, the equations of motion are well defined everywhere [138].

implies that $\tilde{\nabla}_{[\mu}\left(\tilde{X}\,\partial_{\nu]}\phi\right) = 0$, thus $\tilde{X}\partial_a\phi$ is twist-free. Such condition could be regarded as an external constraint to ensure well posedness. In the simple example of Sec 7.1.1, we perform a similar redefinition of the scalar field which is always well defined as it does not depend on X. As an illustration, we show in the nonlinear example of Sec. 7.2 how the twist evolves for several representative cases.

Notice that by working in the Einstein frame, we have straightforwardly recovered the conclusions from [93], *i.e., local well posedness* of this class of Horndeski's theories by virtue of the equations of motion for g_{ab} and ϕ being symmetric hyperbolic. The question of global solutions to this theory is, naturally, far more involved which is not unexpected as this is already a complex question in General Relativity! Nevertheless, some relevant conclusions can be drawn. Namely,

- At the nonlinear level for *weak data*, the equation satisfies Klainerman's *null condition* [139] if $\mathcal{G}$ is at least order X ($\propto \tilde{X}$). Consequently, together with stability of Minkowski results [140] or the weak null energy condition satisfaction by Einstein equations [141], together with contributions of ϕ satisfying Strauss' conjecture [142] would imply the (subclass) of Horndeski's theories considered has a global solution in the small data case. Beyond the weak case however, little is known; though, as mentioned, the propagation speed dependence on the field and its gradient implies a high likelihood of shocks arising and/or a change in character. Would such issues arise and be "invisible" to far observers? It would depend on whether they generically form *inside* a black hole. In such case, pathological issues might be shielded from problematic consequences at the classical level. A priori this seems far from guaranteed; indeed, in the context of ref [137], a change in character of the equations is encountered prior to a black hole being formed. We will also illustrate such a behavior in section 7.2.

- Since the speed of propagation of (perturbations of) metric tensor and scalar field can be different, black holes are defined by the fastest outward propagation speeds. Additionally, gravitational Cherenkov radiation would be possible and high energy cosmic rays can help to draw constraints on this process (e.g. [143]).

Last, we can also check what we can draw from adopting the harmonic gauge in the Einstein frame and its implication in the Jordan frame. For starters, it is trivial to determine that $\tilde{\Gamma}^a = \Omega^{-2}\left(\Gamma^a - 2\nabla^a \ln\Omega\right)$. Thus, in the Jordan frame the harmonic condition from the Einstein frame calls for adopting coordinates that satisfy instead $\Gamma^a = 2\nabla^a \ln\Omega$. Which implies

$$\Gamma^a = \frac{\mathcal{G}_4'}{1+\mathcal{G}_4}\nabla^a\phi \tag{7.14}$$

which is precisely the condition derived in [93] in the Jordan frame to obtain a strongly hyperbolic system of equations and establish local well posedness.

7.1 Illustration in specific cases

7.1.1 Jordan and Einstein frames equations of motion. Hyperbolicity and implications

Within the class of Horndeski's theories, one of the simplest ones is given by,

$$S = \frac{1}{16\pi}\int d^4x\sqrt{-g}\left[\phi R - \frac{\omega}{\phi}g^{\alpha\beta}\nabla_\alpha\phi\nabla_\beta\phi\right] , \tag{7.15}$$

where ω is a function of ϕ only. A comparison with Horndeski's Lagrangian implies,

$$\mathcal{G}_2 = \frac{(2\omega-\phi)}{\phi}X \ , \ \mathcal{G}_4 = \phi - 1\,;$$

with all the other functions (including the potential) set to zero. From our previous discussion, since $\partial_{XX}\mathcal{G}_2 = 0$, it is clear that in the Einstein frame characteristics of both metric tensor and scalar field are determined by the metric. This theory has recently been the subject of fully non-linear studies in the context of binary black neutron star mergers [77, 144, 145]. In such scenarios global solutions describing several orbits, merger and aftermath have been successfully achieved. This suggests an underlying robustness of the equations of motion which can be understood at the analytical level rather simply. To fix ideas, let us consider the vacuum case. The field equations derived from the (Jordan frame) action (7.15) are

$$R_{\mu\nu} - \frac{1}{2}g_{\mu\nu}R = \frac{\omega}{\phi^2}\left(\nabla_\mu\phi\nabla_\nu\phi - \frac{1}{2}g_{\mu\nu}\nabla^\alpha\phi\nabla_\alpha\phi\right) + \frac{1}{\phi}\left(\nabla_\mu\nabla_\nu\phi - g_{\mu\nu}\Box\phi\right) \ , \tag{7.16}$$

$$\Box\phi = -\frac{\phi R}{2\omega} + \left(\frac{1}{2\phi} - \frac{\omega'}{2\omega}\right)(\nabla\phi)^2 \,. \tag{7.17}$$

Upon replacing the Ricci scalar one re-expresses equation (7.17) as,

$$\Box\phi = -\frac{\omega'}{3+2\omega}(\nabla\phi)^2 \,. \tag{7.18}$$

which satisfies the null condition in the weak case. However, a non-trivial coupling –at the level of the principal part– is present in equation (7.16). Furthermore, notice the right hand side of this equation contains second derivatives of the scalar field –thus such terms do belong to the principal part of the system. As well, because of such terms, the right hand side does not seemingly satisfy the null energy condition. Both these observations indicate it is not a priori clear that solutions obtained from this system are well behaved.

However, through the conformal transformation [146],

$$g_{\mu\nu} \longrightarrow \tilde{g}_{\mu\nu} = \phi\, g_{\mu\nu} \,, \tag{7.19}$$

and the scalar field redefinition

$$\phi \longrightarrow \tilde{\phi} = \int \frac{(3+2\omega)^{1/2}}{\phi}\, d\phi \,, \tag{7.20}$$

one recasts the theory in the Einstein frame. In this frame, the theory is defined by the standard Einstein-Hilbert action with an extra field,

$$S = \int d^4x\sqrt{-\tilde{g}}\left[\frac{\tilde{R}}{16\pi} - \frac{1}{2}\,\tilde{g}^{\mu\nu}\tilde{\nabla}_\mu\tilde{\phi}\tilde{\nabla}_\nu\tilde{\phi}\right] \,. \tag{7.21}$$

The field equations are the usual Einstein equations with the scalar field as a source together with a rather trivial equation for the scalar field itself,

$$\tilde{R}_{\mu\nu} - \frac{1}{2}\tilde{g}_{\mu\nu}\tilde{R} = 8\pi\left(\tilde{\nabla}_\mu\tilde{\phi}\tilde{\nabla}_\nu\tilde{\phi} - \frac{1}{2}\,\tilde{g}_{\mu\nu}\tilde{\nabla}^\alpha\tilde{\phi}\tilde{\nabla}_\alpha\tilde{\phi}\right) \,, \tag{7.22}$$

$$\tilde{\Box}\tilde{\phi} = 0 \,. \tag{7.23}$$

The equation for the (conformal) metric $\tilde{g}_{ab}$ is amenable to the standard analysis of well posedness in Einstein equations (e.g. [133]). In particular, adopting *harmonic coordinates* ($\tilde{\Gamma}_a = 0$) the principal part of equation (7.21) becomes just ten wave

equations. Further, the right hand side now obeys the null energy condition. Thus, in the Einstein frame it follows that at least a local in time solution will exist and standard geometrical arguments can be exploited to assess general features of the spacetime behavior.

What does this imply in the Jordan frame? Here, since, $\tilde{\Gamma}_a = \phi^{-2}\left(\phi\Gamma_a - \nabla_a\phi\right)$, the discussion above suggests adopting coordinates satisfying $\Gamma_a = \phi^{-1}\nabla_a\phi$. With this choice, the equations of motion in the Jordan frame can be re-expressed in the following way. Beginning with

$$R_{ab} = \frac{\omega}{\phi^2}\nabla_a\phi\nabla_b\phi + \frac{1}{2\phi}g_{ab}\Box\phi + \frac{1}{\phi}\nabla_a\nabla_b\phi\,, \tag{7.24}$$

we then define $\hat{R}_{ab} + \nabla_{(a}\Gamma_{b)} \equiv R_{ab}$ (i. e. taking out the covariant derivative of the trace of the Christoffels). Now, replacing in such a term the condition on the coordinates, we obtain

$$\hat{R}_{ab} = \frac{\omega+1}{\phi^2}\nabla_a\phi\nabla_b\phi + \frac{1}{2}g_{ab}\phi^{-1}\Box\phi\,. \tag{7.25}$$

A priori we still have second order derivatives in the right hand side of the above equation, but –on shell– we can use the equation for the field ϕ still. Recall,

$$\Box\phi = -\frac{\omega'}{(3+2\omega)}(\nabla\phi)^2\,. \tag{7.26}$$

Thus, the metric equation results in

$$\hat{R}_{ab} = \frac{(1+\omega)}{\phi^2}\nabla_a\phi\nabla_b\phi - \frac{\omega'}{2\phi(3+2\omega)}g_{ab}(\nabla\phi)^2\,. \tag{7.27}$$

And it is evident the right hand side can satisfy the null energy condition for $w \geq 1$.

7.2 Exploring the non-linear behavior

We now turn our attention to Horndeski's theories with a nonlinear kinetic term $\mathcal{G}_2(\phi, X) = -gX^2$, with all other functions, as well as the potential, set to zero for simplicity. This choice, similar to those adopted in [136], can be thought of as the first nonlinear term in a Taylor expansion of the kinetic term in a k-essence theory,

$$S = \int d^4x\sqrt{-g}\left[R + X - gX^2\right]\,. \tag{7.28}$$

Our goal is to study the nonlinear behavior of the theory and explore the possible phenomenology that can arise. While we are restricting to a rather special case, as we shall see, a number of possible pitfalls can appear which are likely to manifest in more general cases. To simplify the treatment and presentation, we concentrate on spherically symmetric scenarios and present several cases defined by different initial conditions as well as the value of the coupling g. For simplicity we adopt Schwarzschild coordinates where the metric can be written as,

$$ds^2 = -\alpha^2 dt^2 + a^2 dr^2 + r^2 d\Omega^2 \,. \tag{7.29}$$

Thus the only dynamical metric functions are the lapse function $\alpha(t, r)$ and $a(t, r)$. Recall that these coordinates become singular when a horizon forms. Such scenario takes place when $l^\mu \nabla_\mu r = 0$, where l^μ is a null vector [136]. In the gauge (7.29), this is simply $\alpha = 0$. Consequently, with our current implementation we can explore up to black hole formation. Despite this limitation, as we shall see below, one can identify several problematic scenarios arising either outside the black hole or even prior to its formation. Thus, severe restrictions to well posedness arise which are not cloaked by a horizon for asymptotic observers.

To simplify the discussion and the numerical implementation, we introduce standard first order variables as used in [40],

$$\Phi \equiv \phi' \,, \qquad \Pi \equiv \frac{a}{\alpha}\dot{\phi} \,, \tag{7.30}$$

using the notation $\dot{f} = \partial_t f$ and $f' = \partial_r f$. In the special case of $\mathcal{G}_2(\phi, X) = \mathcal{G}_2(X)$, as in (7.28), equations (7.9) and (7.10), respectively, take the form

$$R_{\mu\nu} - \frac{1}{2} g_{\mu\nu} R = \left[\frac{X + \mathcal{G}_2(X)}{2}\right] g_{\mu\nu} + \left[\frac{1 + \partial_X \mathcal{G}_2(X)}{2}\right] \nabla_\mu \phi \nabla_\nu \phi \,, \tag{7.31}$$

$$\left[g^{\mu\nu} - \frac{\partial^2_{XX} \mathcal{G}_2(X)}{1 + \partial_X \mathcal{G}_2(X)} \nabla^\mu \phi \nabla^\nu \phi\right] \nabla_\mu \nabla_\nu \phi = 0 \tag{7.32}$$

where the effective inverse metric $\gamma^{\mu\nu}$, as in equation (7.11), is given by

$$\gamma^{\mu\nu} = g^{\mu\nu} - \frac{\partial^2_{XX} \mathcal{G}_2(X)}{1 + \partial_X \mathcal{G}_2(X)} \nabla^\mu \phi \nabla^\nu \phi \,. \tag{7.33}$$

Now, in order to monitor the character of the equation of motion for the scalar field (7.32), the eigenvalues of the effective inverse metric must be computed. In

particular we extract at any given time the two eigenvalues, here labeled as $\lambda_\pm$ for every spatial point. Since we are mainly interested in one of the eigenvalues going to zero, the relevant quantities will be $\min(\lambda_+)$ and $\max(\lambda_-)$, where $\min(\cdot)$ and $\max(\cdot)$ refer to the minimum and maximum in the spatial (radial) direction, at any given time. It is important to keep in mind that although $\lambda_+ > 0$ and $\lambda_- < 0$ for $\phi = 0$, this is not necessarily the case for arbitrary configurations. In fact, the equations will change character when these conditions cease to be satisfied. The two eigenvalues can be expressed as

$$\begin{aligned}\lambda_\pm &= \frac{\gamma^{tt}+\gamma^{rr}}{2} \pm \sqrt{\left(\frac{\gamma^{tt}+\gamma^{rr}}{2}\right)^2 - \gamma^{tt}\gamma^{rr} + (\gamma^{tr})^2} \\ &= \frac{\gamma^{tt}+\gamma^{rr}}{2} \pm \sqrt{\left(\frac{\gamma^{tt}+\gamma^{rr}}{2}\right)^2 - \det(\gamma^{\mu\nu})}\,. \end{aligned} \tag{7.34}$$

It is evident that the system will become parabolic when $\det(\gamma^{\mu\nu}) = 0$, as expected. Additionally, it is important to keep track of the characteristic speeds, or propagation velocities, of the scalar field. This can be done by extracting the eigenvalues, here labeled as $V_\pm$, of the principal part of the (first order) equations of motion for Φ and Π. These eigenvalues determine the shape of the light cones for the scalar field, and can be used to identify features such as sound horizons (horizons for the scalar field [136]). With our conventions, asymptotically $V_+ \to 1$ while $V_- \to -1$ describing, respectively, the incoming and outgoing modes of the field. A sound horizon –with respect to asymptotic observers– will appear[4] when $V_- = 0, V_+ \geq 0$. Again, as in the case of the effective metric, we are interested in $\min(V_+)$ and $\max(V_-)$.

$$V_\pm = -\frac{\gamma^{tr}}{\gamma^{tt}} \pm \sqrt{\left(\frac{\gamma^{tr}}{\gamma^{tt}}\right)^2 - \frac{\gamma^{rr}}{\gamma^{tt}}} = -\frac{\gamma^{tr}}{\gamma^{tt}} \pm \sqrt{-\frac{\det(\gamma^{\mu\nu})}{(\gamma^{tt})^2}}\,. \tag{7.35}$$

As mentioned, when $\det(\gamma^{\mu\nu}) = 0$ the equation changes character. However, the rate at which $(\gamma^{tt})^2 \to 0$ distinguishes two important cases with respect of the *type* of change. Recall that mixed character equations can often be classified in comparison

[4]Naturally the opposite condition still defines a local sound horizon, cloaking some local region from being reached by scalar field perturbations.

to two standard equations ([147]). These are the Tricomi equation

$$\partial_y^2 u(x,y) + y\partial_x^2 u(x,y) = 0\,, \tag{7.36}$$

where the characteristic speeds, $\pm y^{1/2}$, go to zero at the character transition line $y = 0$, and the Keldysh equation

$$\partial_y^2 u(x,y) + \frac{1}{y}\partial_x^2 u(x,y) = 0\,, \tag{7.37}$$

where the speed $\pm y^{-1/2}$ diverges at the transition line.

Notice that the discriminant between the two characteristic speeds (7.35) turns out to be proportional to $-\det(\gamma^{\mu\nu})$. Therefore, as long as $(\gamma^{tt})^2 \to 0$ slower than $\det(\gamma^{\mu\nu}) \to 0$, the characteristic speeds V_+, V_- will coincide and the scalar field light cone becomes degenerate. Thus, there must exist some instant of time, before the system becomes –at least locally– parabolic, when either V_+ or V_- is zero (the latter case implying a sound horizon) indicative of a Tricomi-type transition. On the other hand, if $(\gamma^{tt})^2 \to 0$ faster than $\det(\gamma^{\mu\nu}) \to 0$ the characteristic speeds diverge indicating a transition of Keldysh type. This case is more delicate to tract numerically as the diverging speeds imply the time-step should be adjusted to decrease inversely with the maximum speed with an explicit integration algorithm. (Note: an implicit update could be implemented to bypass this issue, but at the expense of missing physics taking place at smaller scales than the time-step adopted).

Interestingly, in [147], only a Tricomi-type behavior is observed. Anticipating our results, we observe both cases depending on the value of the coupling g: Tricomi-like for $g < 0$ and Keldysh-type transitions $g > 0$. The well posedness of Tricomi equation has been explored in [148, 149] and, as discussed in [147] the initial/boundary conditions to ensure well posedness would be rather unnatural from a time-development point of view.

7.2.1 Implementation details

In the first order variables (7.30) we can extract from the rr and tt components of equation (7.31), respectively, the first order constraint equations

$$\alpha' = \frac{\alpha}{8r}\left[4(a^2-1) + r^2(\Phi^2+\Pi^2)\right] - g\frac{r\alpha}{16a^2}\left[(\Phi^2+\Pi^2)^2 - 4\Phi^4\right]\,, \tag{7.38}$$

$$a' = \frac{a}{8r}\left[4(1-a^2) + r^2(\Phi^2+\Pi^2)\right] + g\frac{r}{16a}\left[(\Phi^2+\Pi^2)^2 - 4\Pi^4\right] . \tag{7.39}$$

Equation (7.32), in terms of the first order variables, is given by

$$\dot{\Pi} = \frac{1}{r^2}\left(r^2\frac{\alpha}{a}\Phi\right)' + \frac{2g}{a^2+g\left(\Phi^2-3\Pi^2\right)}\frac{\alpha}{a}\Bigg[(\Phi^2+\Pi^2)\Phi' - 2\Phi\Pi\Pi' + \left(\frac{r}{4}\Pi^2 - \frac{a'}{a}\right)\left(\Phi^2-\Pi^2\right)\Phi + \frac{gr}{4a^2}\left(\Phi^2-\Pi^2\right)^2\Phi\Pi^2 + \frac{2}{r}\Phi\Pi^2\Bigg] , \tag{7.40}$$

together with the condition that $\partial_t\partial_r\phi = \partial_r\partial_t\phi$, namely

$$\dot{\Phi} = \left(\frac{\alpha}{a}\Pi\right)' . \tag{7.41}$$

The effective inverse metric from equation (7.33) reads

$$\gamma^{tt} = -\frac{1}{\alpha^2}\left(1 - g\frac{2\Pi^2}{a^2+g\left(\Phi^2-\Pi^2\right)}\right) , \qquad \gamma^{rr} = \frac{1}{a^2}\left(1 + g\frac{2\Phi^2}{a^2+g\left(\Phi^2-\Pi^2\right)}\right) , \tag{7.42}$$

$$\gamma^{tr} = -g\frac{2\Pi\Phi}{a\alpha\left(a^2+g\left(\Phi^2-\Pi^2\right)\right)} , \tag{7.43}$$

and the matrix defining the principal part of equations (7.40) and (7.41) is,

$$M = \begin{pmatrix} 0 & \frac{\alpha}{a} \\ -\frac{a\gamma^{rr}}{\alpha\gamma^{tt}} & -2\frac{\gamma^{tr}}{\gamma^{tt}} \end{pmatrix} = \frac{\alpha}{a}\begin{pmatrix} 0 & 1 \\ 1+2g\frac{\Phi^2+\Pi^2}{a^2+g(\Phi^2-3\Pi^2)} & -4g\frac{\Pi\Phi}{a^2+g(\Phi^2-3\Pi^2)} \end{pmatrix} . \tag{7.44}$$

The equations of motion are solved in a constrained evolution scheme. Both $\alpha(t,r)$ and $a(t,r)$ are obtained through a spatial integration while the scalar field is integrated in time through a Runge Kutta 4th order time integrator. At each time step (intermediate or full), given a spatial profile for the fields Φ and Π, the constraint equations (7.38) and (7.39) are integrated in space using also a Runge-Kutta 4th order method (RK4). First, a is integrated radially outwards from $r = 0$ to $r = r_{\max}$ with the initial condition $a(r=0) = 1$. This condition ensures regularity at $(\alpha' = a' = 0)$ at the origin. Then, α is integrated radially inwards with the

condition $\alpha(r_{\max}) = 1/a(r_{\max})$. Notice that, as these integrations are carried out, the fields Φ and Π which are needed at 'virtual radial points' in between grid points are obtained through fourth order (second order near the spatial boundaries) spatial interpolations at any given time step.

Evolution of Φ and Π forward in time is carried out via the method of lines with a RK4 integration using equations (7.40) and (7.41). Spatial derivatives are computed with second order (first order near the boundaries) finite-difference operators satisfying summation by parts. Regularity at the origin is addressed by using l'Hôpital's rule at $r = 0$ to regularize the equation, and we defined totally outgoing boundary conditions at the outer radial boundary. A small amount of fourth order (second order near the boundaries) artificial dissipation is added for convenience as described. For further details see [150–152].

The numerical results displayed in this chapter are performed in a spatial domain ranging from $r = 0$ to $r = r_{\max} = 100$, and a spatial resolution of $\Delta r = 1/80$. (though convergence and consistency of the solutions obtained is checked with resolutions of $\Delta r = 1/20$ and $\Delta r = 1/40$). The Courant number is initially taken to be $C = 1/10$, and therefore $\Delta t = C\Delta r = 1/800$. Numerical output is produced every 40 time steps. For cases displaying very fast changes, or a high speed of propagation of the scalar field, we switch to a Courant parameter of $C = 1/100$ ($\Delta t = 1/8000$) in the last part of the simulation, and we produce output of the solution every 4 time steps. The instants of time where this happens are listed in TABLE 7.1.

Parameter Set	A-	B-	C-	A+	B+	C+
Refinement Time	Never	$t = 56.5$	Never	Never	$t = 54.0$	$t = 68.0$

Table 7.1: Instants in time where resolution is increased.

Further, we compute the order of convergence of solutions Q as

$$2^Q = \frac{|S_{\Delta/2} - S_\Delta|}{|S_{\Delta/4} - S_{\Delta/2}|}\,. \tag{7.45}$$

In Fig. 7.1 the order of convergence is shown as a function of time for the four grid functions, indicating convergence with the expected rate.

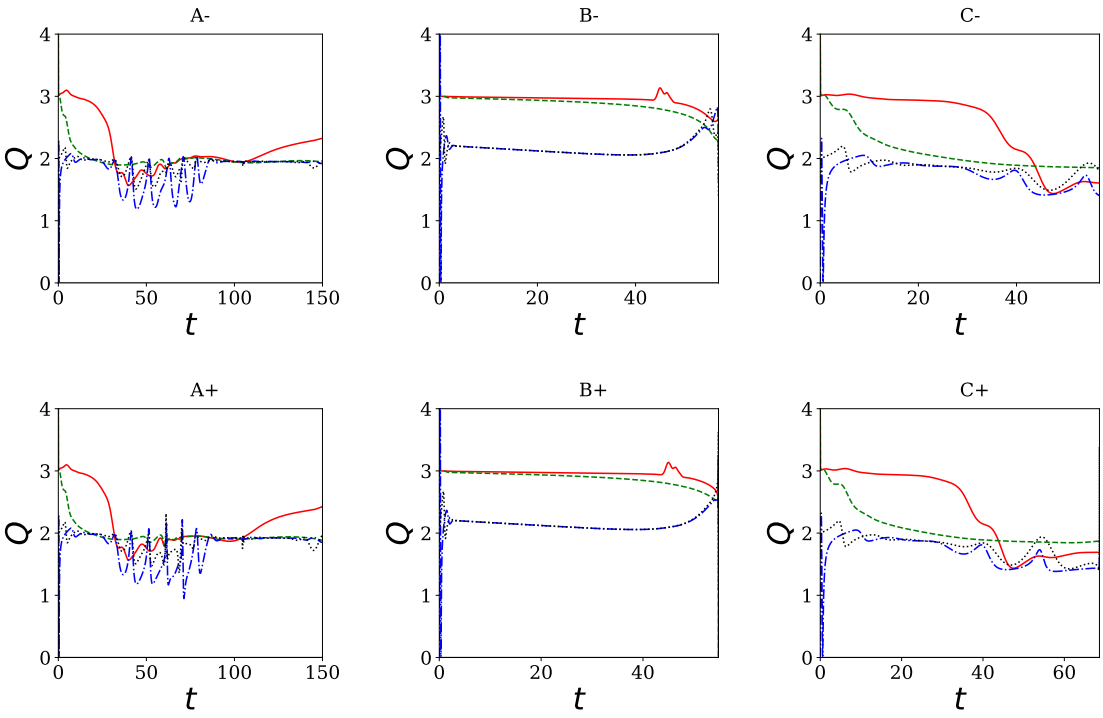

Figure 7.1: Order of convergence Q for the four grid functions α (red solid), a (green dashed), Φ (Blue, dash-dotted) and Π (black dotted).

7.2.2 Initial conditions and coupling parameters

As mentioned, our goal is to explore the possible phenomenology that can arise in this theory. We have performed extensive studies to try and isolate different scenarios and, for concreteness in our presentation, we present three representative cases for positive and negative coupling values. In particular, we adopt initial data for the (first order variables of the) scalar field given by:

$$\Phi(t=0,r) = A \exp\left(-\frac{(r-r_0)^2}{\sigma^2}\right) \cos\left(\frac{\pi}{10} r\right) , \qquad \Pi(t=0,r) = 0\,. \tag{7.46}$$

with $r_0 = 55$. The three cases, labeled **A**, **B** and **C**, are defined by the following parameters:

- Case **A**: $A = 0.02$, $\sigma = 15.0$

- Case **B**: $A = 0.14$, $\sigma = 1.5$
- Case **C**: $A = 0.045$, $\sigma = 15.0$

For each of these parameter sets, we have obtained solutions for $g = +1$ (labeled A+, B+ and C+) and for $g = -1$ (A-, B- and C-). Naturally, the scale over which a non-trivial physical behavior occurs depends on: (i) the initial location and amplitude of the pulse –as it travels towards the origin in spherical symmetry, his associated energy density naturally grows– and (ii) the strength of the coupling parameter g.

7.2.3 Negative coupling constant: $g = -1$

Setting $g = -1$, we observe three different outcomes depending on the initial conditions of the wave pulse as illustrated in Fig. 7.2. If the data is weak enough, case A-, the ingoing pulse reaches the origin, bounces off it and disperses as it propagates to infinity. For configuration B-, the eigenvalue λ_+ of the effective inverse metric crosses zero at $t \approx 56.63, r \approx 1.75$ while the lapse remains bounded from below by $\alpha \approx 0.62$. This indicates the system has become parabolic before a light horizon forms. Further, as predicted by equation (7.35), the characteristic speeds of the scalar field merge together as $\lambda_+ \to 0$ and acquire an imaginary part after that. Before the transition point, the eigenvalue V_- crosses zero at $t \approx 56.52, r \approx 1.90$, and therefore a sound horizon is indeed produced. However, since the lapse function α is positive everywhere, there is no light horizon and perturbations of the metric tensor can still propagate through the sound horizon, thus the transition point is not disconnected from outside observers. This is not the only possible outcome for strong enough initial data, as in configuration C- a light horizon does form, together with a sound horizon at $r \approx 6.5$, without any change in character of the scalar field equation. In Fig. 7.2 C-, the final state at and outside this region is described by a black hole with an outwards propagating field. As mentioned, we can not comment on what takes place inside the horizon. Interestingly, case B- displays characteristic speeds going to zero before going imaginary where the equation changes character to parabolic. This, as discussed in [147], is an indication that the equation is of Tricomi type.

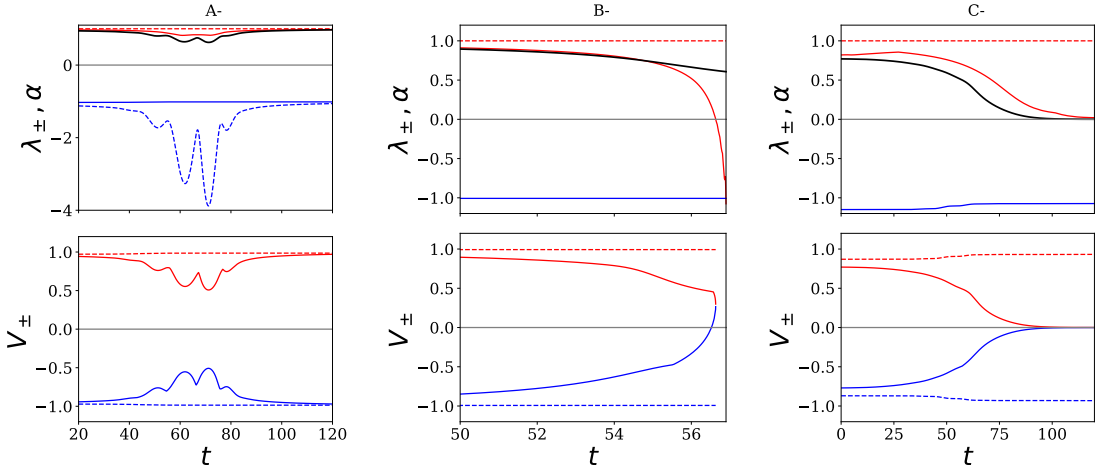

Figure 7.2: Eigenvalues for $g = -1$, in cases A- (left), B- (center) and C- (right). The upper three plots show the (max/min of) eigenvalues $\lambda_\pm$ of the effective inverse metric $\gamma^{\mu\nu}$ and the minimum of α. The lower three plots show the eigenvalues $V_\pm$ of the principal part of the scalar field equations, corresponding to the characteristic speeds of propagation of the scalar. In each plot, the upper red curves correspond to the spatial maximum (red dashed) and minimum (red solid) values of the λ_+ and V_+, while the lower blue curves depict the spatial maximum (blue solid) and minimum (blue dashed) of λ_- and V_-. The thick black solid line is the lapse function α, used to identify the formation of a black hole. A gray line at 0 is added as a guide to the eye.

7.2.4 Positive coupling constant: $g = +1$

For $g = +1$, delicate features in the solution for the same initial conditions developed in a more marked way and, arguably, more violently. The obtained behavior is illustrated in Fig. 7.3. Naturally, there is not much qualitative difference in A+ configuration. This is to be expected since for weak enough data, the impact of the scalar field is considerably suppressed. In cases B+ and C+, however, λ_- crosses zero and the system becomes parabolic in a rather sharp, abrupt way. The transition occurs at $t \approx 54.82, r \approx 1.70$ for case B+, and at $t \approx 68.63, r \approx 0$ for case C+.

In contrast to the previous case, cases B+, C+ display fastly growing characteristic speeds right before becoming imaginary where the equation changes character

to parabolic. This, as discussed in [147], is an indication that the equation is of Keldysh type. Moreover, this implies these regimes have a natural causal horizon significantly larger than that of light (e.g. [153]). Nevertheless, the change of character in the equation signals well-behaved solutions can only be obtained within a finite range of time. Furthemore, this change of character –for both values of coupling– takes place *prior to a shock being formed*.

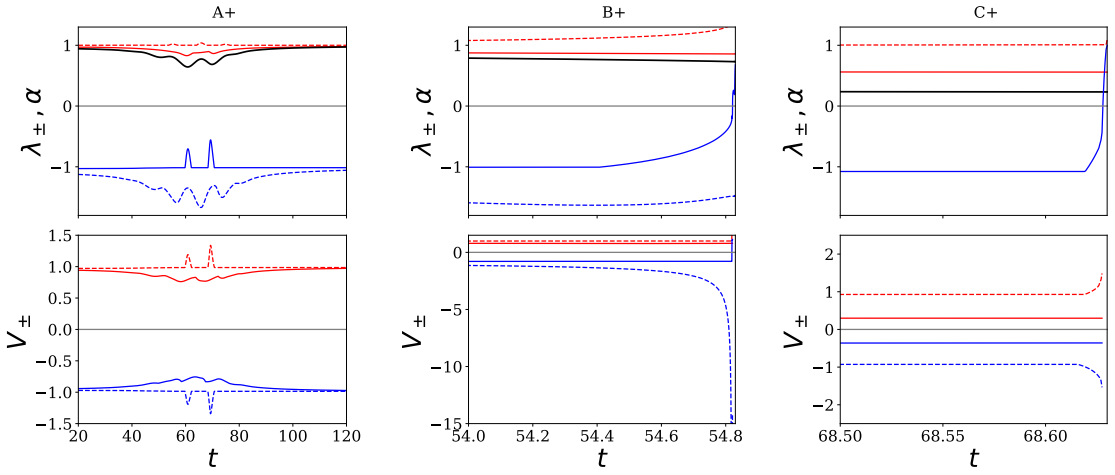

Figure 7.3: Eigenvalues for $g = +1$, in cases A+ (left), B+ (center) and C+ (right). The upper three plots show the (max/min of) eigenvalues $\lambda_\pm$ of the effective inverse metric $\gamma^{\mu\nu}$ and the minimum of α. The lower three plots show the eigenvalues $V_\pm$ of the principal part of the scalar field equations, corresponding to the characteristic speeds of propagation of the scalar. In each plot, the upper red curves correspond to the spatial maximum (red dashed) and minimum (red solid) values of the λ_+ and V_+, while the lower blue curves depict the spatial maximum (blue solid) and minimum (blue dashed) of λ_- and V_-. The thick black solid line is the lapse function α, used to identify the formation of a black hole. A gray line at 0 is added as a guide to the eye.

Finally, we illustrate the behavior of the (only non-trivial) component, τ_{tr}, of the twist

$$\tau_{\mu\nu} = \nabla_{[\mu}(X\partial_{\nu]}\phi)\,, \tag{7.47}$$

in figures 7.4, 7.5 for the negative and positive couplings adopted. As it is evident in the figures, in the weak cases (A-,A+), the twist remains bounded and relatively

small throughout the evolution. In contrast, in all but the C- cases the twist grows without bound. In case C-, however, the twist remains bounded since the large value of a at the horizon causes $X = a^{-2}(\Pi^2 - \Phi^2)/2$ to approach zero.

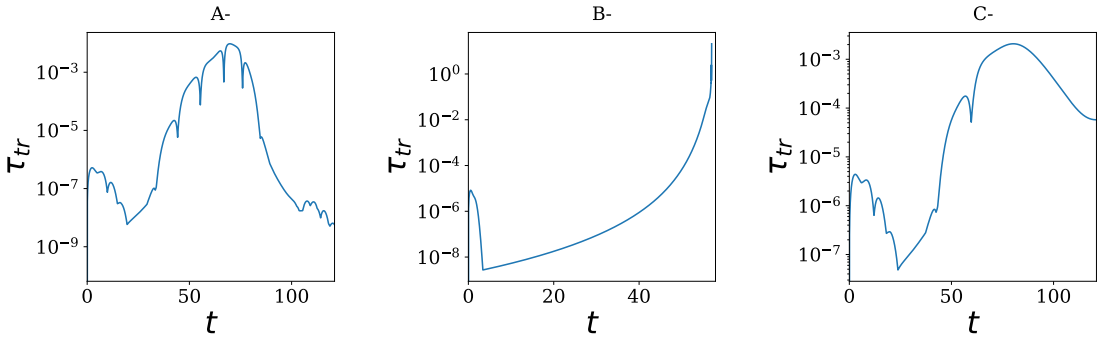

Figure 7.4: $\max|\tau_{tr}|$ for cases A- (left), B- (center) and C- (right).

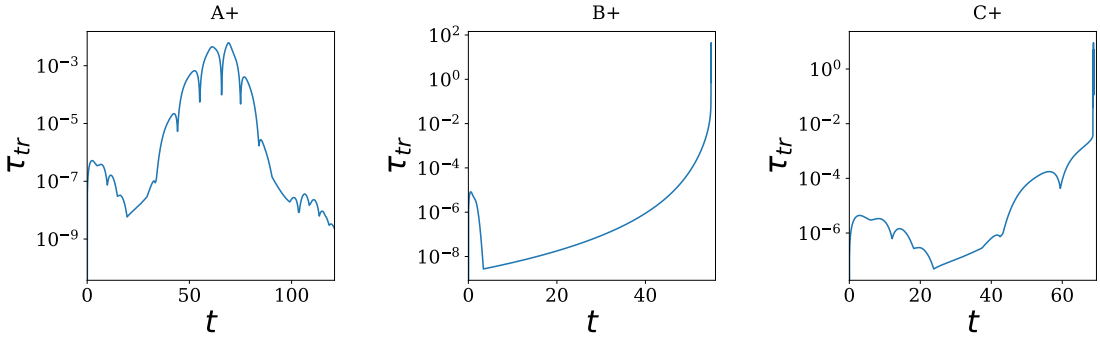

Figure 7.5: $\max|\tau_{tr}|$ for cases A+ (left), B+ (center) and C+ (right).

Chapter 8

Conclusions

8.1 Large D approach to gravity and black holes

The main part of this thesis is focused on the large D expansion of classical gravity as an extremely powerful technique to describe a variety of apparently disconnected physical systems. The description of black branes as an effective membrane, which is characterized by its mass density and momenta, results in a set of very simple parabolic equations that can be treated numerically, and even analytically, with remarkable results. Chapter 2 of this thesis focuses on the derivation of these effective equations, and their possible interpretations. As it turns out, the black branes at large D can be seen as hydrodynamic systems, but also as elastic membranes when they reach equilibrium configurations, giving rise to the concept of hydro-elastic complementarity.

Hydro-elastic complementarity is the manifestation in the limit $D \to \infty$ of what is arguably one of the most basic properties of a black hole, namely, that the same quantity doubles its role as the geometric size and as the mass. In the large-D effective theory of black branes, we can view $m(t, \sigma)$ as the local, fluctuating mass density of a fluid, or as the local radius of an elastic soap bubble embedded in the background spacetime. The effective dynamics can then be alternatively regarded as hydrodynamics, like in (2.26) and (2.27), or as elasticity, like in (2.48), (2.49) and (2.53).

As a first application of the large D effective equations, we analyze in a fair amount of detail the dynamics and phases of black strings. We do so not only at leading order in $1/D$ as introduced in Chapter 2, but as long as $1/D^4$. This allows us to treat the spacetime dimension D as a free parameter, allowing a great increment of the range of phenomena that we can describe. Even at this very high order, the equations become easily solved (even though very lengthy), and conceptually no different than the leading order. There are no constraints to be solved, and issues such as gauge invariance and gauge fixing are absent—they are dealt with once and for all when the effective equations are derived. A second, even more substantial advantage, lies in the possibility of using a sequential construction (sec. 3.4) in which, once the corrections to a given order are computed, then one can combine them to directly generate solutions where D is a continuous parameter that can be freely varied.

It is remarkable that, despite a qualitative change at a finite, critical dimension—often an impassable barrier to a perturbative series—, the large-D expansion is able to correctly capture physics at and even below this dimension. In particular, we have been able to compute D_* analytically as it is manifested in several different magnitudes, with all the 3NLO results (3.41), (3.44) and (3.65) converging on the value

$$D_* = 13.6\,. \tag{8.1}$$

A natural question is whether some of the rich structure observed in the time evolutions in $D = 5$ in [27], in particular the cascading behavior at late times, may be reproduced by evolving the effective large-D equations, which are computationally relatively simple to solve. After all, as we have seen, when sufficiently high-order corrections are included these equations appear to correctly capture many qualitative properties of NUBS in $D < D_*$. Unfortunately, we have found that the time evolution breaks down too early in the development of inhomogeneity to see this. Our simulations do not exhibit any sign of these cascading structures, nor of the self-similar shrinking of the thin tubes that connect the larger blobs on the string in [27]. Indeed, this behavior seems to depend crucially on scaling and homogeneity properties of the equations that are washed away when taking $D \to \infty$. So all those detailed features may be inaccessible to the large-D expansion.

Lacking so far in our investigation of black objects in a Kaluza-Klein circle are the phases of localized black holes. The reason is that, like with numerical analyses, the presence of "exposed" sections of the symmetry axis that are not covered by a horizon requires an approach different than for black string phases. Nevertheless, we expect that the large-D expansion can be a useful means for their investigation. It is straightforward to construct, via a large-D matched asymptotic expansion, solutions for localized black holes of increasing size up until they almost fill up the axis of the compact circle, except for a fraction $\sim 1/D$ of it.[1] Black holes that fill up a larger fraction of the axis and then reach up to the merger configurations,[2] where conifold structures of the type studied in [107, 154, 155] appear, also seem to be accessible in a large-D expansion. Putting together all these pieces of information, it might then

[1] This is a large-D version of the constructions in [36, 37].

[2] These have been numerically studied at finite, low D, in [26, 38, 39]

be possible to obtain a complete characterization of the phases of black objects in a Kaluza-Klein circle across the entire range of dimensions.

Quite surprisingly, the effective large D equations that were initially designed to describe black branes can be used to explore the dynamics of localized black holes. This comes as a consequence of the endpoint of the Gregory-Laflamme instability at infinite dimension, which creates Gaussian blobs on the brane. These blobs are only joined by exponentially thin membranes, and can move independently and interact with each other. It was recently found [43] that the blobs reproduce many of the features of localized black holes, thus opening a whole new world of possibilities to describe higher-dimensional objects (as long as gravitational radiation can be ignored).

In Chapter 4 we show that the resulting object (a black bar) from a black hole collision at large enough J forms a neck that quickly pinches down. Although our methods only allow to follow the evolution into regions of curvature smaller than $\mathcal{O}(D)$, the evidence from [27, 102], and indeed what our simulations suggest, is that the horizon pinches off to zero size, leading to a violation of CC.

Note, however, that our proposal for the breakup, namely, evaporation of a Planck-size neck, is actually independent of this, and we do not claim that the regulated large-D evolution is evidence for it. Indeed, the presence of the regulator is irrelevant for the main outcome of our simulations, which is the formation of an intermediate bar-like configuration that becomes unstable. This convincingly shows that the system is driven towards a situation where CC will be violated, but the detailed features of the singularity and its formation are beyond the reach of our methods, and so are left to future studies.

Another caveat is that the size of the region of the horizon that is captured in the effective theory of (4.1) is only $\mathcal{O}\left(1/\sqrt{D}\right)$. However, as shown very effectively in [102], this range can be enlarged by incorporating $1/D$ corrections until the method reproduces accurately the detailed features of black holes and black strings at finite D (including below the critical dimension). We do not see any apparent reason why *perturbative* $1/D$ corrections should lead to qualitative, instead of merely quantitative, changes in our picture.

More important are the consequences of *non-perturbative* corrections in $1/D$. Of these, the loss of angular momentum through the emission of gravitational radiation

is the main mechanism that opposes the instability: if the rate at which the angular momentum of the bar is shed off is faster than the instability growth, then the black bar may spin down to a stable MP black hole before the neck has time to form and pinch down. We have used the D-dimensional quadrupole formula [45] to estimate the characteristic time scale $\tau_{\rm rad} = \partial_t \ln(\mathbf{J}/\mathbf{M})$ of the radiative spin-down of a rotating ellipsoidal bar. We have then compared it to the shortest characteristic time $\tau_{\rm inst}$ for the growth of the Gregory-Laflamme instability of a black string of the same mass as the black bar. The radiation damping time is longer at large D by a strong factor,

$$\frac{\tau_{\rm rad}}{\tau_{\rm inst}} \sim D^D \,, \tag{8.2}$$

indeed so much so that our more accurate estimate suggests that already when $D \gtrapprox 7$ the spin-down may be much too slow to prevent the contraction of the neck [111].

Intermediate black bar states are in fact plausible only in $D \geq 6$, since only in these dimensions does the MP black hole have linear bar-mode instabilities [156] (however, see [157]). These bar-modes have been followed non-linearly in $D = 6, 7, 8$ and they return back to a stable black hole through radiation emission [158]. However, their long lifetime suggests that their angular momentum is not large enough to reach the unstable regime of black bars (moreover, the horizons in [158] do not result from a collision merger). Our estimates are uncertain, but the suppression of radiation with increasing D is so strong that we find it hard to envisage how the spin-down could be efficient in, say, $D \approx 10$ and possibly even lower dimensions.

At any rate, although at present it is difficult to obtain a more precise estimate, we are confident that our analysis supports the conclusion that the violation of CC proposed here will be present in a high but finite D.

8.2 Strong Cosmic Censorship in the presence of a cosmological constant

In Chapter 5 we leave Weak Cosmic Censorship to address its twin sister conjecture: Strong Cosmic Censorship, in this case at $D = 4$. The main motivation for this study

was to understand whether nonlinear effects could trigger mass inflation, even when the linearized analysis suggests otherwise [51].

We found that nonlinear effects seem not to be strong enough to change the picture. Within a nonlinear evolution, the precise linearized results are difficult to reproduce (for instance, the final spacetime parameters depend on the initial parameters and on the size of the initial data). The linearized analysis of Ref. [51] suggests that no mass inflation should occur for BH charge above a threshold $Q_* \simeq 0.995$. As a consequence of the accretion of the scalar field pulse, the mass of the black hole increases slightly, thus decreasing the extremality of the black hole. Because of the limitations of the numerical code, a large enough pulse is needed to trigger nonlinear effects, such as the blowup of the Kretschmann scalar, in the integration timescale. This in fact drives the black hole below the threshold of extremality Q_*. Clearly, then, the results are still inconclusive. However, we do see an evident and dramatic decrease in mass inflation as we increase the extremality, which seems to suggest that nonlinear effects are not likely to preserve SCC.

The (numerical) solutions presented here are the first solutions of this kind arising from the full nonlinear evolution of exterior data. They contain a Cauchy horizon in their BH interior region that can be seen as ("weakly") singular, due to the divergence of curvature invariants. However, these divergent tidal forces are not necessarily strong enough to lead to a divergent tidal deformation and the consequent unequivocal destruction of all macroscopic objects [117]. Even more problematic, the extrapolated lack of mass inflation indicates that these Cauchy horizons should maintain enough regularity as to allow the field equations to determine (classically), in a highly non-unique way, the evolution of the metric to their future. This corresponds to a potential severe violation of SCC.

Our results concern spherically symmetric spacetimes. The picture is unlikely to change even with asymmetric initial conditions [51]. Thus, from the *conceptual* point of view [52], our results show that SCC is not enforced by the field equations.

In the meantime, interesting suggestions to remedy SCC, in the presence of a positive cosmological constant, have been put forward: these include enlarging the allowed set of initial data by weakening their regularity [159], or restricting the scope of SCC to the uncharged BH setting [160]. It thus seems plausible that the *astrophysical* interpretation of SCC remains valid, once other fields *and* realistic BH

charges are considered.

8.3 Holographic plasma polarization and Love numbers of black branes

Chapter 6 is an example of a simple yet very insightful calculation in the context of AdS/CFT holography. The calculations can be done mostly analytically, with some very simple numerical integrations of ordinary differential equations. Clearly we have only taken a first step. There is still further work ahead if one wants to test a holographic calculation of the polarization response against results from real-world systems. In particular the holographic modelling must be made more sophisticated. But we have identified the basic features of the phenomenon, and the extension to other models developed in AdS/CMT is possible.

In this thesis the initial unperturbed geometry for the field theory has always been Minkowski space, and correspondingly we have worked in the Poincaré patch of AdS in the bulk. But it is also possible and interesting to study the electric and gravitational polarization of black holes in global AdS—in dual terms, the polarization of the plasma on a spherical space. Indeed, the fully non-linear effects of electric polarization for these black holes have been studied numerically already in [161, 162], see also [163–165]. The analysis in global AdS is technically more complicated (spherical harmonics instead of plane waves) and presumably less relevant to systems in the lab, so we have not attempted it here.

8.4 Horndeski's Theory

In Chapter 7 we explore the subset of Horndeski's theories identified as being able to define locally well posed problems. The analysis we build upon, described in [93, 94], relied on identifying and exploiting a specific gauge. Such a choice might a priori be regarded as restrictive, however when seen from the Einstein frame point of view, it can be argued as being quite natural. Further, note the discussion –and problems identified that can arise– for the dynamics of the scalar field holds regardless of the gauge chosen to consider the evolution for the metric sector. In particular, one can

argue for the existence of global well behaved solutions in the weak data case. Beyond this regime, however the truly non-linear character of the equations can induce phenomenology which present serious roadblocks. Avoiding such issues requires satisfying a twist-free condition, but such a case might be too restrictive depending on the application and context of interest. In the general case, the strong possibility of a change in character of the equation –from hyperbolic to elliptic through a parabolic stage– as well as the loss of uniqueness through the appearance of shocks further question the ability to define well-posed problems with these theories. (In simplified settings, similar deficiencies have been identified [166–168]). We mention in passing that since the effective metric depends on the gradient of the scalar field, the transition to parabolic/elliptic regimes is likely to take prior to the formation of shocks in generic situations (also highlihgted in [137]). Hence, considering Horndeski's theories as the leading order in a gradient expansion, problems might arise still within the a priori assumed regime of applicability. The timescale for the identified pathologies to arise depends, naturally, on the coupling value considered and the initial data adopted. Due to these difficulties, the extent to which global solutions obtained within the linearized regime and the information one can draw from them with respect to the original action can be regarded as suspect.

This observation, which is arguably in tension with interesting observations drawn at linearized levels in the cosmological context, perhaps calls for a different philosophy with respect to Horndeski's theories. For instance, to use the linearized equations of motion as a starting point to build a new one free of the (many) problems identified at the nonlinear level through the addition of further suitable operators (for a related discussion, see [169]). However, it might come at the expense of higher derivatives being introduced. A complementary or alternative approach would be to identify the set of behaviors which can be considered physical and, armed with a suitable justification, modify the non-linear equations of motion to control unphysical pathologies (e.g. [135, 170]).

Chapter 9

Catalan Summary
Resum en Català

La Relativitat General ha demostrat ser una teoria de la gravetat extremadament exitosa. Aquesta teoria, formulada en un llenguatge purament geomètric, produeix prediccions que s'han verificat amb molta precisió en una gran quantitat d'experiments històrics. Més recentment, i gairebé precisament un segle després de la formulació de la teoria, LIGO ens va donar una confirmació d'una de les prediccions més espectaculars de la Relativitat General, juntament amb una nova forma d'obtenir informació valuosa a partir d'esdeveniments astrofísics: les ones gravitacionals. Això no obstant, d'un punt de vista fonamental, tenim motius per pensar que la Relativitat General està incompleta. Creiem que la teoria hauria de deixar de ser fiable a una escala d'energia prou gran (o a una escala de longitud prou petita). Aquesta escala ha de ser, com a màxim, l'escala de Planck.

Els forats negres són els objectes més bàsics de la Relativitat General, i posseir-ne un bon coneixement sembla ser clau per comprendre la gravetat. Són extremadament importants com a objectes astrofísics, també de l'univers primerenc (forats negres primordials), en relativitat matemàtica, en teoria de cordes i en gravetat quàntica. També en molts sistemes aparentment no gravitacionals mitjançant dualitats hologràfiques aplicades (AdS / QFT, AdS / QGP, AdS / CMT ...). Els forats negres són probablement els objectes macroscòpics més senzills de la Natura, que es descriuen completament per la seva massa, moment angular i càrrega elèctrica. Aquest fet els fa matemàticament molt atractius i elegants: ens permet descriure objectes de mida astrofísica amb equacions molt simples, sovint fins i tot analíticament. Tot i que semblen molt senzills, tenim pistes, com la termodinàmica dels forats negres o la Paradoxa de la Informació, que ens indiquen que la Relativitat General està fonamentada per una estructura més complexa. És, per tant, el nostre objectiu intentar trobar la teoria adequada de la gravetat quàntica. Ara per ara, els candidats més acceptats estan agrupats en el que es coneix com la teoria de cordes. Adoptar aquesta família de teories té un cost: hem de formular-les en més de quatre dimensions, normalment 10 o 11, i gairebé segur que requereixen supersimetria.

En aquesta tesi aplicarem nous enfocaments i desenvoluparem noves tècniques per tractar diversos temes relacionats amb aspectes fonamentals de la teoria gravitacional moderna i els forats negres. Tenir una dimensió fonamental superior a quatre és un problema que es pot esquivar exigint que les dimensions addicionals es compactin en una varietat diferenciable de dimensió $D-4$. D'aquesta manera,

la física a escales de longitud suficientment llargues es desenvolupa de forma efectiva en un espaitemps de dimensió 4. Aquest fet, però, ens anima a explorar el comportament de la gravetat i els forats negres en dimensions superiors a quatre. La física dels forats negres en dimensions altes és immensament més rica que en dimensió quatre: molts dels teoremes d'unicitat no es mantenen, permetent així una gran varietat de fenòmens gravitacionals. En particular, existeixen forats negres amb direccions extenses (cordes negres i branes negres). Els forats negres extensos també presenten l'anomenada inestabilitat de Gregory-Laflamme, que fa que les cordes negres i les branes negres desenvolupin espontàniament deformacions que poden acabar produint una violació de la conjectura de la Censura Còsmica Feble.

9.1 Branes i cordes negres en dimensions altes

En aquesta tesi estudiem el comportament de les branes negres en l'aproximació *large* D, és a dir, considerem un espaitemps amb un nombre molt gran de dimensions. Al Capítol 2, aquest enfocament ens permet obtenir un conjunt d'equacions molt simples que recullen molts dels fenòmens físics de la gravetat. Aquesta tècnica utilitza el fet que el camp gravitatori al voltant d'un objecte massiu decau més ràpidament com més alta és la dimensió, i per tant, quan es pren el límit $D \to \infty$, queda concentrat en una regió molt fina de mida $1/D$ al voltant de l'horitzó del forat negre. D'aquesta manera, l'horitzó es pot veure com una membrana suspesa en una geometria de fons essencialment plana. La regió on viu el forat negre està (en certa manera) exclosa de l'espaitemps de fons.

Una pregunta bàsica que ens podem fer és si les equacions de la teoria efectiva es poden entendre en termes de la física quotidiana. En efecte, podem descriure l'evolució dinàmica de la brana negra com un fluid, mentre que per a configuracions estacionàries és més natural veure-la com una membrana elàstica o una bombolla de sabó.

Al Capítol 3 utilitzem les equacions efectives *large* D per investigar les fases i l'estabilitat de les cordes negres a diferents valors de la dimensió D i de la longitud de compactificació L. En alguns casos, la inestabilitat de Gregory-Laflamme de les cordes negres uniformes pot conduir a cordes negres no uniformes estables. El tipus transició canvia a un cert valor crític de la dimensió d'espaitemps $D_* \approx 13,5$.

Utilitzem correccions $1/D$ per estimar el valor de la dimensió crítica, que resulta ser molt precisa. De fet, la nostra determinació analítica de les dimensions crítiques proporciona possiblement el valor més exacte fins ara, superant els càlculs numèrics actuals. Utilitzem tant solucions analítiques pertorbatives com càlculs numèrics per obtenir dades termodinàmiques que comparem amb resultats a D finita de la literatura. La comparació mostra que la tècnica *large* D pot donar resultats analítics amb gran precisió.

També realitzem un estudi de cordes negres altament deformades en un nombre creixent de dimensions, per tal de determinar el punt de transició a forats negres localitzats. Aquest estudi seria extremadament feixuc i requeriria molt de temps amb tècniques numèriques convencionals, a causa de la creixent dificultat d'aquests mètodes a mesura que augmenta el nombre de dimensions. Ho fem mitjançant una combinació de mètodes — a través de l'evolució dinàmica de les equacions, i a través estudis de solucions estàtiques que desenvolupen patologies identificables (específicament, tensions negatives) quan la deformació és massa gran.

9.2 Col·lisions i Censura Còsmica Feble

La conjectura de Censura Còsmica Feble de Penrose afirma que no es poden formar singularitats nues a través de l'evolució dinàmica d'un sistema gravitacional a partir de dades inicials clàssiques. També es podria definir com la impossibilitat per a observadors llunyans d'observar la física a l'escala de Plank (i per tant la gravetat quàntica) si l'energia de la configuració inicial és baixa i el sistema segueix l'evolució gravitatòria clàssica de les equacions d'Einstein.

El Capítol 4 explora possibles esdeveniments de violació de la Censura Còsmica en col·lisions de forats negres a $D > 4$. La tècnica de *large* D, mitjançant les equacions efectives, proporciona una eina potent per analitzar aquest tipus d'escenaris que d'altra manera serien molt complicats d'abordar mitjançant simulacions numèriques a D finita. Recentment s'ha demostrat que els forats negres en rotació es poden descriure com protuberàncies sobre una brana negra.

El fenomen de la violació de la Censura Còsmica es pot resumir de la manera següent: Quan dos forats negres xoquen, els seus horitzons d'esdeveniments es fusionen i formen un únic forat negre molt deformat. Si el moment angular és prou

baix, l'horitzó resultant es relaxarà mitjançant vibracions dels modes quasinormals fins arribar a una solució estacionària de Myers-Perry en rotació. En canvi, si el moment angular de la col·lisió està per sobre d'un determinat llindar, el forat negre esdevindrà un objecte allargat en forma de barra.

La barra negra es veu afectada per una inestabilitat, anàloga a la inestabilitat de Gregory-Laflamme, que fa que l'horitzó formi un coll prim al seu centre. L'objecte resultant es pot trencar un cop aquest coll és suficientment prim, i separar-se en dos forats negres (ara estables) que són llançats en direccions diferents. La competició entre la velocitat de creixement de la inestabilitat de Gregory-Laflamme i la pèrdua de moment angular a causa de l'emissió d'ones gravitacionals determinarà si es produeix finalment la violació de la Censura Còsmica Feble.

9.3 Censura Còsmica Forta

Els horitzons de Cauchy apareixen en moltes solucions exactes per a sistemes gravitacionals, particularment en les solucions de Reissner-Nordström i de Kerr. Aquests horitzons són un límit més enllà del qual la Relativitat General deixa de ser una teoria determinista. De fet, el futur d'un observador que entri a la regió de l'espaitemps més enllà de l'horitzó intern d'un forat negre de Reissner-Nordström no es pot predir a partir de les dades inicials externes. L'observador tindrà en aquest moment una singularitat de tipus temps en el seu passat nul, i per tant la informació d'aquesta singularitat pot afectar el futur de l'interior del forat negre.

Generalment es creu que la presència dels horitzons de Cauchy és un artefacte que sorgeix en solucions *eternes* exactes. En exigir que l'espaitemps sigui estacionari, estem impedint l'evolució dinàmica que evitaria la formació d'aquests horitzons. Aquesta idea queda recollida en la conjectura de Censura Còsmica Forta de Penrose. Segons aquesta hipòtesi, les pertorbacions externes que cauen al forat negre patirien un desplaçament cap al blau infinit en arribar a l'horitzó de Cauchy, provocant així una inestabilitat. L'horitzó inestable resultant esdevindria singular, creant un acabament de l'espaitemps.

L'estabilitat dels horitzons de Cauchy depèn per tant del decaïment de les pertorbacions a l'exterior del forat negre. Una pertorbació d'un camp escalar ϕ en un forat negre asimptòticament pla decaurà com una llei de potència donada per la

coneguda llei de Price. Aquest comportament és suficient per garantir el fenomen d'inflació de massa, i per tant la validesa de la Censura Còsmica Forta. Aquest escenari, però, canvia dràsticament quan hi afegim una constant cosmològica $\Lambda > 0$. En aquest cas, ϕ decaurà seguint una llei exponencial. Aquest fet ha fet que recentment es posi en dubte la conjectura de Censura Còsmica Forta per a forats negres de Reissner-Nordström altament carregats en espaitemps asimptòticament de Sitter.

Per anar més enllà dels estudis anteriors, el Capítol 5 resumeix els resultats de simulacions completament no lineals de Reissner-Nordström altament carregats. Per tal de realitzar les integracions no lineals (esfèricament simètriques), s'ha desenvolupat un nou codi espectral en coordenades doblement nul·les. Tot i que els resultats presentats aquí són lluny de ser concloents, mostren una disminució dramàtica de la inflació de massa quan la càrrega del forat s'aproxima al llindar predit a la literatura, fins al punt on no s'observa la inflació de massa dins del domini computacional del codi.

9.4 Polarització de plasmes i nombres de Love

Qualsevol sistema continu que es pugui descriure com una teoria quàntica de camps reaccionarà davant un canvi en la geometria on està situat. Ho farà canviant la distribució de la densitat d'energia, la pressió i el tensor d'esforços. És a dir, el sistema (que anomenarem *plasma*) es polaritza, i el seu tensor d'energia-moment adquireix un valor esperat quàntic no trivial. En general, aquest efecte és bastant difícil de calcular, sobretot si la teoria de camps està fortament acoblada. En aquest cas, la teoria de pertorbacions no és aplicable i només es poden realitzar càlculs numèrics.

En aquest context, la dualitat hologràfica, també coneguda com a correspondència AdS/CFT, és extremadament útil per extreure informació qualitativa i valuosa del sistema. D'acord amb aquesta conjectura, les teories quàntiques de camps fortament acoblades amb invariància conforme (CFT), són duals a la gravetat clàssica dins l'espaitemps Anti-de Sitter (AdS). Per tant, hi ha una correspondència entre la gravetat clàssica en AdS en dimensió $n+1$ i les teories conformes fortament acoblades en dimensió n (en particular, les teories Super Yang-Mills amb grup de galga $SU(N)$) situades a la frontera d'AdS. Aquest fet es pot utilitzar per extreure informació de

la teoria quàntica, altrament molt difícil d'obtenir, a partir de càlculs de gravetat.

Les pertorbacions en la geometria de la frontera d'AdS produiran deformacions de marea en la geometria de l'interior. Per calcular aquesta deformació, resolem les equacions per a una pertorbació linealitzada de la geometria que satisfà una condició de contorn adequada a l'infinit. Aquest és exactament l'objectiu del Capítol 6. Tenir una teoria quàntica a temperatura finita equival a introduir un forat negre a l'interior d'AdS. En particular, una brana negra, les direccions espacials de la qual corresponen a les direccions espacials de la frontera.

Si les pertorbacions són prou petites, les deformacions de la brana es descriuen bé mitjançant coeficients de resposta lineal, anomenats nombres de Love. El valor esperat quàntic del tensor d'energia moment s'obté a partir dels nombres de Love.

9.5 Teories de Horndeski

Quan s'intenten construir extensions a la Relativitat General, és natural considerar la inclusió de nous graus de llibertat per descriure el camp gravitatori. És important, però, que les equacions de moviment resultants siguin com a màxim de segon ordre, per garantir l'absència de fantasmes d'Ostrogradski, que potencialment conduirien a inestabilitats catastròfiques de la teoria. La riquesa de possibles teories augmenta dràsticament si es permet que la gravetat estigui descrita tant per una mètrica $g_{\mu\nu}$ com per un camp escalar ϕ. Així, la teoria més general que conté una mètrica i un camp escalar, que és invariant sota difeomorfismes, i que condueix a equacions de moviment de segon ordre és coneguda com la teoria de Horndeski.

Independentment de les dades experimentals, generalment se suposa que una teoria que pretén descriure la Natura ha de ser matemàticament *ben plantejada*. Les teories ben plantejades són aquelles que tenen una solució única que depèn de forma contínua de les condicions inicials i de contorn. Una teoria que no està ben plantejada no pot donar cap predicció física fiable.

El Capítol 7 estudia un subconjunt de les teories de Horndeski les equacions del moviment de les quals són localment ben plantejades. Tot i això, cal determinar si existeixen solucions globals i si aquestes solucions són prou ben comportades. És important tenir en compte que, en aquest cas, la velocitat de propagació del camp escalar no coincideix en general amb la "velocitat de la llum" i, per tant, podem

trobar *horizons de so* per al camp escalar i *horitzons de llum* per a la mètrica. Atès que $g_{\mu\nu}$ i ϕ estan acoblats, només l'horitzó més intern serà un veritable límit per a la connexió causal amb l'infinit. La velocitat de propagació de l'escalar no està fitada superiorment i, fins i tot, pot divergir en determinades circumstàncies especials.

Una altra possibilitat preocupant (que s'ha confirmat amb simulacions numèriques), és un canvi del caràcter de l'equació de moviment, d'hiperbòlica a parabòlica i finalment a el·líptica. Això produeix un canvi en l'estructura causal de la geometria.

Bibliography

[1] LIGO Scientific, Virgo collaboration, *Observation of Gravitational Waves from a Binary Black Hole Merger*, *Phys. Rev. Lett.* **116** (2016) 061102 [1602.03837].

[2] J. M. Maldacena, *The Large N limit of superconformal field theories and supergravity*, *Int. J. Theor. Phys.* **38** (1999) 1113 [hep-th/9711200].

[3] R. Gregory and R. Laflamme, *Black strings and p-branes are unstable*, *Phys. Rev. Lett.* **70** (1993) 2837 [hep-th/9301052].

[4] R. Gregory and R. Laflamme, *The Instability of charged black strings and p-branes*, *Nucl. Phys.* **B428** (1994) 399 [hep-th/9404071].

[5] T. Andrade, R. Emparan, D. Licht and R. Luna, *Cosmic censorship violation in black hole collisions in higher dimensions*, *JHEP* **04** (2019) 121 [1812.05017].

[6] J. Camps, R. Emparan and N. Haddad, *Black Brane Viscosity and the Gregory-Laflamme Instability*, *JHEP* **05** (2010) 042 [1003.3636].

[7] V. Asnin, D. Gorbonos, S. Hadar, B. Kol, M. Levi and U. Miyamoto, *High and Low Dimensions in The Black Hole Negative Mode*, *Class. Quant. Grav.* **24** (2007) 5527 [0706.1555].

[8] R. Emparan, R. Suzuki and K. Tanabe, *The large D limit of General Relativity*, *JHEP* **06** (2013) 009 [1302.6382].

[9] R. Emparan, D. Grumiller and K. Tanabe, *Large-D gravity and low-D strings*, *Phys. Rev. Lett.* **110** (2013) 251102 [1303.1995].

[10] R. Emparan, R. Suzuki and K. Tanabe, *Decoupling and non-decoupling dynamics of large D black holes*, *JHEP* **07** (2014) 113 [1406.1258].

[11] R. Emparan, T. Shiromizu, R. Suzuki, K. Tanabe and T. Tanaka, *Effective theory of Black Holes in the 1/D expansion*, *JHEP* **06** (2015) 159 [1504.06489].

[12] S. Bhattacharyya, A. De, S. Minwalla, R. Mohan and A. Saha, *A membrane paradigm at large D*, *JHEP* **04** (2016) 076 [1504.06613].

[13] R. Suzuki and K. Tanabe, *Stationary black holes: Large D analysis*, *JHEP* **09** (2015) 193 [1505.01282].

[14] R. Suzuki and K. Tanabe, *Non-uniform black strings and the critical dimension in the* $1/D$ *expansion*, *JHEP* **10** (2015) 107 [1506.01890].

[15] R. Emparan, R. Suzuki and K. Tanabe, *Evolution and End Point of the Black String Instability: Large D Solution*, *Phys. Rev. Lett.* **115** (2015) 091102 [1506.06772].

[16] K. Tanabe, *Black rings at large D*, *JHEP* **02** (2016) 151 [1510.02200].

[17] S. Bhattacharyya, M. Mandlik, S. Minwalla and S. Thakur, *A Charged Membrane Paradigm at Large D*, *JHEP* **04** (2016) 128 [1511.03432].

[18] R. Emparan, T. Harmark, V. Niarchos and N. A. Obers, *Essentials of Blackfold Dynamics*, *JHEP* **03** (2010) 063 [0910.1601].

[19] T. Damour, *Black Hole Eddy Currents*, *Phys. Rev.* **D18** (1978) 3598.

[20] T. Wiseman, *Static axisymmetric vacuum solutions and nonuniform black strings*, *Class. Quant. Grav.* **20** (2003) 1137 [hep-th/0209051].

[21] B. Kleihaus, J. Kunz and E. Radu, *New nonuniform black string solutions*, *JHEP* **06** (2006) 016 [hep-th/0603119].

[22] E. Sorkin, *Non-uniform black strings in various dimensions*, *Phys. Rev.* **D74** (2006) 104027 [gr-qc/0608115].

[23] P. Figueras, K. Murata and H. S. Reall, *Stable non-uniform black strings below the critical dimension*, *JHEP* **11** (2012) 071 [1209.1981].

[24] M. Kalisch and M. Ansorg, *Highly Deformed Non-uniform Black Strings in Six Dimensions*, in *Proceedings, 14th Marcel Grossmann Meeting on Recent Developments in Theoretical and Experimental General Relativity, Astrophysics, and Relativistic Field Theories (MG14) (In 4 Volumes): Rome, Italy, July 12-18, 2015*, vol. 2, pp. 1799–1804, 2017, 1509.03083, DOI.

[25] M. Kalisch and M. Ansorg, *Pseudo-spectral construction of non-uniform black string solutions in five and six spacetime dimensions*, *Class. Quant. Grav.* **33** (2016) 215005 [1607.03099].

[26] M. Kalisch, S. Mckel and M. Ammon, *Critical behavior of the black hole/black string transition*, *JHEP* **08** (2017) 049 [1706.02323].

[27] L. Lehner and F. Pretorius, *Black Strings, Low Viscosity Fluids, and Violation of Cosmic Censorship*, *Phys. Rev. Lett.* **105** (2010) 101102 [1006.5960].

[28] R. Penrose, *Gravitational collapse: The role of general relativity*, *Riv. Nuovo Cim.* **1** (1969) 252.

[29] E. Sorkin, *A Critical dimension in the black string phase transition*, *Phys. Rev. Lett.* **93** (2004) 031601 [hep-th/0402216].

[30] B. Kol, *The Phase transition between caged black holes and black strings: A Review*, *Phys. Rept.* **422** (2006) 119 [hep-th/0411240].

[31] T. Harmark, V. Niarchos and N. A. Obers, *Instabilities of black strings and branes*, *Class. Quant. Grav.* **24** (2007) R1 [hep-th/0701022].

[32] G. T. Horowitz, ed., *Black holes in higher dimensions*. Cambridge Univ. Pr., Cambridge, UK, 2012.

[33] M. Kalisch, *Numerical construction and critical behavior of Kaluza-Klein black holes*, Ph.D. thesis, Jena U., 2018. 1802.06596.

[34] M. Rozali and A. Vincart-Emard, *On Brane Instabilities in the Large D Limit*, *JHEP* **08** (2016) 166 [1607.01747].

[35] . J. C. Dias, J. E. Santos and B. Way, *Lattice Black Branes: Sphere Packing in General Relativity*, *JHEP* **05** (2018) 111 [1712.07663].

[36] T. Harmark, *Small black holes on cylinders*, *Phys. Rev.* **D69** (2004) 104015 [hep-th/0310259].

[37] D. Gorbonos and B. Kol, *A Dialogue of multipoles: Matched asymptotic expansion for caged black holes*, *JHEP* **06** (2004) 053 [hep-th/0406002].

[38] H. Kudoh and T. Wiseman, *Connecting black holes and black strings*, *Phys. Rev. Lett.* **94** (2005) 161102 [hep-th/0409111].

[39] M. Headrick, S. Kitchen and T. Wiseman, *A New approach to static numerical relativity, and its application to Kaluza-Klein black holes*, *Class. Quant. Grav.* **27** (2010) 035002 [0905.1822].

[40] M. W. Choptuik, *Universality and scaling in gravitational collapse of a massless scalar field*, *Phys. Rev. Lett.* **70** (1993) 9.

[41] P. Figueras, M. Kunesch, L. Lehner and S. Tunyasuvunakool, *End Point of the Ultraspinning Instability and Violation of Cosmic Censorship*, *Phys. Rev. Lett.* **118** (2017) 151103 [1702.01755].

[42] H. Bantilan, P. Figueras, M. Kunesch and R. Panosso Macedo, *End point of nonaxisymmetric black hole instabilities in higher dimensions*, *Phys. Rev.* **D100** (2019) 086014 [1906.10696].

[43] T. Andrade, R. Emparan and D. Licht, *Rotating black holes and black bars at large D*, *JHEP* **09** (2018) 107 [1807.01131].

[44] T. Andrade, R. Emparan and D. Licht, *Charged rotating black holes in higher dimensions*, *JHEP* **02** (2019) 076 [1810.06993].

[45] V. Cardoso, O. J. C. Dias and J. P. S. Lemos, *Gravitational radiation in D-dimensional space-times*, *Phys. Rev.* **D67** (2003) 064026 [hep-th/0212168].

[46] E. Poisson and W. Israel, *Inner-horizon instability and mass inflation in black holes*, *Phys. Rev. Lett.* **63** (1989) 1663.

[47] R. H. Price, *Nonspherical perturbations of relativistic gravitational collapse. 1. Scalar and gravitational perturbations*, *Phys. Rev.* **D5** (1972) 2419.

[48] J. L. Costa, P. M. Girão, J. Natário and J. D. Silva, *On the Occurrence of Mass Inflation for the EinsteinMaxwell-Scalar Field System with a Cosmological Constant and an Exponential Price Law*, *Commun. Math. Phys.* **361** (2018) 289 [1707.08975].

[49] J. L. Costa and A. T. Franzen, *Bounded energy waves on the black hole interior of Reissner-Nordström-de Sitter*, *Annales Henri Poincare* **18** (2017) 3371 [1607.01018].

[50] P. Hintz and A. Vasy, *Analysis of linear waves near the Cauchy horizon of cosmological black holes*, *J. Math. Phys.* **58** (2017) 081509 [1512.08004].

[51] V. Cardoso, J. L. Costa, K. Destounis, P. Hintz and A. Jansen, *Quasinormal modes and Strong Cosmic Censorship*, *Phys. Rev. Lett.* **120** (2018) 031103 [1711.10502].

[52] V. Cardoso, J. L. Costa, K. Destounis, P. Hintz and A. Jansen, *Strong cosmic censorship in charged black-hole spacetimes: still subtle*, 1808.03631.

[53] O. J. C. Dias, H. S. Reall and J. E. Santos, *Strong cosmic censorship: taking the rough with the smooth*, 1808.02895.

[54] Y. Mo, Y. Tian, B. Wang, H. Zhang and Z. Zhong, *Strong cosmic censorship for the massless charged scalar field in the Reissner-Nordstrom-de Sitter spacetime*, 1808.03635.

[55] O. J. C. Dias, H. S. Reall and J. E. Santos, *Strong cosmic censorship for charged de Sitter black holes with a charged scalar field*, 1808.04832.

[56] A. Donos and S. A. Hartnoll, *Interaction-driven localization in holography*, *Nature Phys.* **9** (2013) 649 [1212.2998].

[57] A. Donos and J. P. Gauntlett, *Novel metals and insulators from holography*, *JHEP* **06** (2014) 007 [1401.5077].

[58] A. Donos, B. Goutraux and E. Kiritsis, *Holographic Metals and Insulators with Helical Symmetry*, *JHEP* **09** (2014) 038 [1406.6351].

[59] A. Donos, J. P. Gauntlett and C. Pantelidou, *Conformal field theories in $d = 4$ with a helical twist*, *Phys. Rev.* **D91** (2015) 066003 [1412.3446].

[60] T. Damour and A. Nagar, *Relativistic tidal properties of neutron stars*, *Phys. Rev.* **D80** (2009) 084035 [0906.0096].

[61] T. Binnington and E. Poisson, *Relativistic theory of tidal Love numbers*, *Phys. Rev.* **D80** (2009) 084018 [0906.1366].

[62] E. E. Flanagan and T. Hinderer, *Constraining neutron star tidal Love numbers with gravitational wave detectors*, *Phys. Rev.* **D77** (2008) 021502 [0709.1915].

[63] T. Hinderer, *Tidal Love numbers of neutron stars*, *Astrophys. J.* **677** (2008) 1216 [0711.2420].

[64] P. K. Kovtun and A. O. Starinets, *Quasinormal modes and holography*, *Phys. Rev.* **D72** (2005) 086009 [hep-th/0506184].

[65] S. Bhattacharyya, R. Loganayagam, S. Minwalla, S. Nampuri, S. P. Trivedi and S. R. Wadia, *Forced Fluid Dynamics from Gravity*, *JHEP* **02** (2009) 018 [0806.0006].

[66] S. Bhattacharyya, R. Loganayagam, I. Mandal, S. Minwalla and A. Sharma, *Conformal Nonlinear Fluid Dynamics from Gravity in Arbitrary Dimensions*, *JHEP* **12** (2008) 116 [0809.4272].

[67] J. Lennon and P. McCartney, *All you need is Love*, *Parlophone* (1967) .

[68] P. Chesler, A. Lucas and S. Sachdev, *Conformal field theories in a periodic potential: results from holography and field theory*, *Phys. Rev.* **D89** (2014) 026005 [1308.0329].

[69] R. P. Woodard, *Avoiding dark energy with 1/r modifications of gravity*, *Lect. Notes Phys.* **720** (2007) 403 [astro-ph/0601672].

[70] G. W. Horndeski, *Second-Order Scalar-Tensor Field Equations in a Four-Dimensional Space*, *International Journal of Theoretical Physics* **10** (1974) 363.

[71] C. Deffayet, X. Gao, D. A. Steer and G. Zahariade, *From k-essence to generalised Galileons*, *Phys. Rev.* **D84** (2011) 064039 [1103.3260].

[72] A. Nicolis, R. Rattazzi and E. Trincherini, *The Galileon as a local modification of gravity*, *Phys. Rev.* **D79** (2009) 064036 [0811.2197].

[73] C. Deffayet, G. Esposito-Farèse and A. Vikman, *Covariant Galileon*, *Phys. Rev.* **D79** (2009) 084003 [0901.1314].

[74] P. G. Ferreira, *Cosmological Tests of Gravity*, 1902.10503.

[75] T. Kobayashi, M. Yamaguchi and J. Yokoyama, *Generalized G-inflation: Inflation with the most general second-order field equations*, *Prog. Theor. Phys.* **126** (2011) 511 [1105.5723].

[76] T. Damour and G. Esposito-Farèse, *Tensor - scalar gravity and binary pulsar experiments*, *Phys. Rev.* **D54** (1996) 1474 [gr-qc/9602056].

[77] E. Barausse, C. Palenzuela, M. Ponce and L. Lehner, *Neutron-star mergers in scalar-tensor theories of gravity*, *Phys. Rev.* **D87** (2013) 081506 [1212.5053].

[78] S. Mirshekari and C. M. Will, *Compact binary systems in scalar-tensor gravity: Equations of motion to 2.5 post-Newtonian order*, *Phys. Rev.* **D87** (2013) 084070 [1301.4680].

[79] L. Sagunski, J. Zhang, M. C. Johnson, L. Lehner, M. Sakellariadou, S. L. Liebling et al., *Neutron star mergers as a probe of modifications of general relativity with finite-range scalar forces*, *Phys. Rev.* **D97** (2018) 064016 [1709.06634].

[80] F.-L. Julié and N. Deruelle, *Two-body problem in Scalar-Tensor theories as a deformation of General Relativity : an Effective-One-Body approach*, *Phys. Rev.* **D95** (2017) 124054 [1703.05360].

[81] E. W. Hirschmann, L. Lehner, S. L. Liebling and C. Palenzuela, *Black Hole Dynamics in Einstein-Maxwell-Dilaton Theory*, *Phys. Rev.* **D97** (2018) 064032 [1706.09875].

[82] L. Bernard, *Dynamics of compact binary systems in scalar-tensor theories: Equations of motion to the third post-Newtonian order*, *Phys. Rev.* **D98** (2018) 044004 [1802.10201].

[83] H. Witek, L. Gualtieri, P. Pani and T. P. Sotiriou, *Black holes and binary mergers in scalar Gauss-Bonnet gravity: scalar field dynamics*, *Phys. Rev.* **D99** (2019) 064035 [1810.05177].

[84] B. Ratra and P. J. E. Peebles, *Cosmological Consequences of a Rolling Homogeneous Scalar Field*, *Phys. Rev.* **D37** (1988) 3406.

[85] R. R. Caldwell, R. Dave and P. J. Steinhardt, *Cosmological imprint of an energy component with general equation of state*, *Phys. Rev. Lett.* **80** (1998) 1582 [astro-ph/9708069].

[86] C. Armendariz-Picon, V. F. Mukhanov and P. J. Steinhardt, *A Dynamical solution to the problem of a small cosmological constant and late time cosmic acceleration*, *Phys. Rev. Lett.* **85** (2000) 4438 [astro-ph/0004134].

[87] C. Armendariz-Picon, V. F. Mukhanov and P. J. Steinhardt, *Essentials of k essence*, *Phys. Rev.* **D63** (2001) 103510 [astro-ph/0006373].

[88] J. Khoury and A. Weltman, *Chameleon fields: Awaiting surprises for tests of gravity in space*, *Phys. Rev. Lett.* **93** (2004) 171104 [astro-ph/0309300].

[89] J. Khoury and A. Weltman, *Chameleon cosmology*, *Phys. Rev.* **D69** (2004) 044026 [astro-ph/0309411].

[90] T. Baker, E. Bellini, P. G. Ferreira, M. Lagos, J. Noller and I. Sawicki, *Strong constraints on cosmological gravity from GW170817 and GRB 170817A*, *Phys. Rev. Lett.* **119** (2017) 251301 [1710.06394].

[91] P. Creminelli and F. Vernizzi, *Dark Energy after GW170817 and GRB170817A*, *Phys. Rev. Lett.* **119** (2017) 251302 [1710.05877].

[92] J. M. Ezquiaga and M. Zumalacárregui, *Dark Energy After GW170817: Dead Ends and the Road Ahead*, *Phys. Rev. Lett.* **119** (2017) 251304 [1710.05901].

[93] G. Papallo and H. S. Reall, *On the local well-posedness of Lovelock and Horndeski theories*, *Phys. Rev.* **D96** (2017) 044019 [1705.04370].

[94] A. Ijjas, F. Pretorius and P. J. Steinhardt, *Stability and the Gauge Problem in Non-Perturbative Cosmology*, 1809.07010.

[95] . D. Kovács, *Well-posedness of cubic Horndeski theories*, 1904.00963.

[96] J. Hadamard, *Sur les problèmes aux dérivées partielles et leur signification physique*, *Princeton University Bulletin* **13** (1902) 49.

[97] R. Emparan, K. Izumi, R. Luna, R. Suzuki and K. Tanabe, *Hydro-elastic Complementarity in Black Branes at large D*, *JHEP* **06** (2016) 117 [1602.05752].

[98] M. M. Caldarelli, J. Camps, B. Goutraux and K. Skenderis, *AdS/Ricci-flat correspondence and the Gregory-Laflamme instability*, *Phys. Rev.* **D87** (2013) 061502 [1211.2815].

[99] M. M. Caldarelli, J. Camps, B. Goutraux and K. Skenderis, *AdS/Ricci-flat correspondence*, *JHEP* **04** (2014) 071 [1312.7874].

[100] M. M. Caldarelli, R. Emparan and B. Van Pol, *Higher-dimensional Rotating Charged Black Holes*, *JHEP* **04** (2011) 013 [1012.4517].

[101] R. Emparan, T. Harmark, V. Niarchos and N. A. Obers, *Blackfolds in Supergravity and String Theory*, *JHEP* **08** (2011) 154 [1106.4428].

[102] R. Emparan, R. Luna, M. Martnez, R. Suzuki and K. Tanabe, *Phases and Stability of Non-Uniform Black Strings*, *JHEP* **05** (2018) 104 [1802.08191].

[103] S. S. Gubser, *On nonuniform black branes*, *Class. Quant. Grav.* **19** (2002) 4825 [hep-th/0110193].

[104] T. Harmark and N. A. Obers, *New phase diagram for black holes and strings on cylinders*, *Class. Quant. Grav.* **21** (2004) 1709 [hep-th/0309116].

[105] T. Harmark and N. A. Obers, *Phase structure of black holes and strings on cylinders*, *Nucl. Phys.* **B684** (2004) 183 [hep-th/0309230].

[106] R. Emparan, R. Suzuki and K. Tanabe, *Quasinormal modes of (Anti-)de Sitter black holes in the 1/D expansion*, *JHEP* **04** (2015) 085 [1502.02820].

[107] B. Kol, *Topology change in general relativity, and the black hole black string transition*, *JHEP* **10** (2005) 049 [hep-th/0206220].

[108] R. Emparan and K. Tanabe, *Universal quasinormal modes of large D black holes*, *Phys. Rev.* **D89** (2014) 064028 [1401.1957].

[109] J. Bezanson, A. Edelman, S. Karpinski and V. B. Shah, *Julia: A fresh approach to numerical computing*, *SIAM review* **59** (2017) 65.

[110] C. Rackauckas and Q. Nie, *Differentialequations. jl–a performant and feature-rich ecosystem for solving differential equations in julia*, *Journal of Open Research Software* **5** (2017) .

[111] T. Andrade, R. Emparan, D. Licht and R. Luna, *Black hole collisions, instabilities, and cosmic censorship violation at large D*, *JHEP* **09** (2019) 099 [1908.03424].

[112] R. Luna, M. Zilhão, V. Cardoso, J. L. Costa and J. Natário, *Strong Cosmic Censorship: the nonlinear story*, *Phys. Rev.* **D99** (2019) 064014 [1810.00886].

[113] M. Dafermos, *Black holes without spacelike singularities*, *Commun. Math. Phys.* **332** (2014) 729 [1201.1797].

[114] J. Luk, *Weak null singularities in general relativity*, *J. Am. Math. Soc.* **31** (2018) 1 [1311.4970].

[115] M. Dafermos and J. Luk, *The interior of dynamical vacuum black holes I: The C^0-stability of the Kerr Cauchy horizon*, 1710.01722.

[116] S. Klainerman, I. Rodnianski and J. Szeftel, *The Bounded L2 Curvature Conjecture*, *Invent. Math.* **202** (2015) 91 [1204.1767].

[117] A. Ori, *Inner structure of a charged black hole: An exact mass-inflation solution*, *Phys. Rev. Lett.* **67** (1991) 789.

[118] J. L. Costa, P. M. Girão, J. Natário and J. D. Silva, *On the global uniqueness for the Einstein-Maxwell-scalar field system with a cosmological constant. Part 3: Mass inflation and extendibility of the solutions*, *Ann. PDE* **3** (2017) [1406.7261].

[119] E. Eilon and A. Ori, *Adaptive gauge method for long-time double-null simulations of spherical black-hole spacetimes*, *Phys. Rev.* **D93** (2016) 024016 [1510.05273].

[120] L. M. Burko and A. Ori, *Late time evolution of nonlinear gravitational collapse*, *Phys. Rev.* **D56** (1997) 7820 [gr-qc/9703067].

[121] J. Hansen, A. Khokhlov and I. Novikov, *Physics of the interior of a spherical, charged black hole with a scalar field*, *Phys. Rev.* **D71** (2005) 064013 [gr-qc/0501015].

[122] P. P. Avelino, A. J. S. Hamilton, C. A. R. Herdeiro and M. Zilhao, *Mass inflation in a D dimensional Reissner-Nordstrom black hole: a hierarchy of particle accelerators ?*, *Phys. Rev.* **D84** (2011) 024019 [1105.4434].

[123] M. Dafermos, *The Interior of charged black holes and the problem of uniqueness in general relativity*, *Commun. Pure Appl. Math.* **58** (2005) 0445 [gr-qc/0307013].

[124] J. Sbierski, *The C_0-inextendibility of the Schwarzschild spacetime and the spacelike diameter in Lorentzian geometry*, *J. Diff. Geom.* **108** (2018) 319 [1507.00601].

[125] P. R. Brady, C. M. Chambers, W. Krivan and P. Laguna, *Telling tails in the presence of a cosmological constant*, *Phys. Rev.* **D55** (1997) 7538 [gr-qc/9611056].

[126] R. Emparan, A. Fernandez-Pique and R. Luna, *Geometric polarization of plasmas and Love numbers of AdS black branes*, *JHEP* **09** (2017) 150 [1707.02777].

[127] V. Balasubramanian and P. Kraus, *A Stress tensor for Anti-de Sitter gravity*, *Commun. Math. Phys.* **208** (1999) 413 [hep-th/9902121].

[128] B. Assel, D. Cassani, L. Di Pietro, Z. Komargodski, J. Lorenzen and D. Martelli, *The Casimir Energy in Curved Space and its Supersymmetric Counterpart*, *JHEP* **07** (2015) 043 [1503.05537].

[129] M. Ammon and J. Erdmenger, *Gauge/gravity duality*. Cambridge University Press, Cambridge, 2015.

[130] R. Emparan, C. V. Johnson and R. C. Myers, *Surface terms as counterterms in the AdS / CFT correspondence*, *Phys. Rev.* **D60** (1999) 104001 [hep-th/9903238].

[131] L. Bernard, L. Lehner and R. Luna, *Challenges to global solutions in Horndeskis theory*, *Phys. Rev.* **D100** (2019) 024011 [1904.12866].

[132] Y. Fourès-Bruhat, *Théorème d'existence pour certains systèmes d'équations aux dérivées partielles non linéaires*, *Acta Math.* **88** (1952) 141.

[133] O. Sarbach and M. Tiglio, *Continuum and Discrete Initial-Boundary-Value Problems and Einstein's Field Equations*, *Living Rev. Rel.* **15** (2012) 9 [1203.6443].

[134] H. S. Reall, N. Tanahashi and B. Way, *Shock Formation in Lovelock Theories*, *Phys. Rev.* **D91** (2015) 044013 [1409.3874].

[135] G. Allwright and L. Lehner, *Towards the nonlinear regime in extensions to GR: assessing possible options*, *Class. Quant. Grav.* **36** (2019) 084001 [1808.07897].

[136] R. Akhoury, D. Garfinkle and R. Saotome, *Gravitational collapse of k-essence*, *JHEP* **04** (2011) 096 [1103.0290].

[137] J. L. Ripley and F. Pretorius, *Hyperbolicity in Spherical Gravitational Collapse in a Horndeski Theory*, 1902.01468.

[138] G. Papallo, *On the hyperbolicity of the most general Horndeski theory*, *Phys. Rev.* **D96** (2017) 124036 [1710.10155].

[139] G. Holzegel, S. Klainerman, J. Speck and W. Wong, *Shock Formation in Small-Data Solutions to $3D$ Quasilinear Wave Equations: An Overview*, *arXiv e-prints* (2014) arXiv:1407.6276 [1407.6276].

[140] D. Christodoulou and S. Klainerman, *The Global nonlinear stability of the Minkowski space*, .

[141] H. Lindblad and I. Rodnianski, *The Global stability of the Minkowski space-time in harmonic gauge*, math/0411109.

[142] C. Wang and X. Yu, *Recent works on the Strauss conjecture*, *arXiv e-prints* (2011) arXiv:1110.4454 [1110.4454].

[143] R. Kimura and K. Yamamoto, *Constraints on general second-order scalar-tensor models from gravitational Cherenkov radiation*, *JCAP* **1207** (2012) 050 [1112.4284].

[144] C. Palenzuela, E. Barausse, M. Ponce and L. Lehner, *Dynamical scalarization of neutron stars in scalar-tensor gravity theories*, *Phys. Rev.* **D89** (2014) 044024 [1310.4481].

[145] M. Shibata, K. Taniguchi, H. Okawa and A. Buonanno, *Coalescence of binary neutron stars in a scalar-tensor theory of gravity*, *Phys. Rev.* **D89** (2014) 084005 [1310.0627].

[146] C. Brans and R. H. Dicke, *Mach's principle and a relativistic theory of gravitation*, *Phys. Rev.* **124** (1961) 925.

[147] J. Ripley and F. Pretorius, *Gravitational Collapse in Einstein Dilaton Gauss-Bonnet Gravity*, 1903.07543.

[148] C. S. Morawetz, *The dirichlet problem for the tricomi equation*, *Communications on Pure and Applied Mathematics* **23** (1970) 587 [https://onlinelibrary.wiley.com/doi/pdf/10.1002/cpa.3160230404].

[149] T. H. Otway, *Elliptichyperbolic partial differential equations: A mini-course in geometric and quasilinear methods*, .

[150] G. Calabrese, L. Lehner, D. Neilsen, J. Pullin, O. Reula, O. Sarbach et al., *Novel finite differencing techniques for numerical relativity: Application to black hole excision*, *Class. Quant. Grav.* **20** (2003) L245 [gr-qc/0302072].

[151] G. Calabrese, L. Lehner, O. Reula, O. Sarbach and M. Tiglio, *Summation by parts and dissipation for domains with excised regions*, *Class. Quant. Grav.* **21** (2004) 5735 [gr-qc/0308007].

[152] F. S. Guzman, L. Lehner and O. Sarbach, *Do unbounded bubbles ultimately become fenced inside a black hole?*, *Phys. Rev.* **D76** (2007) 066003 [0706.3915].

[153] C. Bonvin, C. Caprini and R. Durrer, *A no-go theorem for k-essence dark energy*, *Phys. Rev. Lett.* **97** (2006) 081303 [astro-ph/0606584].

[154] B. Kol and T. Wiseman, *Evidence that highly nonuniform black strings have a conical waist*, *Class. Quant. Grav.* **20** (2003) 3493 [hep-th/0304070].

[155] R. Emparan and N. Haddad, *Self-similar critical geometries at horizon intersections and mergers*, *JHEP* **10** (2011) 064 [1109.1983].

[156] . J. C. Dias, G. S. Hartnett and J. E. Santos, *Quasinormal modes of asymptotically flat rotating black holes*, *Class. Quant. Grav.* **31** (2014) 245011 [1402.7047].

[157] M. Shibata and H. Yoshino, *Nonaxisymmetric instability of rapidly rotating black hole in five dimensions*, *Phys. Rev.* **D81** (2010) 021501 [0912.3606].

[158] M. Shibata and H. Yoshino, *Bar-mode instability of rapidly spinning black hole in higher dimensions: Numerical simulation in general relativity*, *Phys. Rev.* **D81** (2010) 104035 [1004.4970].

[159] M. Dafermos and Y. Shlapentokh-Rothman, *Rough initial data and the strength of the blue-shift instability on cosmological black holes with* $\Lambda > 0$, 1805.08764.

[160] O. J. C. Dias, F. C. Eperon, H. S. Reall and J. E. Santos, *Strong cosmic censorship in de Sitter space*, *Phys. Rev.* **D97** (2018) 104060 [1801.09694].

[161] M. S. Costa, L. Greenspan, M. Oliveira, J. Penedones and J. E. Santos, *Polarised Black Holes in AdS*, *Class. Quant. Grav.* **33** (2016) 115011 [1511.08505].

[162] M. S. Costa, L. Greenspan, J. Penedones and J. E. Santos, *Polarised Black Holes in ABJM*, *JHEP* **06** (2017) 024 [1702.04353].

[163] C. Herdeiro and E. Radu, *Anti-de-Sitter regular electric multipoles: Towards EinsteinMaxwell-AdS solitons*, *Phys. Lett.* **B749** (2015) 393 [1507.04370].

[164] C. Herdeiro and E. Radu, *EinsteinMaxwellAnti-de-Sitter spinning solitons*, *Phys. Lett.* **B757** (2016) 268 [1602.06990].

[165] C. A. R. Herdeiro and E. Radu, *Static Einstein-Maxwell black holes with no spatial isometries in AdS space*, *Phys. Rev. Lett.* **117** (2016) 221102 [1606.02302].

[166] S. Appleby and E. V. Linder, *The Paths of Gravity in Galileon Cosmology*, *JCAP* **1203** (2012) 043 [1112.1981].

[167] A. De Felice and S. Tsujikawa, *Conditions for the cosmological viability of the most general scalar-tensor theories and their applications to extended Galileon dark energy models*, *JCAP* **1202** (2012) 007 [1110.3878].

[168] R. Brito, A. Terrana, M. Johnson and V. Cardoso, *Nonlinear dynamical stability of infrared modifications of gravity*, *Phys. Rev.* **D90** (2014) 124035 [1409.0886].

[169] C. de Rham, *The gravitational rainbow beyond Einstein gravity*, *Int. J. Mod. Phys.* **D28** (2019) 1942003.

[170] J. Cayuso, N. Ortiz and L. Lehner, *Fixing extensions to general relativity in the nonlinear regime*, *Phys. Rev.* **D96** (2017) 084043 [1706.07421].